University of Strathclyde

Department of Naval Architecture, Ocean and Marine Engineering

Experimental and Numerical Quantification of Influences of Drugs on Zebrafish Larvae Swimming Kinematics and Energetics

ZHENKAI ZHAO

The thesis submitted in fulfillment of the requirements for the degree of

Doctor of Philosophy

July 2020

Acknowledgements

First and foremost, I would like to thank my principal supervisor Dr Qing Xiao and my second supervisor Dr Huirong Jiang for their inspiring advice and kind help. Dr Xiao was always encouraging and helpful with her expertise in CFD related problems. Her efforts in supervising me with my PhD study will always be appreciated.

I would like to thank Dr Xinhua Shu from Glasgow Caledonian University and Dr Gen Li from Japan Agency for Marine-Earth Science and Technology for their kind help in developing the numerical tool and providing lab and apparatus for experiment. Their valuable supports are much appreciated.

I would like to thank University of Strathclyde for the financial support during my study in the UK.

I would like to thank Ms Susan Pawson and other staff in the Department of NAOME for their kind help in administrative and technical issues.

I would like to thank the technical supports from ARCHIE-WeSt HPC based at University of Strathclyde and CIRRUS HPC based at University of Edinburgh for providing CFD simulation resources.

I would like to thank all my amazing colleagues and friends in Glasgow. They were always supportive and encouraging and the time spent with them made my life in Scotland much more enjoyable.

Finally, I am deeply indebted to my loving family for their endless love and support. I am grateful to my parents for their selfless support on my study and life. They always understand me and support all my decisions on study and development. I am proud of being their son.

Publications

Journal Articles

- Laibing Jia, Kotapati Raghupathy, R., Albalawi, A., **Zhenkai Zhao**, Reilly, J., Qing Xiao. & Xinhua (2017). A colour preference technique to evaluate acrylamide induced toxicity in zebra-fish. *Comparative Biochemistry and Physiology Part C: Toxicology and Pharmacology,* **199**, 11-19.

- **Zhenkai Zhao**, Gen Li, Qing Xiao, Hao Liu and Xinhua Shu (2020). Quantification of the influence of medicine on zebrafish larvae swimming behaviours and energetics. *PeerJ*, **8:e8374**

- **Zhenkai Zhao**, Qing Xiao, Gabriel Mbuta Tchivelekete, James Relly, Huirong Jiang, Xinhua Shu. Quantification of computational fluid dynamics simulation assists the evaluation of Gypenoside protection in a zebrafish pain model. *Physiology & Behavior* (under review).

Conference paper

- **Zhenkai Zhao**, Qing Xiao, Gen Li, Hao Liu and Xinhua Shu (2018) A study of zebrafish locomotion using experimental and numerical simulation. In proceedings of the *2018 7th International Symposium on Aero Aqua Bio-mechanisms*, Senju, Tokyo, Japan

Abstract

The use of zebrafish larvae has aroused wide-interest in the medical field for its potential role in the development of new therapies. Compared to other species, the zebrafish larvae grow extremely quickly, and the embryos are nearly transparent, which allows easy examination of its internal structures using fluorescent imaging techniques. Its complete genome sequence has already been published and is quite similar to that of human beings. Together with other advantages such as 2-6mm tiny body size for large scale screening, zebrafish has been grown to be a valuable model to test drugs and human diseases. Different types of drugs might have different influences on zebrafish behaviors, these behavior changes are related to functional changes of motoneurons in the spinal cord in the central nervous system (CNS) and transformations of the zebrafish body such as muscle mechanical power and force variation, which cannot be measured directly by pure experimental observation. Therefore, a knowledge of internal muscle mechanics can assist the understanding of the effects of drugs on swimming activity. In this study, a novel methodology has been developed to investigate the influences of drugs on zebrafish larvae kinematics and energetics including the internal muscle mechanics, which can supply additional information on zebrafish swimming behavior changes induced by drug applications.

The method includes both experimental measurement and numerical simulation. The experimental study is carried out with high-speed camera recordings on real zebrafish larvae swimming behaviors and post-processing with multi-function in-house *MATLAB* code to capture and extract the body motion data. The numerical simulation is based on coupling between open-source CFD toolbox *OpenFOAM*, and an open-source multi-body dynamics software *MBDyn* to accurately quantify influences of drug applications on zebrafish larvae kinematic and energetic performances, and especially internal muscle mechanics. For the interactions between zebrafish larvae and surrounding fluid, *OpenFOAM* is used to solve fluid dynamics and deal with dynamic internal mesh motion; *MBDyn* is used for solid body analysis and provide kinematic data for

OpenFOAM. The coupling of these two solvers is achieved by establishing an interface library to exchange data with the help of the TCP/IP protocol.

Test cases are studied to validate the feasibility and accuracy of the numerical methodology. The first step validation includes comparisons with past research of a 2-D jellyfish-like multi-body structure to prove that numerical coupling between *OpenFOAM* and *MBDyn* is feasible in simulating multi-body structure. The second step validation includes comparisons between 3-D zebrafish model and experimentally observed results with high-speed camera. To be specific, tail-beat angles and averaged forward velocity of zebrafish larvae are compared, and all the quantitative comparisons show acceptable similarities. Also, zebrafish body curvatures are compared between experiment and CFD during one period of time to supplement the validation for accuracy of numerical simulation.

Applications of our methodology include nociceptive and neuroactive drug influences on zebrafish locomotion and additional information from our results such as internal muscle mechanisms, to assist the evaluation of Gypenosides protection from high concentration acetic acid. We firstly provide comparisons of zebrafish locomotion before and after treatments with 0.01% acetic acid, 500 μM diphenylhydantoin (DPH), and 100mg/ml yohimbine to test whether our novel zebrafish model can simulate different types of drug effects (positive, negative and no effect) on zebrafish larvae or not. The reason of choosing the three drugs is based on previous studies showing apparent physiology and behavioural changes under biological experiments. Based on our results, the three different drugs show positive, negative, and no impact on zebrafish swimming activities, respectively. These effects have been accurately quantified with parameters such as forward velocity, forces, and hydrodynamic and mechanical power distributions, etc.

Besides, we have evaluated the damage caused by 0.1% acetic acid to the muscle of 5 days post-fertilization (dpf) zebrafish larvae, and the effects of protection with saponin

Gypenoside (GYP) extracted from *Gynostemma pentaphyllum* to demonstrate that our technique can support biological experiment. Quantitative real-time polymerase chain reaction (qRT-PCR) has been used to examine the effects of acetic acid and GYP on oxidative stress and inflammation, leading to the fact that co-treatment of GYP can mediate damage caused by acetic acid. At the same time, we have quantified the parameters related to muscle such as muscle power and the resultant hydrodynamic force, proving that GYP can alleviate the detrimental effect of acetic acid on zebrafish larvae, in the form of alleviation from swimming debility, and that the muscle status can be quantified to represent the degree of muscle damage due to the acetic acid and the recovery due to GYP. We have also linked the behavioral changes to alteration of antioxidant and inflammation gene expression.

These results provide novel insights into the reasons for pain-related behavioral changes in zebrafish larvae, especially from an internal muscle perspective which is hard to be provided with traditional biological experimental analysis. Using this approach, we might focus on evaluating potential analgesic drugs for pain relief and neuroactive drug effects on fish behaviors, which might help to understand the functions of the nervous system and explain drug effects on zebrafish larvae locomotion.

Table of Contents

1 Introduction

1.1. Background

Zebrafish (also called Danio rerio) is a tropical freshwater fish (displayed in **Fig. 1-1**) distributed across parts of India, Bangladesh, Nepal, and Pakistan [1]. Over the past thirty years, zebrafish has become a pre-eminent vertebrate model to study genes as well as drug discovery in medical research. Zebrafish embryo has a nearly transparent body and develop externally, allowing scientists to observe the morphological changes such as cell motion, organ formation, heartbeat, and development during the first few days of life [2]. Zebrafish can produce a large number of offspring, and the 2-6mm body length for larval stage allows massive number of specimens to be manipulated in a flexible space to generate a large number of mutants simultaneously [3, 4]. Mutants can be used to discover the specific stages of embryogenesis being disrupted by different types of mutations, which is essential for elucidating the conserved molecular mechanisms underlying early vertebrate development [5, 6]. Compared with human beings, zebrafish has a similar genetic structure and shares 70% of genes with human beings, which makes it possible to study human diseases on zebrafish. In the following sections, a brief introduction of zebrafish applications and contributions in drug discovery and medical treatment will be stated to provide an essential background for readers on part of the research scopes of zebrafish.

Figure 1-1. A sketch of zebrafish development from the embryo stage (left-most image), larvae stage (middle image) (scale bar = 1mm) to the adult stage (right-most model). (isoft iStock)

1.1.1. Zebrafish contributions in toxicological study and new drug development

In recent years, zebrafish has become a valuable model for drug discovery. As shown in **Fig. 1-2**, publications on zebrafish related to toxicology have grown over 4-fold in the last ten years. At early stages, zebrafish larvae are cheap, and they can produce large numbers of offspring, from which scientists can test the efficacy and toxicity of new drugs before applying to more expensive and complicated mammalian animals.

Toxicology, by definition, is tightly constrained to the need to prevent diseases. Specifically, whether a chemical is safe or a given disease is caused or influenced by a specific chemical exposure is at the core of the discipline. Therefore, evaluating the toxicity of a new drug is vital as the unaccepted toxicity will fail the check at clinical trials. Determination of toxicity includes various compounds such as heavy metals, pesticides, and compounds causing environmental contaminations. An important parameter to be determined for toxicity testing is the LC_{50} value (the concentration that is lethal to 50% of testing fish) [7]. A comparison of LC_{50} value between zebrafish and mammals based on 18 chemical compounds has been made, showing that zebrafish embryo is more sensitive than mammals to the toxic treatment [8]. Similar researches have also been applied to evaluate the embryotoxicity and safety of drug application [9].

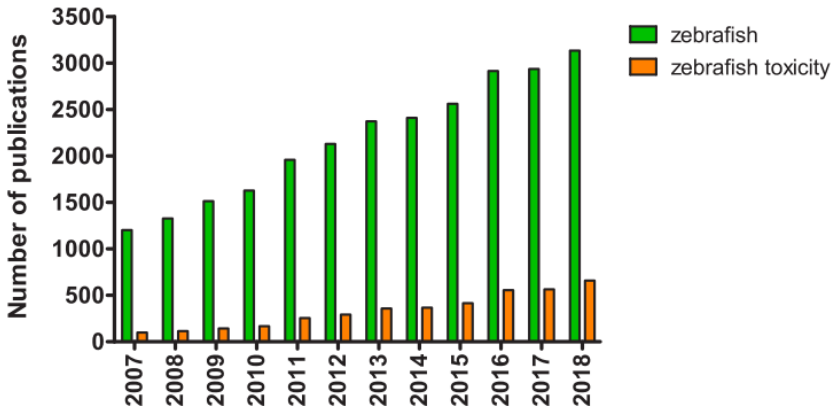

Figure 1-2. Studies on zebrafish and toxicity studies with zebrafish. [10]

1.1.1.1. Zebrafish as a model to study environmental toxicology

Early zebrafish models have been used to evaluate the environmental toxins more than pharmaceutical compounds [11]. Environmental toxins, including toxic heavy metals, endocrine disruptors, and organic pollutants, have been widely studied. Sandrine *et al* have tested the effect of MPTP, rotenone, and paraquat in both adult and larval zebrafish [12].These neurotoxins can not only influence the aquatic environment but also induce Parkinson's disease for human beings, which are meant to be studied. Decreased locomotor activity induced by MPTP has been observed on adult zebrafish, in contrast, larvae zebrafish exhibited developmental, behavioural, and DA sensitivity to agents mentioned above, suggesting that zebrafish could be a valuable model for testing environmental toxins' effects. Other researchers have also studied similar terms in this field. Goolish *et al* have tested the behavioural response of adult zebrafish to hypergravity conditions to prove that zebrafish can access the air-water interface for initial swimbladder inflation [13]. Inspired by the fact that a mix of noxious agents can affect the aquatic embryo ignoring the protection of chorion, Merle *et al* have studied the effects of single chemicals and chemical mixtures on zebrafish and medaka embryos' development [14]. Part of the treated results on zebrafish are shown in **Table 1-1** and **Table 1-2**, and the author has tested the effects of toluene and a mixture of TCDD and Benzene of dechorionated zebrafish. As displayed by two tables, dechorionated zebrafish embryos exposed to both single and mixed chemicals develop cardiovascular defects (Heart defects), and the mixture chemicals can cause more severe problems.

1.1.1.2. Zebrafish as a model in toxicology and drug discovery

By definition, drug discovery is the process of identifying potential new medicines, involving a wide range of scientific disciplines, including biology, chemistry, and pharmacology. Modern drug discovery involves the identification of high throughput screening (HTS), which requires significant investments by pharmaceutical companies, therefore, cost control for preclinical testing is necessary.

Following the 3Rs criteria, replacement, reduction, and refinement in animal research [15, 16], zebrafish is gaining its popularity as an alternative animal model. According to the European Commission Directive from 2010, experiments with the earliest life-stages of some animals are not regulated as animal models [10]. Therefore, zebrafish under five dpf can be considered as the earliest life-stage subject to regulation mentioned above.

Table 1-1. Survival of dechlorinated zebrafish after 30 min static exposure to toluene

	N	24 h	48 h	Heart defects	72 h	96h (Swim up)
100 ppm toluene	10	2(20%)	2(20%)	2/2	2(20%)	0
10 ppm toluene	11	5(45%)	5(45%)	3/5	5(45%)	2(18%)
1 ppm toluene	36	25(69%)	21(58%)	1/21	20(56%)	17(47%)
0.1 ppm toluene	20	12(60%)	11(55%)	1/11	11(55%)	10(50%)
0.01 ppm toluene	20	15(75%)	15(75%)	1/15	14(70%)	14(70%)
0.001 ppm toluene	16	14(88%)	12(75%)	0	12(75%)	12(75%)
0.0001ppm toluene	16	13(81%)	13(81%)	0	13(81%)	13(81%)

Table 1-2. Survival of dechlorinated zebrafish after 30 min static exposure to a mixture of TCDD and Benzene

	N	24 h	48 h	Heart defects	72 h	96 h (Swim up)
1 ppm TCDD/benz	16	6(38%)	4(25%)	2/4	4(25%)	2(13%)
0.1 ppm TCDD/benz	16	10(63%)	8(50%)	1/8	6(38%)	5(31%)
0.01 ppm TCDD/benz	16	16(100%)	16(100%)	0	11(69%)	8(50%)
0.001 ppm TCDD/benz	16	13(81%)	10(63%)	0	10(63%)	10(63%)
0.0001 ppm TCDD/benz	16	14(68%)	12(76%)	0	12(75%)	12(75%)

Drug discovery used to be achieved occasionally by observing phenotype changes of whole animals exposed to small molecules. As zebrafish have high fecundity, a large scale and systematic screening can be performed to study new drugs and toxicology. In drug discovery, the biological effects of toxins and chemicals have been studied extensively [17]. Peterson *et al* have examined the impact of 1100 molecules with large scale screening on the central nervous system and heart of zebrafish embryos, and found that some molecules can disturb the development of embryos [18].Yu *et al* have designed a screen to find a compound that could inhibit targeted bone morphogenetic protein (BMP) receptors [19]. They have found an inhibitor called dorsomorphin which can perturb dorsoventral axis formation in zebrafish. As shown in **Fig. 1-3**, zebrafish applied with different concentrations' dorsomorphin can affect the formation of body trunk

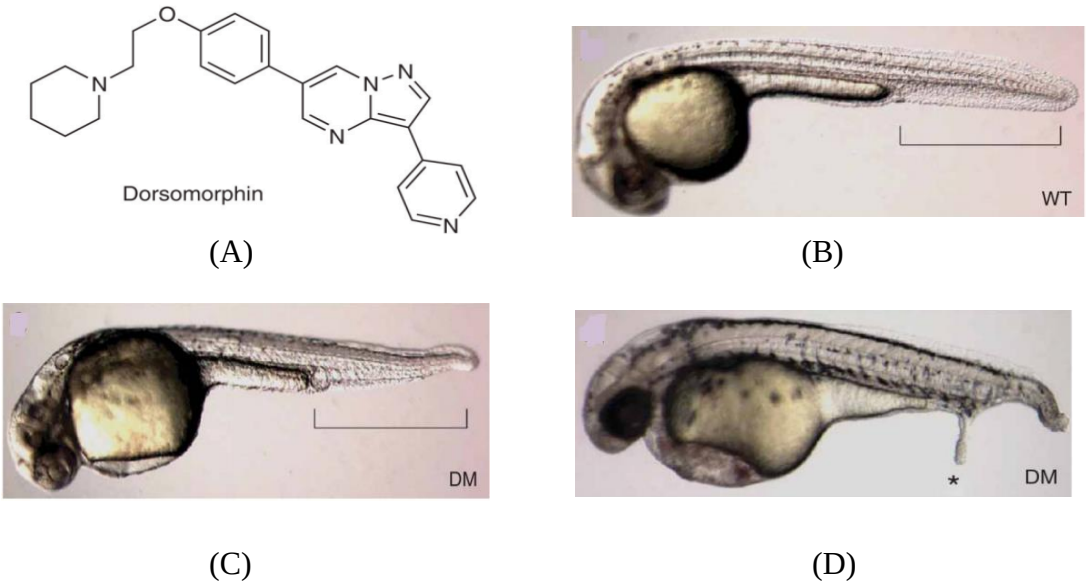

Figure 1-3. Dorsomorphin induces dorsalization in zebrafish embryos. (A) Structure of dorsomorphin. (B) WT zebrafish embryo at 36 (hours post-fertilization) hpf. Ventral tail fin is highlighted in brackets. (C) Zebrafish embryo treated with 10 μM dorsomorphin (DM) at 6-8 hpf and photographed at 36 hpf. (D) Zebrafish embryo treated with 10 μM dorsomorphin at 6 hpf, occasionally develop ectopic tails at 48 hpf.[19]

Besides, neurotoxicity is also widely concerned in drug discovery with zebrafish embryos and larvae. Neurotoxicity testing is the initial stage for studying mechanisms of neurological disorders and diseases [20]. By definition, neurotoxicity represents a form of toxicity in which a specific toxin produces adverse effects on the function of a

particular region of the central/peripheral nervous system [21]. As the central/peripheral nervous system controls the motor neurons in the spinal cord of fish embryos and thus the musculature, it is necessary to record the locomotion of fish samples to screen the neurotoxic compounds [22]. A wide range of drugs have been tested, such as diphenylhydantoin, pentylenetetrazol, and picrotoxin, to study the influences on locomotor behaviors [23-25]. Examples of part of those results are shown in **Fig. 1-4**. In this figure, most researchers choose to use distance moved by the fish embryos during a period, which is the most straightforward measurement. The current results suggest that the influences from neurotoxic drugs on locomotor activities are dose-dependent; compared with rodent animals; these results are proved to be similar [10]. Although there exist some untranslatable results, it is prudent to say that zebrafish can be an alternative model for neurotoxicity study.

1.1.2. Zebrafish contributions in human disease modeling

It has been reported that more than 80% of human genes associated diseases have a zebrafish homolog [26], which means some common conditions such as muscle, cardiovascular and intestine diseases in human beings that cause changes to human body tissues could theoretically be modelled in zebrafish. However, some tissues and body parts with pathological changes in human beings do not exist in zebrafish, such as lungs, should be examined with other animals.

Currently used genome editing approach is called CRISPR/Cas9, or artificial site-specific nucleases such as zinc-finger nuclease, and transcription activator-like nucleases [27-29]. With the genome editing approach, scientists can knock-in or knock-out the target genes in vivo to mimic human phenotypes and observe the symptoms on mutant zebrafish. These models can also be used to test cures for the disease. Compared with rodent lab animals, zebrafish's high fecundity can achieve a large number of samples being observed repeatedly.

Many severe diseases have already been studied with mutant zebrafish models, including muscle diseases such as Duchenne muscular dystrophy, and neurodegenerative diseases such as Alzheimer's disease [20, 30-36].

Muscular dystrophy

Muscle dystrophy is one of the most commonly seen diseases in human beings. Induced by the mutations in the dystrophin gene, different types of muscle dystrophy have been classified, including Duchenne Muscular Dystrophy and Becker Muscular Dystrophy [37]. The critical feature of muscular dystrophy is a loss of muscle function, which will lead to necrotic and abnormally sized muscle fibres. This kind of degeneration of skeletal muscles is always fatal to human beings. To address the severity of muscle dystrophy, many animal models have been well established to model the disease. Zebrafish larvae are particularly suited to study muscle-related diseases as the transparent and somatic muscle comprises a large proportion of body and is accessible [31].

Early studies on muscle diseases with zebrafish include isolation of specific mutated muscle genes [37] and screening of zebrafish mutant families [5, 38, 39]. Muscle disorganization is observed with birefringence technique. As the highly ordered somatic muscle has the ability to rotate polarized light, it is possible to observe the amount of rotated light to determine the muscle conditions. For example, a decrease in the amount of rotated light indicate a loss of the muscle structure, and dark patches might suggest that muscle is teared or muscle fibre is disorganized [40]. As shown in **Fig. 1-5**, one kind of mutant, *Sapje* mutant is presented and shows that compared to wildtype zebrafish, the swimming blade pointed with black arrow is un-inflated. Large screens of zebrafish genes have identified a large number of mutants that influence the muscle functions, including mutations at different positions along body trunk. Here a specific locus, *sapje* (sap), is taken as an example to display the affected muscle formation of the mutant zebrafish model. As shown in **Fig. 1-6**, dystrophin is lost from

the end of muscle fibres in *sap* mutant zebrafish model, the fibre of zebrafish with *sap* mutation detaches compared with wild type zebrafish [31].

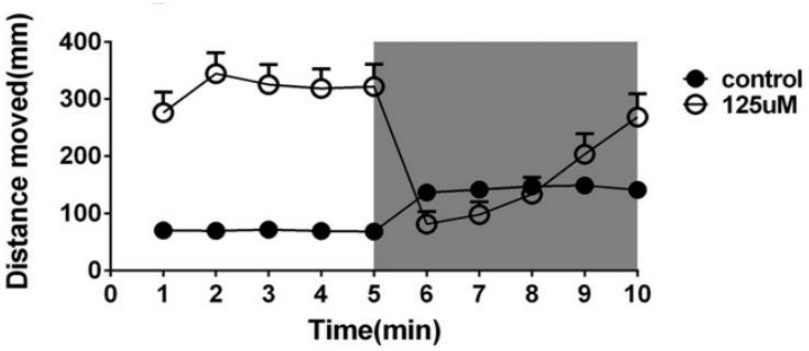

(A)

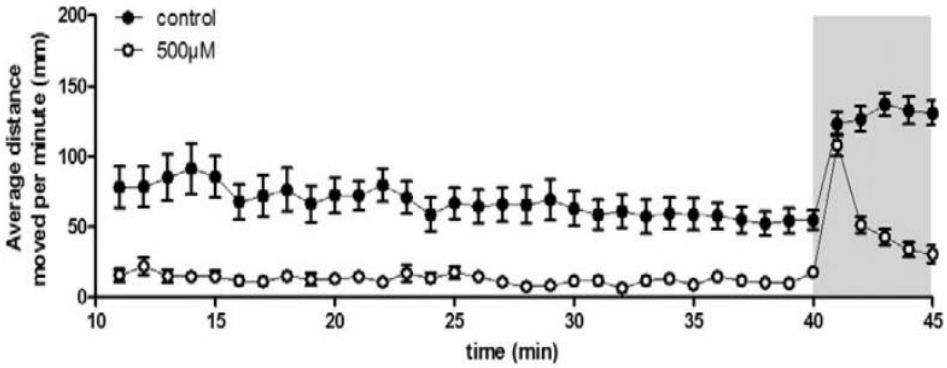

(B)

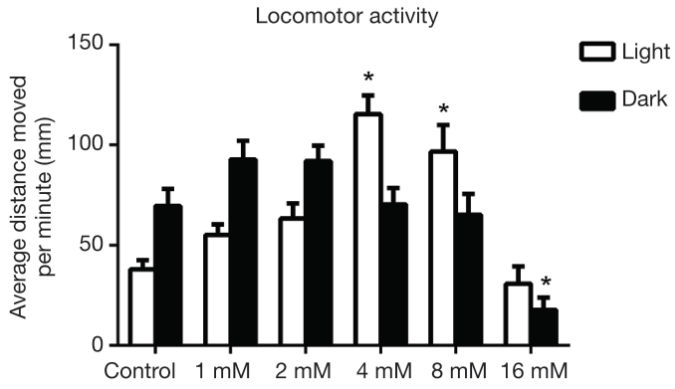

(C)

Figure 1-4. Examples of locomotor behaviors of zebrafish treated with different neurotoxic drugs. (A) Distance moved by zebrafish larvae under continuous illumination followed by alternative light and dark conditions. Comparisons are made between the control group and 125 μM picrotoxin. (B) Average distance moved by zebrafish larvae per minute within 35 minutes under continuous illumination, followed by a 5 minutes' dark condition. Comparisons are made between the control group and 500 μM diphenylhydantoin. (C) Effects of pentylenetetrazol on averaged distances moved by the zebrafish larvae within 1-min time under both light and dark conditions. The horizontal axis represents the concentration of pentylenetetrazol. [23-25]

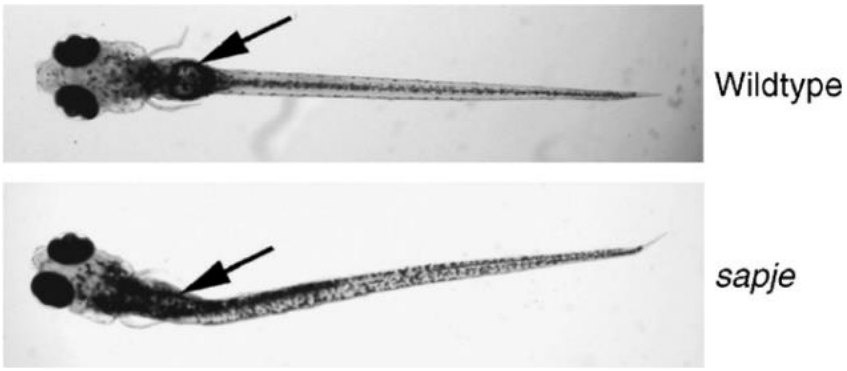

Figure 1-5. Sapje mutants show decreased birefringence and un-inflated swim-bladder compared to wildtype zebrafish [38]

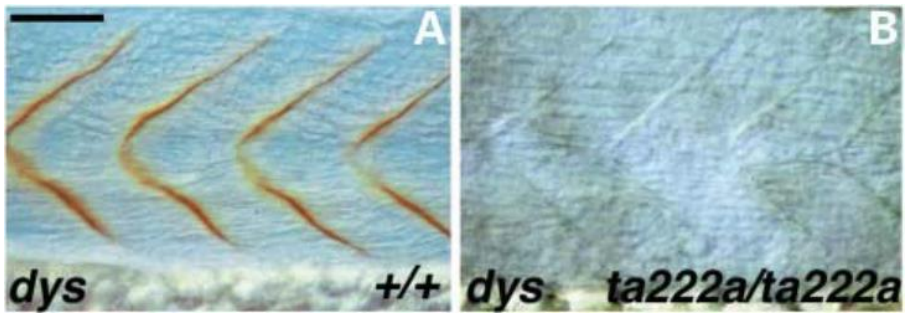

Figure 1-6. Fibre detachment caused by mutation of zebrafish. The left picture is the wild type zebrafish model with dystrophin, and the right image represents the mutant zebrafish model which lacks dystrophin [31]

Alzheimer's disease

Alzheimer's disease (AD) is the most common form of neurodegenerative disease. Unfortunately, no effective therapies have been developed till now. By definition, AD is characterized by progressive memory loss including impairment of speech and motor ability [41]. Before zebrafish being applied as a model to study AD, rodent models had been extensively used to investigate the mechanisms of AD. Compared to rodent animals, zebrafish lack the complex cognitive behaviors. Still, they possess orthologous genes to those mutated in familial Alzheimer's disease (FAD), which are difficult to observe in rodent animals [33]. Advantages of zebrafish as a model to study Alzheimer's disease are shown in **Table 1-3**. There is a high conservation of brain organization between zebrafish and human beings, and a similarity between neuroanatomic and neurochemical pathways [42, 43], which are closely related to AD research. Scientists can investigate the functions of some relevant genes involved in FAD in mutant zebrafish such as the presenilin genes, blockage, and loss of presenilin

gene expression that can lead to lack of production of motor neurons in the developing spinal cord of zebrafish larvae [44]. However, limitations exist for zebrafish as an AD model. Due to the tiny body size, the whole body of zebrafish will be exposed to the chemical compounds, thus the quantification entering zebrafish body is unpredictable as the chemicals can be absorbed randomly by gills and skin. To better study the pathology of FAD with the zebrafish model, a deeper understanding of zebrafish's brain structure and function are required. Also, fields like the behavior, physiology, and neuroanatomical circuitry of the fish and the link between neurodevelopment and neurodegeneration need to be better elucidated.

Table 1-3. Advantages over zebrafish as an AD model

Embryos	Larva	Adult
Rapid development	Optically transparent	Vertebrate neural structure
Optically transparent	Similar genome	Low cost, easy maintenance
Similar genome	High-throughput screening	Genome comprises orthologs of human FAD genes
External development		

1.2. Motivation & research aim

As mentioned above, in recent years, zebrafish have been extensively used in the research fields as an alternative to rodent animals for toxicology and drug discovery; at the same time, many types of zebrafish models have been built to test chemical influences on the physiology and behaviors of zebrafish. In this part, depending on the purposes of experiments, critical features of affected zebrafish under chemical treatment can be described with images of damaged/deformed body tissues or changing swimming behaviors characterized by distance travelled/body bending angle. These two aspects are connected as the damaged body tissue will probably affect the swimming behaviors as well. Inspired by the connections between body tissues and swimming behaviors, we intend to build a novel zebrafish model different from the traditional biological model, this model will help to understand the internal muscle mechanics during swimming and quantify the effect of internal muscle before and after

drug treatment. Also, considering the potential ability to assess the internal muscle performance during swimming, it might be feasible to evaluate the muscle status under different types of muscle diseases. For example, as mentioned above, by comparing the internal muscle characteristic differences between wild type zebrafish larvae and mutant fish larvae induced by muscular dystrophy related genes with the numerical simulation tool, it might be possible to compare the muscle power at specific locations to justify to what extent the muscle has been damaged or degenerated, suggesting that the methodology can be potentially used in pathological study.

The novel model aims at combining an advanced flow analysis technology and experimental tools to investigate the variation of zebrafish swimming behaviors subject to pharmaceutical influences. The experimental tools include a biological observation of the in vivo zebrafish locomotion and the subsequent data analysis. The developed flow analysis tool can simulate the swimming behaviors of zebrafish larvae to quantify several important swimming characteristics, including body force and power consumption which cannot be acquired with biological experiments only. With assistance from flow analysis technology, we can quantify to what extent the tissue has been damaged from the toxins and compare the effect of different chemicals with specific values and percentages.

Besides, the feasibility of the model with different types of drugs and chemicals is going to be discussed, including neuroactive medicines and chemicals, which will stimulate the nociception of zebrafish. A drug-induced recovery from body pain is applied as well. Using this approach, our zebrafish model could potentially contribute to studying the effects of new drugs on zebrafish larvae.

1.3. Thesis structure

The thesis is divided into six chapters. A brief introduction about zebrafish and its biological implications are stated in Chapter 1. A review of the past research on

different species related to nociceptive study and pain relief and comparisons to zebrafish have been discussed in Chapter 2. Methodology, including Experimental setup, animal treatment, drug application, and *MATLAB* post-processing are shown in Chapter 3. CFD simulations on the zebrafish larvae model are also shown in the methodology chapter. Validations of the methodology regarding biological observations, *MATLAB* post-processing, and CFD software coupling have been displayed in Chapter 4. Applications on drug treatment of the zebrafish larvae with three different types of drugs, and pain relief with Gypenosides including biologically observed kinematic performance and CFD simulated kinematics and energetics results on zebrafish larvae locomotion are displayed in Chapter 5. The conclusion of the whole work and discussions about future studies related to pain relief on zebrafish larvae a given in Chapter 6.

2 Literature Review

2.1. Nociception study on mammalian

Due to the above advantages of zebrafish, in recent years, it has been widely used to study one of the most concerned topics, body pain. Pain has been defined as a "complex constellation of unpleasant sensory, emotional, and cognitive experience provoked by real or perceived tissue damage and manifested by certain automatic, psychological, and behavioural reactions" [45]. For human beings, they experience these pains over extreme temperatures and pressures that could potentially injure tissues [46]. Pains are perceived by a peripheral sensory neuron known as nociceptor, which is distributed in skin, muscle, and joints and plays the role of sending potential threats to multiple brain regions via the dorsal horn of the spinal cord [8]. The concept of nociception was inspired by the Latin *nocere*, which means 'to harm', and developed by Sherrington in 1910 [47]. It is a sensory system of the peripheral and central nervous system to detect potentially harmful stimulus. Due to the origins of different stimuli, nociceptors can be divided into three types, thermal, mechanical, and chemical nociceptors. A schematic diagram sketching the development of the perception of pain is shown as **Fig. 2-1.** Once contacting potential harmful stimulus, the peripheral nociceptors will be activated, the noxious stimuli will be transduced into neuronal signals and signals will be transmitted to CNS. Integration of these information in brain regions results in complex cortical structure responses, and finally, modulation occurs via reciprocal and descending tracts [48, 49].

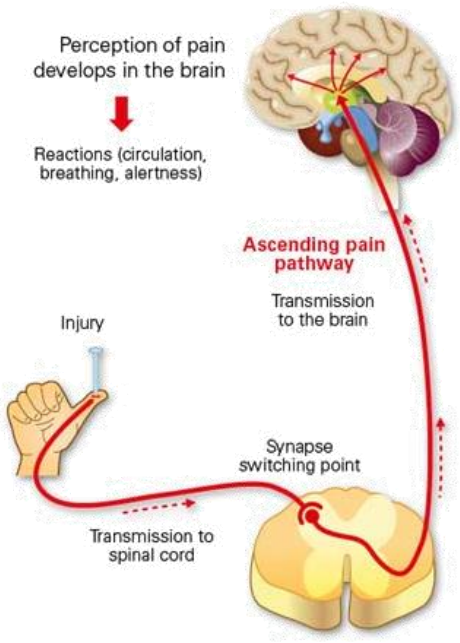

Figure 2-1. Development of the perception of pain [50]

As mentioned above, pain can be induced by many factors such as temperature, pressure, and chemical substances, scientists have followed these factors and a large number of animal models possessing nociception system have been developed to understand pain better before zebrafish model was applied. Transmissions of nociception study started from mammalian such as rodents as they have many similarities to human beings such as anatomy, physiology, and genetics [51]. Bennett *et al* have found a peripheral mononeuropathy in adult rat that produces disorders of pain sensation like human beings [52], postoperative behaviors such as hyperalgesia, allodynia, and spontaneous pain were found. Sluka has examined the differences of pain processing from skin to muscle; the author has injected Capsaicin into rats' skin, muscle, and joint respectively, and recorded the level of pain. They have found that nociceptive processing from cutaneous tissue injury is different from that of grave tissue injury as the lasting time for dermal tissue and muscle are different for mechanical allodynia and heat hyperalgesia [53]. Similar research has been done by Hargreaves's team by providing a new method to measure thermal nociception in cutaneous hyperalgesia, which possessed higher bioassay sensitivity than the traditional way [54].

Stiles *et al* have studied the effect of morphine sulfate solution (MSS) on signs of pain and wound healing in dogs with corneal ulcers. Twelve dogs were tested, and ten out of twelve dogs have artificially created corneal ulcer in the right eyes, these dogs were treated with 1% MSS and saline solution topically on the right eye to observe the effect on healing. The results indicated that 1% of MSS could provide analgesia and did not interfere with routine would healing [55].

Radhakrishnan *et al* have tested whether the Carrageenan could produce long-lasting hyperalgesia except short-time acute inflammation. By injecting different concentrations of Carrageenan into rats' muscle and joints, a dose-dependent influence on chronic hyperalgesia of muscle or joint from Carrageenan has been proposed, supporting that injection on deeper tissues could result in long-lasting hyperalgesia compared to cutaneous insult [56].

2.2. Nociception study on zebrafish

From an ethical point of view and compared with mammals' experiments mentioned above, vertebrates like fish, reptiles, and birds are lower in the evolution scale, thus less sentient [57]. Considering the welfare of animals and the principles of the Three R's, which are replacement, reduction, and refinement [10], vertebrates have becoming demanded for biomedical and behavioural research. In vertebrates, fish is popular to be used to study nociceptive pain. Different species have been considered to determine the existence of specific responses.

Rainbow trout is a commonly used species for biological research. Newby has tested the effect of acetic acid in conscious rainbow trout [58]. The author has injected saline, 2%, and 5% concentrations' acetic acid into the lip of rainbow trout and compared the behavior response with the control group. The injection of acetic acid has significantly extended the recovery time to pre-treatment levels of respiratory rate. The author's team has also compared their results with Sneddon's results [59, 60]; they did not observe

similar rocking or rubbing behavior as reported in Sneddon's study, but different from Sneddon's treatments, the author did not anesthetize the fish in advance, which might be the reason for that disagreement. Also, without pre-treatment with anaesthesia, the fish might be nervous as well, and thus under severe stress, this might also contribute to the different observation results.

Studies related to nociception on fish have been divided into two controversial groups, debating whether fish have nociceptors and could perceive pains. Studies on three species of elasmobranch fish indicated that fish do not have nociceptors similar to mammals and human beings [61-63] and presented the difference between responses to noxious stimulus and pain perception [63]. Those researches stood on the point that fish lack the most necessary brain structure, a neocortex, for pain perception compared to human beings. The opposite party stated that although some bird species do not have a neocortex, they have been proved to be able to perceive pain as well [64]. Moreover, by using techniques in neuroanatomy and electrophysiology, scientists have confirmed the presence of nociceptors. As shown in **Fig. 2-2,** there exists A-delta and C fibres in trigeminal nerves of rainbow trout, *Oncorhynchus mykiss*. In higher vertebrates, A-delta and C fibres in the trigeminal nerve convey nociceptive information to the brain[65]. Sneddon also showed that rainbow trout could perceive pain by injecting noxious stimulus into trout lips [66]. Several complex reactions have been observed, such as rubbing of the lips against the sides of the container, which imply that trout could perceive pain instead of simple reflex responses [59]. Until now, relationships between nociception and pain perception cannot reach an agreement due to the fact that it can be determined based on specific fish species.

2.2.1. Zebrafish behavior study with high-speed camera

Zebrafish, as a well-established laboratory model, could be excellent to study nociception. In mammals, there exist mainly two types of analgesics, one is opioids, and the other one is Nonsteroidal Anti-Inflammatory Drugs (NSAIDs) [67]. The existence of these analgesics can validate that certain stimuli can induce pain to

mammals. Zebrafish have opioid receptors in their body which have functional characteristics similar to mammals [68]. The effect has been tested by morphine, suggesting that opioids in zebrafish work identical to those in mammals [69-71]. Whereas considering the NSAIDs, two of the commonly used NSAIDs are aspirin and Ibuprofen. They can reduce inflammation but induce some side effects at the same time. Lopez *et al* have tested the effect of aspirin on behavioural changes after applying zebrafish to different concentrations' acetic acid, and the results indicated that receptors for NSAIDs exist in zebrafish [72]. Moreover, toxicology studies have addressed the effects of NSAIDs on freshwater vertebrates, including zebrafish, by showing that ibuprofen is rapidly absorbed by embryos and larvae [73]. Therefore, it is convictive to use zebrafish for nociception study.

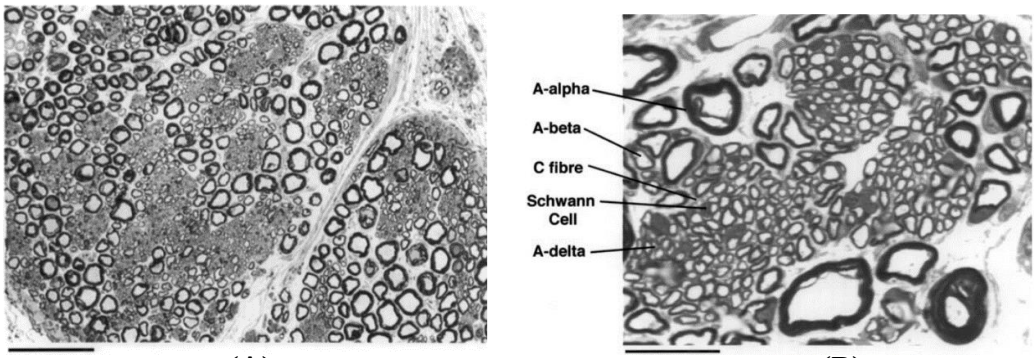

(A) (B)

Figure 2-2. (A) Section of the maxillary branch of the trigeminal nerve of the rainbow trout (x 400, scale bar = 4μm) (B) Section of the maxillary branch of the trigeminal nerve showing the presence of A-delta and C fibres (x 1000, scale bar = 2μm). [65]

As nociceptors can detect a direct or potential noxious stimulus and pass the signal to the spinal cord to control muscle contractions and trigger body deformation [74], it can be visualized and studied by observing behavioural changes of fish body. Thus zebrafish has been used as a pain model to study nociception effects. Swimming behaviors of zebrafish are traditionally captured with a high-speed camera shown in **Fig. 2-3** for the sake of 2-6mm body length. Seth has given a general introduction of locomotion repertoire of larval zebrafish, including prey capture, turning behaviors such as escape turns, routine turns, etc. [75]. The author has explained how the neurons

control the different swimming patterns and deduced that different neurons can be activated by signals from different swimming patterns.

Followed by various *MATLAB* functions or other post-processing tools, different research purposes can be satisfied. Muller has studied three swimming patterns of zebrafish larvae at different ages, cyclic swimming, slow and fast starts [76]. The author has recorded the midline of zebrafish at each instant of time to get the body wave envelop, as shown in **Fig. 2-4(A)**. Based on these midlines, it is possible to derive some kinematic parameters such as tail beat amplitude and frequency, and swimming speed. From this point, the author has calculated the corresponding parameters for zebrafish larvae at different ages' (shown in **Fig. 2-4(B-D)**). Muller has also compared her results with other species like eel [77]and mackerel [78], and found that body wave amplitude increases along the larvae zebrafish body, which is in contrast to eel and mackerel, and even adult zebrafish. Muller later extended her research on zebrafish locomotion by applying 2-D particle image velocimetry (PIV) technique to study the influence of the intermediate flow regime (Reynolds number). Flow generated during the cyclic swimming of a larva has been displayed (as shown in **Fig. 2-5**); from the figure, it is evident that the flow pattern differs between the stiff anterior part and the undulating posterior part. It explains the formation and propagation of vorticity from head towards tail and finally detached at the tail. The black arrow indicates the propulsive jets pointing in the opposite direction of forward motion. Muller has also compared wake differences between larva and adult zebrafish. As stated by the author, this might be caused by different Reynolds numbers as adult zebrafish swim under a higher Reynolds number. Besides, different morphologies of adult zebrafish might also influence the kinematic performance and forming of vorticity. This point has been further studied in corporation with Li with computational fluid dynamics, reporting the influences from fin fold (only in larva zebrafish) on zebrafish locomotion behaviors [79].

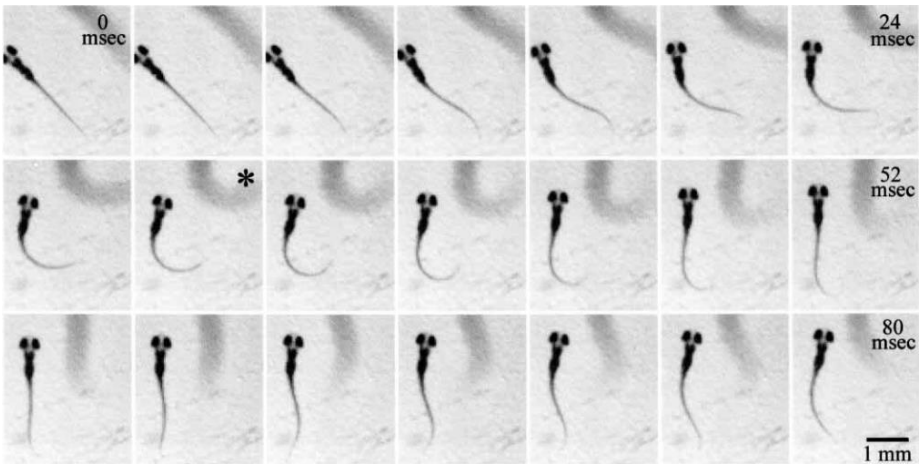

Figure 2-3. High-speed camera captured zebrafish larvae motion within 80 msec. body curvatures of zebrafish larvae at each time step are shown. [75]

2.2.2. Nociception study on zebrafish

Depending on the development stages of zebrafish, chemicals can be injected into adult zebrafish's body trunk or lips [80]. For zebrafish larvae, the fish samples will be submerged in the solution for the sake of 2-6mm body size. Commonly used noxious stimuli include extreme temperature and pressure, and chemicals such as acetic acid, citric acid [54, 67, 72, 81-84]. Malafoglia *et al* have developed a zebrafish model to study pain induced by extreme temperatures. The intense high or low heat will lead to burns of tissues and cause damage. The damage can be attributed to both inflammation and axonal degeneration (neuropathic-like pain). Malafoglia *et al* have tested two events linked to the onset of injury, one is the degeneration of axons innervating the affected tissues, and the other one is the over-expression of specific genes in sensory tissues and found that both of them are conserved from zebrafish to mammals, suggesting that zebrafish larvae could be potentially used to study cellular and genetic networks related to neuropathic and inflammatory pain system in mammals. Curtright *et al* have studied the temperature-related nociception with zebrafish in a different way [85]. He focused on the temperature aversion of 5 dpf zebrafish larvae and found that zebrafish larvae tend to stay in 28.5℃, either it is colder or hotter. The application of AITC (an inflammatory compounds that can reduce the threshold of stimuli to invoke nociception responses) promoted thermal aversion and reverses cool aversion. In this

condition, when analgesics were used, such as buprenorphine, the temperature aversion can be reversed. Buprenorphine significantly reduced 24.5℃ and 32.5℃ aversion for both control and target group. Although there was no significant difference at different temperatures, it is prudent to judge that it is possible to model nociception in zebrafish larvae.

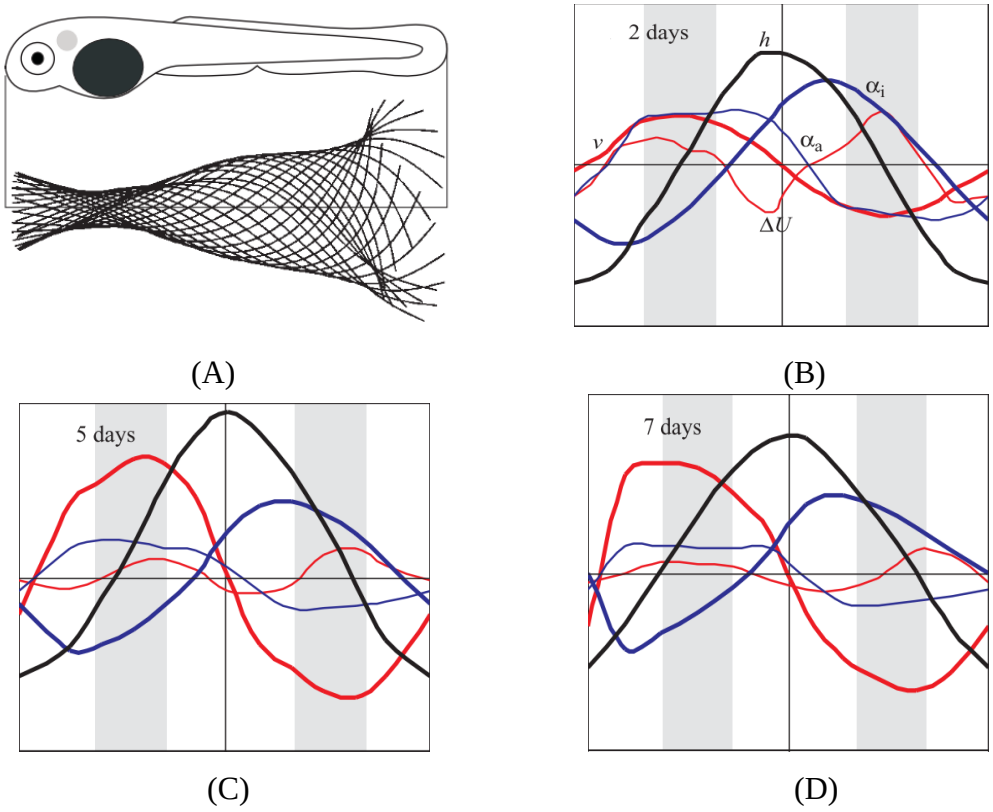

Figure 2-4. Midline curves of zebrafish larvae and the calculated tail beat kinematics. (A) Sketch of the side view of a zebrafish larva and midlines in a fish-based frame of reference. Lateral position of tail tip (h, black), swimming speed (ΔU, thin red), lateral velocity of the tail tip (v, thick red), angle of incidence (α_i, opaque blue), and angle of attack (α_a, thick black) are depicted at (B) 2 dpf, (C) 5 dpf and (D) 7 dpf [76]

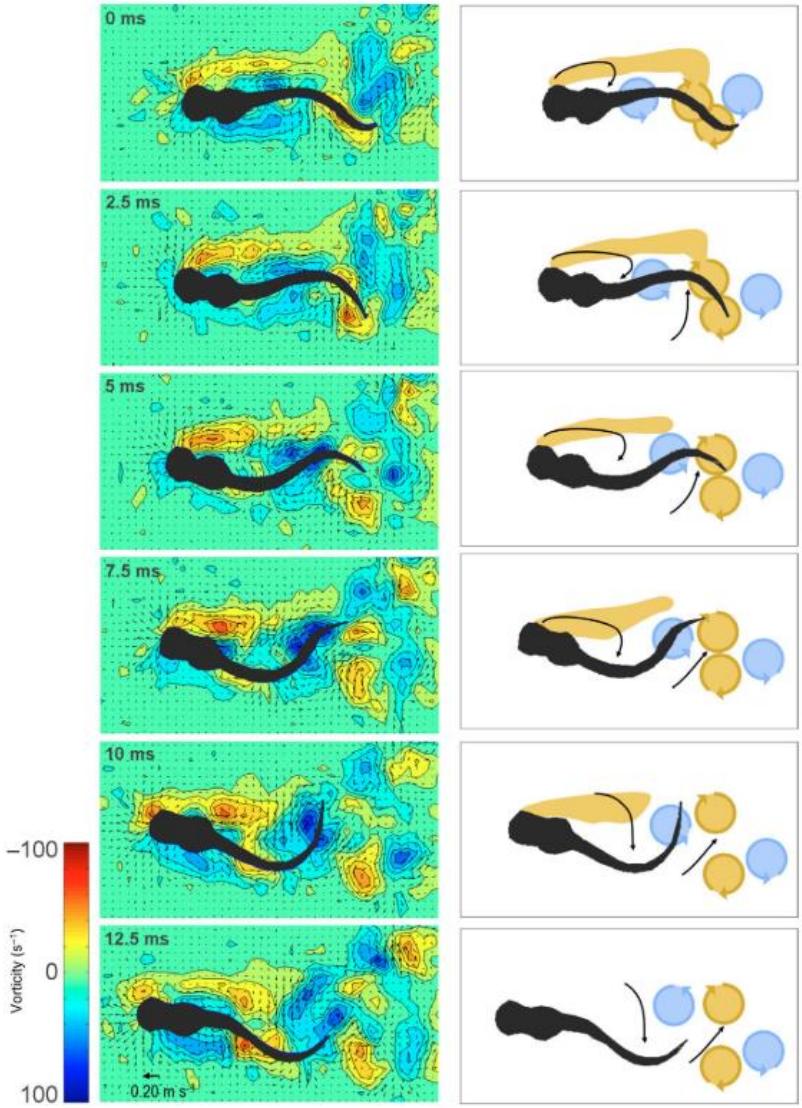

Figure 2-5. Flow generated during a tail beat of a cyclically swimming zebrafish larva (age three dpf). The left column indicates the vorticity field in the colour map. The right column sketches the most relevant flow features, with vorticity generated at the head region (elongate ochre area) and travels along the body, detach at the tail. The black arrow indicates propulsive jets, which gradually reorients more caudally as it goes down the body [77]

Correia *et al* have proposed that zebrafish is an appropriate behavioural model of nociception and has tested its sensitivity and robustness [81]. He has applied two different doses of acetic acid to study the threshold level of nociception. He has also tested the effect of morphine analgesics. As shown in **Fig. 2-6A,** the fish activity shows a significant decrease after injection of 10% and 5% acetic acid compared to the control group. In contrast, after treated with morphine (shown in **Fig. 2-6B**), the fish activity increases, and the value is getting closer to control group, suggesting that as a

commonly used analgesic drug, morphine works similar in zebrafish as human being and zebrafish with acetic acid is a reasonable model to test analgesics.

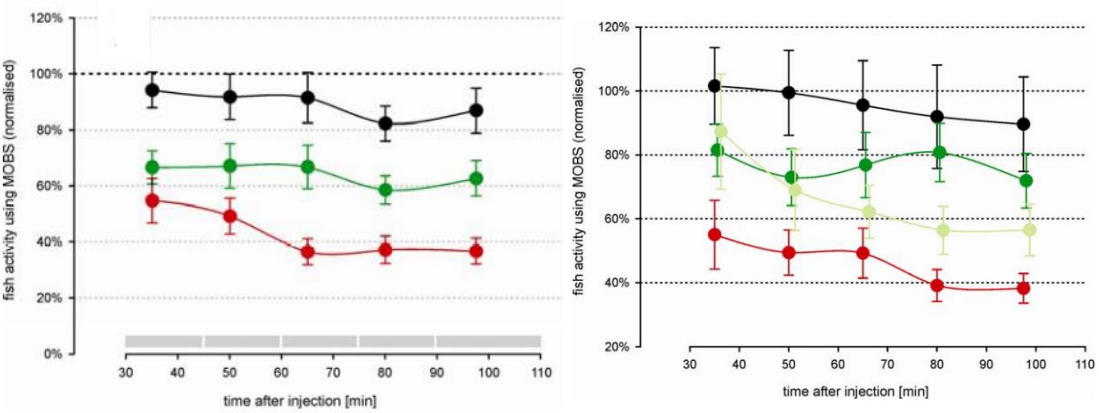

(A) (B)

Figure 2-6. Time course changes in zebrafish activity after the injection of different doses of acetic acid (A) and morphine (B). In Figure A, the control saline solution group (black line) has a higher activity than 5% acid (green line) and 10% acid (red line). In Figure B, after injection of 3mg/kg morphine (light green line) and 6 mg/kg morphine (dark green line), the activity increases compared to 10% acid-treated group (red line) and the value is getting closer to the control saline group (black line) [81]

Observations on swimming behavior differences such as time spent active and average swimming speed can also reflect the influences of the noxious stimulus. As shown in **Fig. 2-7**, Taylor *et al* have tested the acetic acid concentration influences on mean distance and swimming speed, compared with the untreated group, it is evident that acetic acid has a negative effect on the swimming speed and mean distance travelled (time spend active) [84]. Steenberger has tested the anti-nociceptive effect of buprenorphine on zebrafish larvae [86]. The effect of acetic acid on zebrafish locomotion showed similar results compared to part of Taylor's results (shown as **Fig. 2-8A**), and it is also a supplement for the low concentration range of acetic acid. As depicted in **Fig 2-8B**, when the larvae were pre-treated with $0.1\mu g/ml$ buprenorphine, there is no significant increasing locomotion activity compared to control group due to the application of low concentration acetic acid. The author has also compared the levels of cyclooxygenase-2 (cox-2) in zebrafish larvae and found that activation of nociceptive pathways in a low-concentration acetic acid environment produced behavioural changes that were accompanied by changes in levels of cox-2. As the

associated gene is involved in the nociceptive process [87], it seems reasonable to say that the acid-induced behavioural changes can be attributed to nociception.

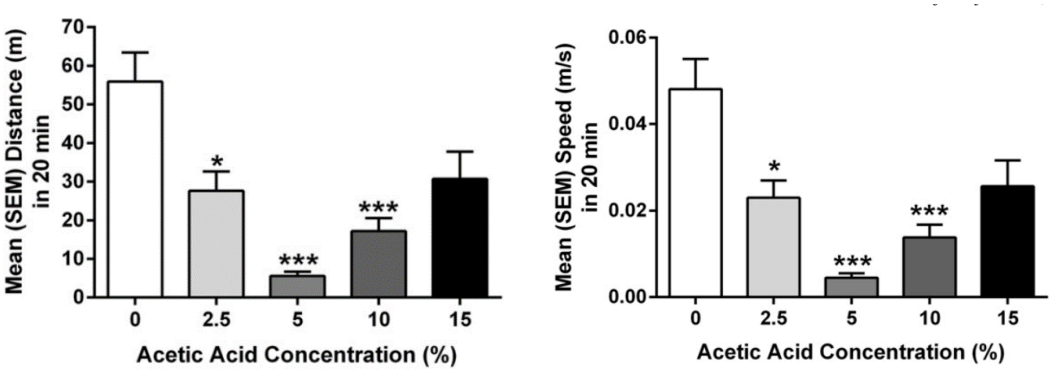

(A) (B)

Figure 2-7. Taylor's results of acetic acid concentrations' influences on zebrafish's kinematic performance. (A) Mean distance in 20 minutes (B) Mean speed in 20 minutes. [84]

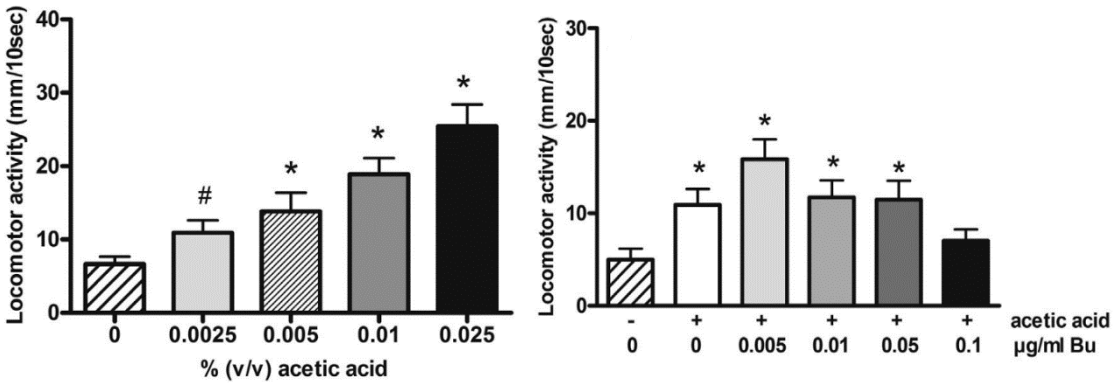

(A) (B)

Figure 2-8. Zebrafish sensitivity to chemical stimulus-acetic acid. (A) Locomotion activity of zebrafish under acetic acid concentrations ranging from 0-0.025%. (B) Influences of buprenorphine on acetic acid-treated zebrafish. Only zebrafish larvae pre-treated with 0.1$\mu g/ml$ buprenorphine do not have a noticeable increase of locomotion activity [86]

Considering the verification of zebrafish larvae as a suitable model for nociception study, Lopez *et al* have verified that unprotected five dpf zebrafish could replace the adult zebrafish [88]. Based on the findings, Lopez *et al* have tested several new analgesic drugs. Starting from verifications on morphine, caffeine and another commonly used analgesia among human beings, expected protections of those drugs from noxious stimulus have been found on zebrafish, such as heartbeat changes and vitality recovery [89-92], proving that zebrafish could perceive pains and nociception of zebrafish works similar to that of human beings. In conclusion, as the zebrafish

(adult/larva) displays similar reactions to both rodents and human beings when experiencing pain, it can be a suitable model for nociception study and new analgesic drugs discovery

2.3. Pain relief research on zebrafish with Gypenoside

As the zebrafish pain model has already been constructed, pain alleviation and recovery are well-reasoned to be focused on studying the effect of analgesic drugs. Starting from ethanol and morphine, which are commonly used analgesia among human beings, expected recovery from noxious stimuli such as temperature and chemicals have been found on zebrafish after applying with these analgesic drugs, such as heartbeat changes and vitality recovery [59, 89-92]. Behavioural improvements after analgesia treatments have also been studied with time spend active, body curvature alteration, and averaged velocity over a period [72, 88].

Gypenosides (GYP) , saponin extracted from *Gynostemma pentaphyllum*, have been widely used in the past centuries on human beings [93]. Nowadays, Gypenosides have been approved by the Central Drug Administration of China to be used as a traditional Chinese OTC in clinics [94]. The compound has been proved to have different effects, such as antioxidation, antilipidemia, neuroprotective, and inflammation reduction [95]. A previous study showed that the antioxidant effect has been validated with the protection of GYP from oxidative stress on retinal pigment epithelium cells [96] and vascular endothelial cells [97]. Besides, the effective extraction from Chinese plant has been proved to lower triglyceride, cholesterol and nitrite in acute hyperlipidaemia of rats. Also, GYP has been tested to have anti-inflammatory effect on aortic lesions of rats and human osteoarthritis chondrocytes [91, 98].

However, protection of GYP on zebrafish were rarely discussed, only including oxidative stress related to retinal degeneration [96], and most of the biological studies including the zebrafish pain model study mainly focused on the kinematic and

hydrodynamic performance caused by the surrounding fluid but desalinated the effect of internal muscle mechanics. The locomotion of fish larvae is powered by axial muscle system driven by motoneurons in the spinal cord [99]. Swimming kinematics are influenced by internal body mechanics and fluid mechanics [100, 101], forces generated by muscle induce body deformation, and the deformation will change the fluid dynamics of the surrounding water, i.e., hydrodynamic force. In return, this hydrodynamic force changes the body deformation as well [102]. Under this circumstance, these coupled mechanical interaction determines the motion of the fish through the water. Therefore, internal body mechanics are significant in the study of body motion.

2.4. Applications with Particle Image Velocimetry (PIV)

Particle image velocimetry (PIV) is an optical method of flow visualisation to obtain instantaneous velocity measurements and related properties in fluids [103]. By allocating sufficiently small tracer particles into the fluid, scientists can assume that the particles follow the flow dynamics. Applications of particle image velocimetry (PIV) techniques enable visualization of the flow field around the fish, and calculation of resultant hydrodynamic force [104]. A sample of apparatus and resultant images are shown in **Fig. 2-9**. However, it is limited to the 2-D flow field, which automatically ignores the flow passing through the dorsal and ventral side of the fish, thus the resultant hydrodynamic force will not be accurate enough to describe fish's swimming performance. Although 3-D PIV can compensate for the deficiency, its high cost makes it not universally applicable to the majority of researchers.

Many recent studies have presented flow field measurements using PIV techniques. Muller *et al* have applied a 2-D PIV technique to study the interactions between body movement of eel and the surrounding fluid [105]. As shown in **Fig. 2-10**, the author plotted the wake generated behind the eel body, and deduced that the wake structure is determined by phase lag between the vorticity shed from the tail and vortices produced

along the body. Besides, she suggested that eels can achieve different propulsive mode by adjusting their body wave. Tytell *et al* have studied the hydrodynamics of American eels systematically with high-resolution PIV to quantify wake structure, swimming efficiency, and force and power output. They also compared the results with other species [106]. A sketch of force and power from the PIV technique and elongated body theory is shown in **Fig. 2-11,** indicating that lateral force is pulsatile. Compared with the PIV method, elongated body theory has underestimated the values of force and total power, as depicted in **Fig. 2-11B**. Besides, the author has stated the differences of wake structure between an eel and carangiform swimmers, such as lacking of significant downstream flow for eels.

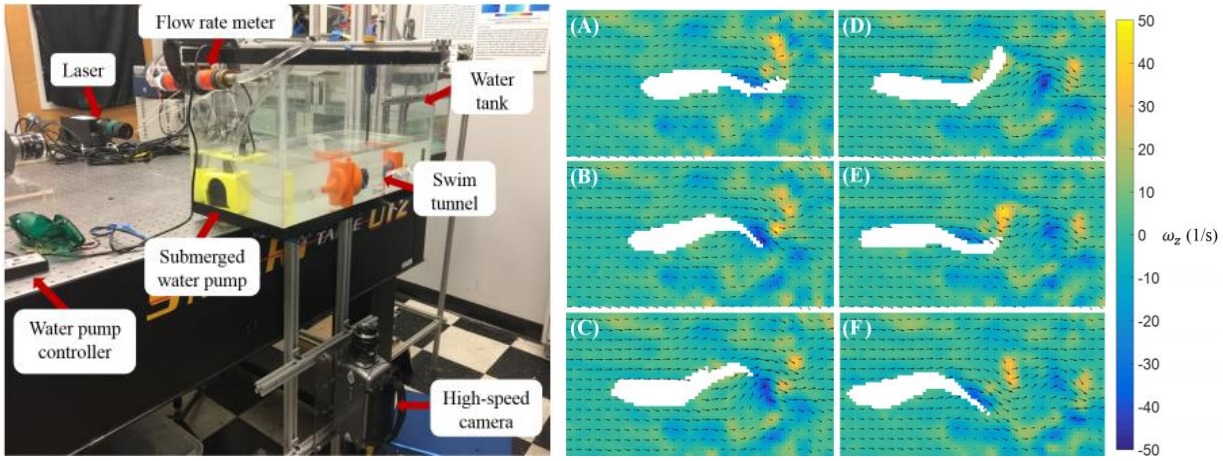

(A) (B)

Figure 2-9. (A) PIV apparatus used to measure flow patterns and kinematic performance of fish (B) Resultant velocity and vorticity field of a cruising fish. The time interval between consecutive snapshots is 1/32s. [104]

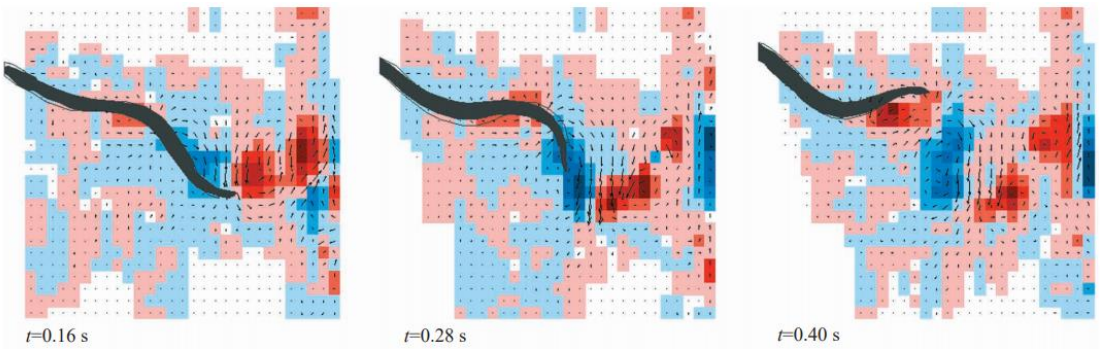

Figure 2-10. Instances during the time course of wake generation behind a steadily swimming eel. The black arrow indicates the swimming velocity, and blue shades indicate clockwise vorticity, red shades indicate counter clockwise vorticity. Darker shades indicate a higher level of vorticity. [105]

2.5. Fish swimming performance study with CFD simulation

Another popular method used to study interactions between fish and surrounding fluid is computational fluid dynamics (CFD) simulation. Compared to PIV method, although it cannot reflect the most accurate wake patterns behind fish body due to the computational model differences and limitations in numerical calculations, CFD simulation has less limitations on fish body characteristics such as length and weight, after setting up body kinematics according to real fish, simulations on hydrodynamic forces can be more systematic and accurate, and the cost is much lower than PIV experiments.

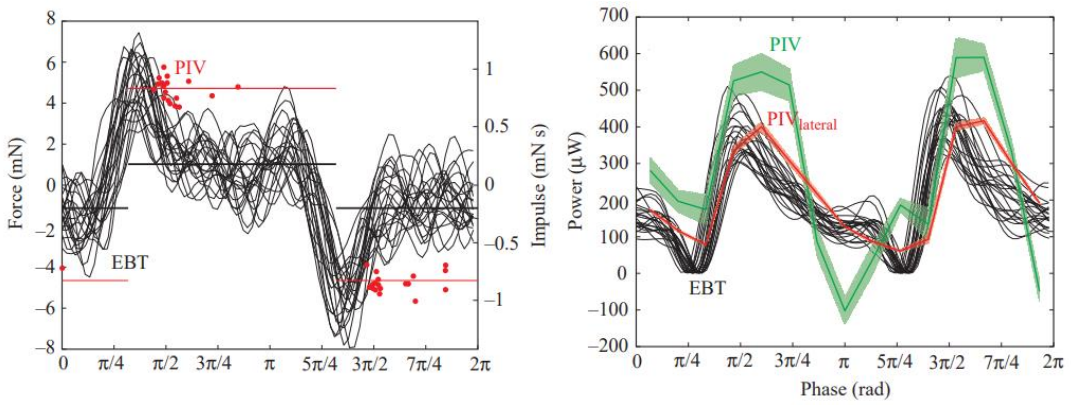

(A) (B)

Figure 2-11. Representative traces for force (A), Impulse, and power (B) from large-amplitude elongated body theory (black curve) and particle image velocimetry (red and green curve). Each black line shows force and energy for a single tail beat [106]

In previous studies, the hydrodynamic study of aquatic locomotion relied on the assumption that the water is inviscid [107, 108]. Some other researchers considered that it is necessary to quantify viscous effects to calculate drag forces acting on the body more accurately, and this requires CFD techniques. Starting from a simple aquatic model, Liu *et al* have studied the fluid dynamics of a swimming tadpole. The author have discussed the mechanisms of thrust generation and flow patterns of swimming of both 2-D and 3-D tadpole models [109, 110]. Carling *et al* have built a 2-D anguilliform fish model with shape in the form of a backward-traveling wave with increasing

amplitude from head to tail, and the fish model is constrained by lateral displacement equation and the equation describing the shape of the fish body is expressed as **Eqn 2.1**. In the equation, *s* represents the distance along the body measured from the nose, *l* is the total length of the body, and *b* is an amplitude parameter used to allow an amplitude other than zero at the nose of the creature, whose value is 0.25 in the paper.

Flow around the self-propelled animal is presented, as shown in **Fig. 2-12A**, another parameter, the mean swimming speed in x and y directions has been calculated as well (shown in **Fig. 2-12B**)[111]. Kern *et al* have built a three-dimensional self-propelled anguilliform fish model to study the fluid-body interactions shown in **Fig. 2-13A**, not only the quantitative information, but also the different swimming modes were linking the kinematic of the motion with the forces acting on the body. He has also compared with two-dimensional condition with the existing data from Carling to study the roles of 2-D and 3-D in quantifying the fluid dynamics, and the results are shown in **Fig. 2-13(B-C)**. It can be seen that compared with the 3-D model, swimming velocity is significantly higher for the 2-D case, and the structure of the vorticity is different as well. Besides, an optimization of swimming efficiency and burst swimming speed have been provided. [112]. Borazjani *et al* have expanded the study of 3-D fish model interactions with fluid to different types of fish locomotion, including carangiform and anguilliform as the Reynolds number and Strouhal number can be systematically varied. The author have discussed the differences of fluid dynamics between anguilliform and carangiform swimmers and the effects of Reynolds number and Strouhal number on forces and swimming efficiency. As depicted in **Fig. 2-14**, the sketch of time history of the axial force for both anguilliform and carangiform virtual swimmers shows similarities and differences between the two swimmer types. For instance, for all *St* values, there exist two peaks of the axial force coefficient in each cycle. However, the amplitude of the fluctuations above the mean value of the axial force coefficient is different, for which carangiform shows higher fluctuation amplitudes. Also, differences exist between two modes of swimming, such as wake structure (single row of vortices for carangiform and double rows of vortices for anguilliform) and Froude efficiency, at

the same time, some aspects of undulatory locomotion do not depend on the specific mode of swimming. For example, for a given Reynolds number, there is a unique Strouhal number at which body undulations produce sufficient thrust to cancel the hydrodynamic drug [113, 114].

$$y_s = \frac{(s/l+b)}{1+b}\sin[2\pi(s/l)-t] \tag{2.1}$$

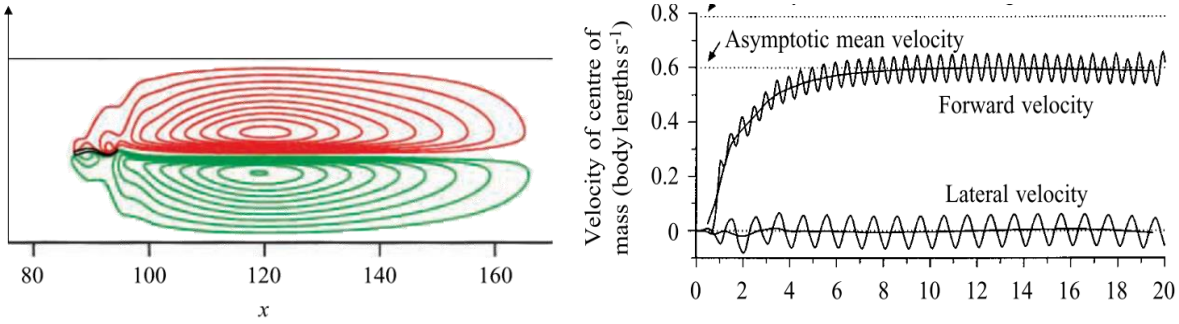

(A) (B)

Figure 2-12. Results for Carling's paper on (A) Streamlines in the wake region of a forward traveling 2-D fish model. (B) Forward and lateral velocity of the centre of mass. [111]

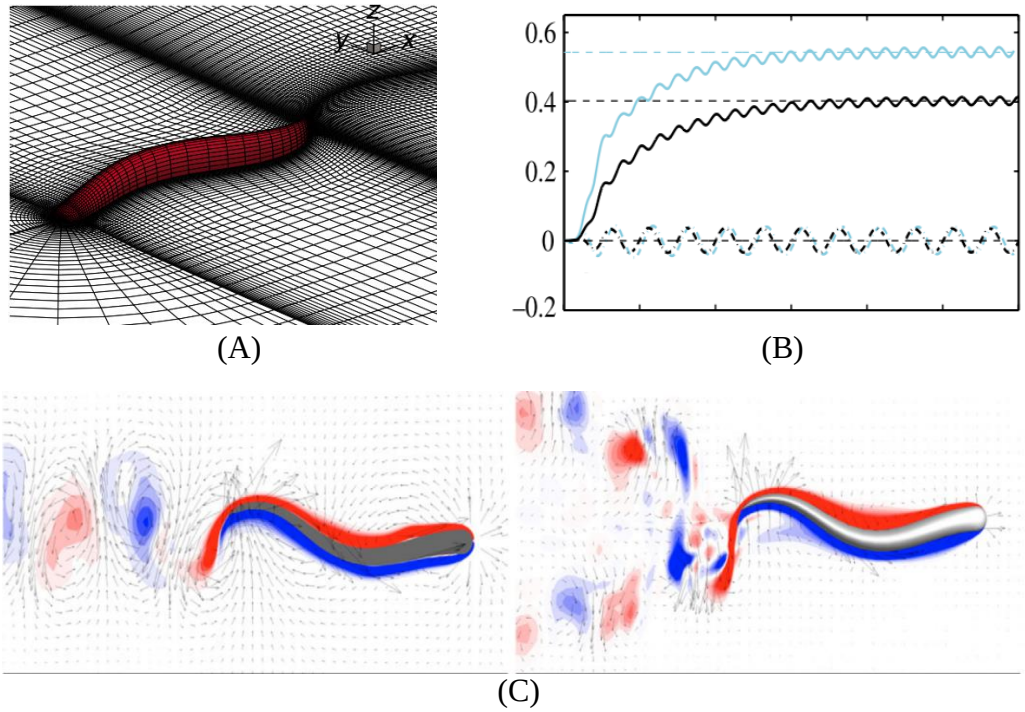

(A) (B)

(C)

Figure 2-13. Results for Kern's paper on (A) 3-D anguilliform fish model (B) Velocity comparisons between the 3-D case and 2-D case, the black curves represent longitudinal velocity (solid line) and lateral velocity (dashed line) for the 3-D example, and the cyan curves represent velocity for the 2-D case. (C) Vorticity comparisons for 3-D (right) and 2-D (left) case. [112]

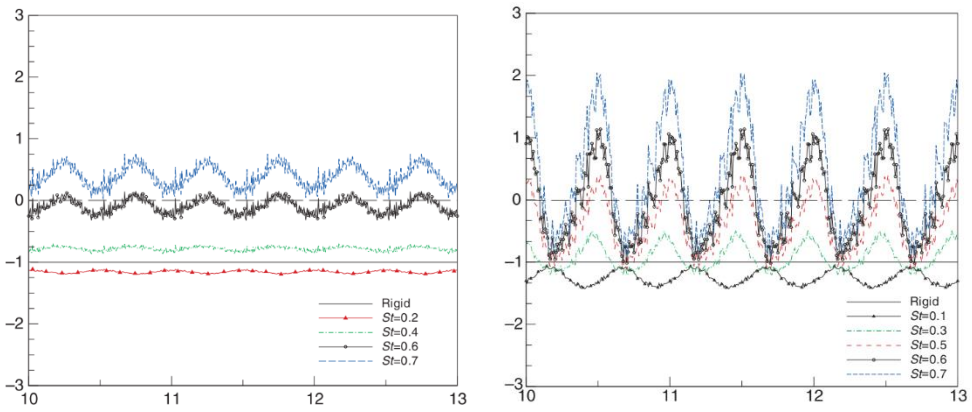

(A) (B)

Figure 2-14. Time history of the axial force coefficient normalized by the rigid body drag coefficient for different St at Re = 4000. (A) Anguilliform virtual swimmer (B) Carangiform virtual swimmer. Positive and negative values indicate thrust and drag force, respectively [114]

So far, the mentioned researches mainly focused on cyclic swimming of adult fish, but ignored the unsteady swimming of larvae fish. Aiming at making up for this part of the study, Katumata *et al* have built a 3-D zebrafish larva model to study the kinematics and hydrodynamics of a self-propelled swimming larva fish [115]. The zebrafish larva model was built based on the real zebrafish larva outline and is shown in **Fig. 2-15A.** When a fish starts swimming from stand-still, an acceleration happens, and the fish bends its body into a C shape, which is called C-starts. The phase comprises a preparatory and a propulsive stroke. As shown in **Fig. 2-15B**, when the fish starts to bend the body, a blue vortex is formed behind the tail tip at t=1/4T and followed by a red vortex generated at the tail tip at t=2/4T. However, the first blue vortex is not strong enough and dies off quickly, which makes the first vortex ring not complete. The complete vortex ring starts from the propulsive stroke. A much clearer sketch of the process of C-start is displayed in **Fig. 2-15C**.

Li *et al* have provided a more systematic computational study on the kinematics and hydrodynamics of a 3-D zebrafish larvae model [104]. He has studied the kinematic and hydrodynamic performance of cyclic swimming and spontaneous C-start, and compared results with the 2-D particle image velocimetry to prove that CFD simulation

can accurately predict fish locomotion. As shown in **Fig. 2-16**, the author has examined the flow patterns generated during cyclic swimming between CFD simulation and PIV results. In this figure, he has also displayed similarities and slight differences between CFD and PIV results and explained the possible reasons, supporting the viewpoint that CFD simulation can accurately predict the motion of zebrafish larvae.

Similar to what have done by Katumata, Li has evaluated the swimming speed of zebrafish larva at Reynolds number equals 550 (experimentally measured Reynolds number) but included comparisons with experimental results. As shown in their **Fig. 2-17**, it is evident that the simulated forward speed matches well with the experimentally measured results, which consolidates the simulation results on the hydrodynamic part. Li has also studied the fin fold influences of zebrafish larvae on vorticity and propulsion based on his previously built zebrafish larvae model [79]. By excluding the fin-fold structure, the author found that the fin fold helps larva achieve higher swimming speeds, yet requires higher power. Therefore, the author suggested that the propulsion of zebrafish larva, partly relies on the fin fold structure, providing a persuasive explanation for the omnipresence of the fin fold in bony-fish larvae.

In our study, inspired by previous work involving CFD simulation on fish swimming [104, 107, 111-114], a novel drug-related zebrafish larvae model combining a biological methodology and a CFD simulation analysis tool to quantify drug influences on zebrafish locomotion has been developed and described in the thesis. Specifically, we have used not only observation of live zebrafish swimming behavior with a high speed camera, but also a CFD simulation tool to quantify several important swimming characteristics, including internal body forces and consumption power, which are hard to acquire with experiments only. By applying appropriate solid-body simulation toolbox and coupling with CFD software, internal forces, torque, and energy could also be quantified. Therefore, it is worthwhile to use CFD software to assist in the analysis of drug influences on zebrafish locomotion.

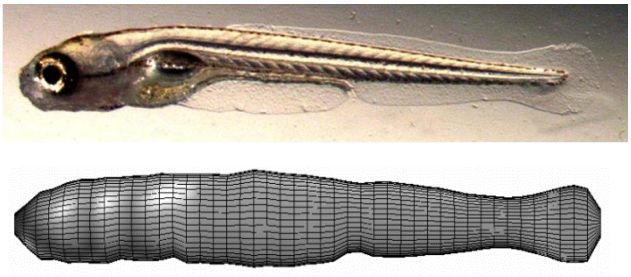

(A)

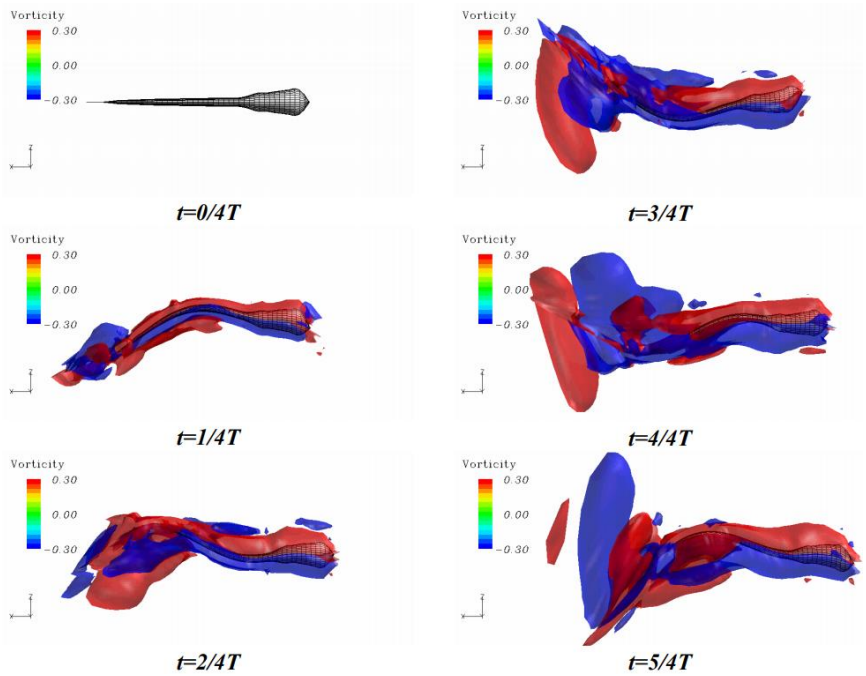

(B)

(C)

Figure 2-15. (A) Sketch of zebrafish model extracted from the real fish larva outline. (B) Iso-vorticity surfaces in the burst phase. (C) Real-time image of the C-start process, the left figure represents a stand-still state, the central figure represents preparatory stroke, and the right figure represents a propulsive stroke. [115, 116]

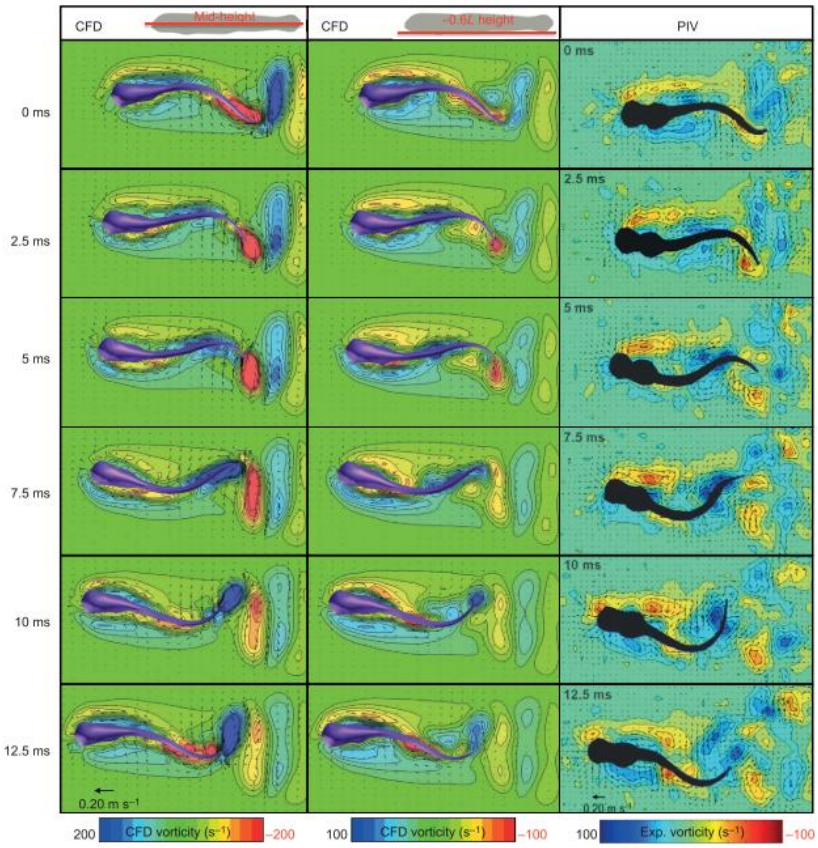

Figure 2-16. Comparison of flow patterns between CFD and Experimental PIV results. The computational results are shown with two planes, one is the medio-frontal plane (left column), and another one is 0.6L below medio-frontal plane (centre column), which is close with the position of PIV plane (right column). Slight differences in flow patterns between CFD results and PIV results might be caused by weak turning manoeuvres of the CFD fish model, which may lead to imperfect and unsymmetrical cyclic swimming. [104]

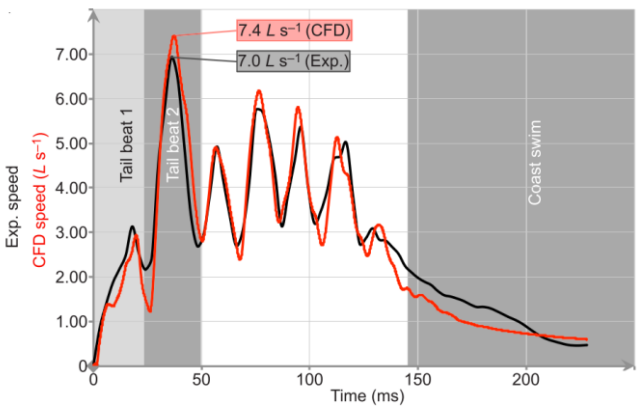

Figure 2-17. Velocity comparison between Experiments and CFD simulation of self-propelled zebrafish larva. [104]

2.6. Concluding Remarks

In this chapter, past researches on zebrafish as a model to study nociceptive responses are firstly discussed. Nociception is an ability of animals to detect potential noxious stimuli, such as extreme temperatures and chemicals. It is closely related to perception of pains or any substances harmful to animals. Early stage nociceptive study focused on transmission of nociception in mammalian animals as they are quite similar to human beings in many aspects. Compared to mammalians such as rodent animals, vertebrate animals such as bird and fish are less sentient, which means they are suitable to be used as a model for pain related nociceptive study from an ethical point of view. Although it has been argued that some fish and birds do not have core structures to perceive pain, behaviors of some species after stimulated with noxious stimuli support that they can perceive pains.

Advantages of zebrafish for biomedical research have been mentioned in the first chapter. As a vertebrate animal, zebrafish have been proved to have pain receptors to perceive pain, and certain types of analgesic drugs have similar effects on zebrafish compared to human beings, making zebrafish a suitable model for nociceptive study. The research includes medical treatment of zebrafish with side effects and recovery and protection from certain analgesic drugs. Techniques used in the research involve high-speed camera and PIV, they are the most straightforward methods to observe the physical changes including body trunk deformation and swimming behaviors. Followed by more precise measurements, such as microscopic observations and post-processing toolbox, affected tissues and cells can be observed, and altered swimming behaviors can be quantified such as body gestures, locomotion activity and swimming distance. As nociceptors can pass the signals received to the spinal cord, behavioural changes can be closely related to nociceptive responses; therefore, techniques mentioned above can be used together to better study the nociceptive responses and transmissions.

Besides, another method used to study the zebrafish swimming behaviors is mentioned in the chapter, which is the CFD simulation. Different from methodologies stated in the above paragraphs, CFD simulation focuses on the quantification of swimming behaviors and can provide more systematic and accurate force values and flow field data. Also, the cost is lower than biological experiments. Based on the previous research, thrust generation, power consumption, and flow field visualization have been achieved for zebrafish locomotion. Data acquired from CFD simulation on zebrafish swimming is important for biological experiment as the nociceptive responses induce body movement alterations. However, connections between the two terms have rarely been studied. Inspired by previous CFD simulation and nociception related biological experiment, studies in the thesis are aimed at filling the gaps mentioned above [84, 85, 104, 113, 114], with a combination of experimental measurements and numerical simulation on zebrafish swimming behaviors.

3 Methodology

3.1. A brief introduction of methodology

We simulate the real zebrafish motion with the help of experiment and open-source CFD software *OpenFOAM* (https://www.openfoam.com/) coupling with solid multibody motion solver *MBDyn* (https://www.mbdyn.org/). The actual fish motion is captured with a high-speed camera and post-processed with in-house *MATLAB* code. Details of the methodology are stated in the following sections.

3.2. Experimental motion capture & post-processing

Apparatus

Apparatus shown in **Fig. 3-1** was used to record the fish motion for further analysis. Zebrafish larvae (in all of the experiments, five dpf zebrafish larvae were used and put inside the Petri dish, and the diameter of the Petri dish is 100mm). The diameter of petri dish is used for calibration of the high speed camera and convert the number of pixels travelled by zebrafish larvae into *SI* unit. The depth of solution in petri dish is approximately twice the fish body length, which allows zebrafish larvae to be fully submerged. Also, according to our observations, 5 dpf zebrafish larvae randomly choose to approach the water surface, instead, they spend most of time beneath the water surface. High-speed camera right above the petri dish recorded the motion of the fish with 500 fps setup. The position of petri dish was adjusted to ensure that the high-speed camera is in alignment with the petri dish to ensure desired region to be included in the camera lens. The real-time zebrafish swimming was displayed on the computer and only the circular region of petri dish was included and recorded. Due to the limitations and purposes of our post-processing tools, each time only one zebrafish larva existed in the petri dish to exclude zebrafish interaction influences and the locomotion was recorded. Depending on different treatments, some fish larvae were pre-treated before five dpf. Still, all of the zebrafish larvae were allowed for 10 minutes

to acclimate to the environment before recording commenced. The recorded videos were collected and post-processed with in-house *MATLAB* code. The experiments were carried out in a room maintained at $27 \pm 1°C$. Water temperature was set at 27℃ for all groups at the beginning by adding water from the homothermal water tank into the petri dish, but the temperature was slightly lower than 27℃ during the experiment as the experiment lasted for a long time. For the entire experiment, lighting condition was kept only by the light-emitting diode (LED) panel beneath the petri dish to provide constant light, without any environmental light. The strength of the light was driven by an adjustable DC power supply (CSI5003XE, Circuit Specialists, and the USA).

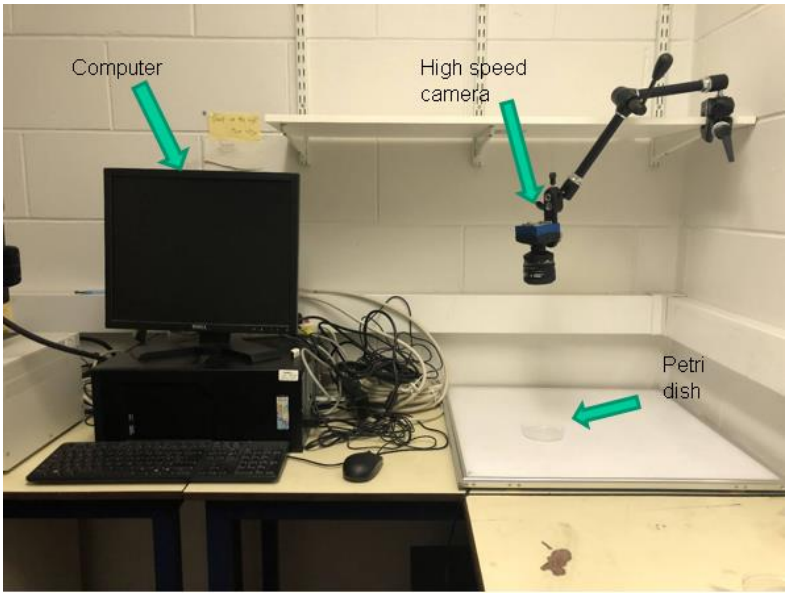

Figure 3-1. Apparatus used to record zebrafish larvae motion. The recorded video will be stored in the computer and processed with MATLAB code

Ethics statement

Animal work was carried out in compliance with the Animal Ethics and Welfare Committee, Department of Life Sciences, Glasgow Caledonian University, and UK Home Office under Project License PPL 60/4169.

The methodology of the experiment was divided into two parts, the first part is validation experiments including multiple types of medicine and drugs, and the second

part is the protection of zebrafish larvae from acetic acid with GYP with qRT-PCR analysis.

3.2.1. Nociceptive & neuroactive drug experiments

Experiment setup

The experiment setup and main methodology were developed based on our previous study for the determination of the toxicity of acrylamide on zebrafish locomotion via a colour preference experiment [117]. In the present study, eighty five dpf wildtype zebrafish (Danio rerio) larvae siblings were used in this stage, and the entire zebrafish samples were divided into four groups. Any larva not used in the study were kept for further experiment or humanely killed before reaching six dpf with Tricaine methane-sulfonate (MS-222). The overdose usage of this anesthetic can kill zebrafish larvae without pains [118]. All fish were immersed in E3 medium (5mM NaCl, 0.17mM KCl, 0.33mM $CaCl_2$, 0.22mM $MgSO_4$, and 0.1% methylene blue) initially, with one hour's time to adapt to the environment. The larvae were then gently placed individually into four Petri dishes with twenty larvae in each Petri dish, corresponding to four groups. To avoid mutual effect, the configuration of solutions in four petri dishes are shown in **Table 3-1**. The first group was regarded as control group, and the rest three groups were drug treated groups. Each larva had ten minutes to stay in the petri dish before observation commenced and was gently moved to the prepared petri dish for recording. Only one zebrafish larva was recorded each time by moving the zebrafish from previously prepared four petri dishes to a new petri dish containing the desired solution. A high-speed video camera (Mikrotron EoSens CL MC1362) was used to record fish swimming behaviors. The frame rate of the camera was set at 500 fps during the entire experiment process. As in the subsequent CFD numerical modelling, the selected fish with a tail beat frequency being less than 70Hz; thus, 7-8 frames within one beat cycle is sufficient to capture the fish tail motion and extract the motion equations. Once recording commenced, there was no stimulation to panic the fish or force the fish swimming forward. Potential stimulation from the light provided by panel beneath petri

dish was avoided by 10 minutes' time to get used to the environment. In this study, only the quasi-steady cruising swimming regime was investigated, excluding the burst-start process. Cruising is a process of steady forward swimming with cyclic tail beat and body motion, and the path is nearly straightforward. The limitation is evident from previous research that cruising with cyclical motion is essential for fish larvae to cover the distance for migration and dispersal [119]. Besides, cruising has been studied extensively, which makes it easier to compare with other researcher's results. In the post-processing part with *MATLAB*, frames containing cyclic swimming behaviours were selected for further processing. Zebrafish fish larvae were gently moved from the petri dish into another container, each group had its own container. Once the experiment completed, the used zebrafish were killed with MS-222 and the unused zebrafish were stored in an incubator for further experiments.

Table 3-1. Experiment configurations on drug selections

Group number	Drug configuration
1	E3 medium (control)
2	0.01% acetic acid
3	500 μM diphenylhydantoin (DPH)
4	100mg/L yohimbine

3.2.2. Gypenosides protection experiment

3.2.2.1. Zebrafish locomotion recording

The experiment was divided into two parts, and the first part is the observation of zebrafish locomotion under different treatments to study GYP (Sigma-Aldrich, UK) protections from high concentration acetic acid damage on zebrafish larvae. GYP (purity 98%) was bought from Xi'an Jiatian Biotech Co. Ltd, China. Eighty four dpf zebrafish larvae were prepared and divided into four groups. Details of treatments are displayed in **Table 3-2**. In the experiment, group 2 and 4 were control groups, and group 1 and 3 were drug treated groups. The zebrafish larvae stayed in homothermal incubator at 27±1℃ and lasted for one day without acid treatment. At five dpf, larvae in group 1

and group 3 were treated with 0.1% acetic acid, and the other two groups remained unchanged. For all groups, fish larvae stayed under the camera and swam freely without any environmental or artificial influence. Swimming behaviors of all the fish samples were recorded for ten minutes and post-processed with in-house *MATLAB* code to be prepared as input for the CFD simulation. Once the experiment has completed, the used zebrafish were killed with MS-222 and the unused zebrafish were stored in an incubator for further experiments.

Table 3-2. Experiment configurations on drug selections

Group number	Drug configuration
1	5 $\mu g/mL$ GYP+0.1% acid
2	5 $\mu g/mL$ GYP
3	E3 medium+0.1% acid
4	E3 medium

3.2.2.2. Quantitative real-time polymerase chain reaction (qRT-PCR)

The second part of the experiment was the toxicity tests of acetic acid and Gypenosides protection (Sigma-Aldrich, UK) performed in 48-well plates. All experiments were performed in triplicate wells, which contained ten embryos in 400μl drug solutions. The sample was exposed to 0.1% acetic acid, 0.1% acetic acid+5μg/mL GYP, 5μg/mL GYP as well as an untreated group.

Different from the experiment explained in the previous subsection, the GYP protection experiment included analysis of relative expression of several target genes (listed in **Table 3-3**) related to Gypenosides and acetic acid. This could be achieved with the help of quantitative real-time polymerase chain reaction (qRT-PCR). Quantitative real-time polymerase chain reaction is a method to determine the amount of PCR product in real time [120]. As the target is the expressions of some specific genes, several steps need to be carried out before the Q-PCR reaction.

The first step was RNA extraction from zebrafish larvae cells. To attain sufficient amount of RNA, 50 zebrafish larvae have been collected. Total RNA was isolated from untreated and treated zebrafish embryos with 120 hours post-fertilization (hpf) using Trizol Reagent (Sigma, UK) according to the manufacturer's guidance. The second step was the complementary deoxyribonucleic acid (cDNA) synthesis, or reverse transcription, which can produce cDNA from RNA template. Synthetization of the cDNA using a High-Capacity cDNA Reverse Transcription Kit (Applied Biosystems, UK) was made to produce cDNA with high fidelity that can accurately represent the target DNA. After cDNA has been produced, the qRT-PCR analysis can be carried out to study the gene expression. The quantification of genes expression was measured by qRT-PCR assay using a Platinum® SYBR® Green PCR kit (Thermos Fisher Scientific, UK) under the PCR condition as described in the protocol. Relative expression of the target gene was determined by normalization to the expression of the housekeeping gene (β-actin) in the untreated and treated samples, using 2^-ΔΔCT formula. The primer sequences of the genes used are listed in **Table 3-3**.

Table 3-3 Primers used for qRT-PCR

Genes	Forward primers 5′-3′	Reverse primers 5′-3′	TM°C	PCR product (bp)
β-ACTIN	ACTGTATTGTCTGGTGGTAC	ATCTCCTGCTTGCTAATCC	69.7	198
IL-1β	TTCCCCAAGTGCTGCTTATT	AAGTTAAAACCGCTGTGGTCA	54.6	149
IL-6	TCAACTTCTCCAGCGTGATG	TCTTTCCCTCTTTTCCTCCTG	55.1	75
TNF-α	ACCAGGCCTTTTCTTCAGGT	GCATGGCTCATAAGCACTTGTT	56.5	147
SOD1	CGCATGTTCCCAGACATCTA	GAGCGGAAGATTGAGGATTG	53.9	100
SOD2	CTAGCCCGCTGACATTACATC	TTGCCCACATAGAAATGCAC	54.5	101
GPX1	AGGCACAACAGTCAGGGATT	CAGGAACGCAAACAGAGGG	56.45	241

Statistical analysis

Graphpad Prism (version 7.0 from Graphpad Software Inc. San Diego, CA, USA) (https://www.graphpad.com/scientific-software/prism/) has been used for statistical analysis. All multiple comparisons were performed using the one-way ANOVA with Bonferroni multiple comparison test. The one-way ANOVA is used to determine whether there exists any significant difference between two or multiple unrelated groups of data. Bonferroni multiple comparison is a method to lower the risk of getting inaccurate significance level. Statistical significance was considered when a level of p is less than 0.05.

3.2.3. Data processing algorithm

An in-house *MATLAB* code has been developed and used to post-process the recorded videos and extract zebrafish swimming kinematic characteristics, i.e. body curvature equations. A real zebrafish larva picture taken from the high-speed camera is shown in **Fig. 3-2A**, and the full path of fish motion can be extracted as well (shown in **Fig. 3-2B**). Frames containing cruising were selected to be prepared for further processing, and this was achieved by observing the recorded video to extract the cruising period in real time and converted to frame data. Key steps of body curvature extraction are shown in **Fig.3-2C**. The entire video was divided into frames, and each frame was used as the original image to be processed with *MATLAB* functions. The original image was firstly converted to a binary image consisting of the sketch of zebrafish larvae with the help of *'im2bw'* function in *MATLAB* image processing toolbox to get rid of unwanted parts in the picture such as edges of the petri dish and impurities. With some adjustments and *'bwboundaries'* function in *MATLAB*, a binary image of zebrafish was extracted, the entire position vector expressed as (x_i, y_i) was obtained for points distributed on the fish outline. x_i and y_i were expressed as pixel values and were converted to the SI unit of length for further calculations. All images were skeletonized into a single backbone curve using functions' *bwmorph'* and *'thin'* operations.

The coordinated pixels on the backbone curve were then divided into equal-distant curves, and each curve represents one body segment. These segments were simplified as connected straight lines to calculate relative orientation variation with time between two adjacent segments using *MATLAB* curve fitting toolbox. Physical representation of the intersection angle is shown in **Fig. 3-2D** and the 3-D intersection angle is expressed by **Fig. 3-2E**, and calculated with **Eqn 3.1**, where i denotes points numbering from one. In **Fig. 3-2D**, each straight black line represents one segment of the fish body, the prescribed relative orientation can mimic the body curvature, and angular displacement represents the lateral displacement of the fish body. As elucidated by [76], the travelling wave of curvature travels along the fish body at a near-constant rate. Thus an averaged frequency was selected for the entire relative orientation functions along the body. To express how the relative orientation equation along fish body have been fitted, an example of detailed extracted relative orientation values are shown with **Table 3-4**. **Eqn 3.1 and 3.2** represent a sample prescribed deformation equation for relative angle between each two body segments, and a set of sample equations are written in **Table 3-5**. **Fig 3-2F** depicts a comparison of curve fitting method on the body curvature functions. The black dots are data collected from *MATLAB* post-processing, indicating the relative angle values between two randomly selected segments. The curve was fitted with non-linear Fourier series regression to minimize the influence of points far from the fitted line, and Bisquare remain robust was used in regression. The bisquare weighting method minimizes a weighted sum of squares, where the weight given to each data point depends on how far the point is from the fitted line. To get rid of influences of some points away from the fitted curve which could be caused by inaccuracy of the post-processing, bisquare robust method was used to fit the curve most relevant to the real condition.

$$\arctan\left(\frac{y_{i+2}-y_{i+1}}{x_{i+2}-x_{i+1}}\right) - \arctan\left(\frac{y_{i+1}-y_i}{x_{i+1}-x_i}\right) \tag{3.1}$$

$$a\cos(\omega t) + bsin(\omega t) \tag{3.2}$$

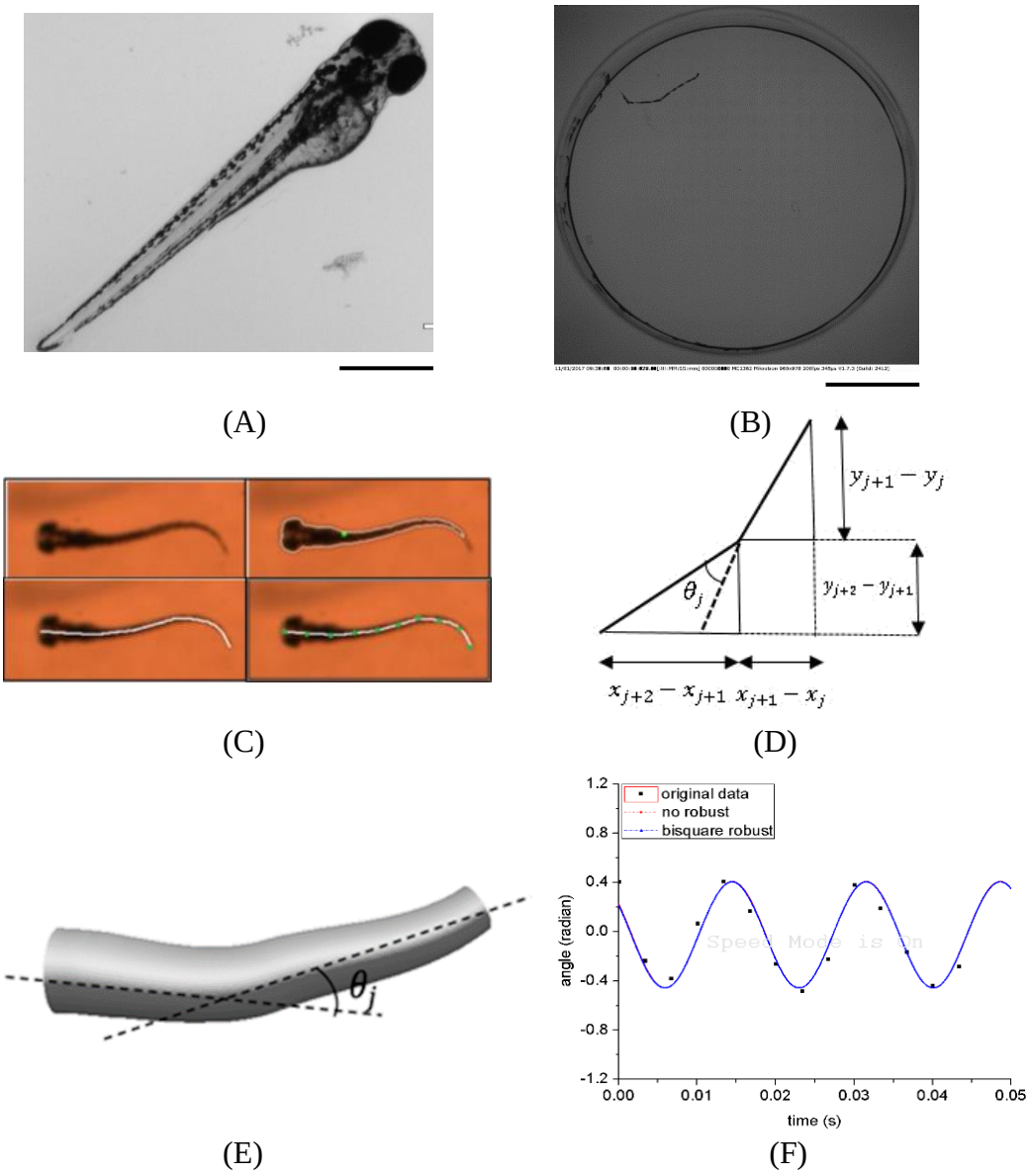

Figure 3-2. Mechanisms of processing zebrafish swimming video. (A) Real zebrafish larvae transparent body (scale bar = 1mm). (B) Fish swimming trajectory captured with high speed camera (scale bar = 25mm). (C) Key steps on getting a central line of zebrafish and equal-distant division of the central line (D) Mathematical expressions of relative intersection angle between two segments of the fish body (E) Analytical expressions of relative orientation between each two segments. (F) Different curve fitting methods for sinusoidal-like relative orientation equations. Bisquare robust method fitted curve coincides with no robust method.

Table 3-4. Detailed orientation angles for the entire fish body

Time (s)	A2(rad)	A3(rad)	A4(rad)	A5(rad)	A6(rad)	A7(rad)	A8(rad)
0	-0.1069	-0.1073	-0.1578	-0.1926	-0.4647	-0.195	-0.2018
0.0033	0.1087	0.1127	-0.4663	-0.4209	-0.2655	-0.454	-0.571
0.0067	0.3033	0.3623	-0.1431	-0.1473	0.1677	0.1059	0.2366
0.0100	-0.0867	-0.0702	0.144	0.1294	0.4787	0.4812	0.5591
0.0133	-0.3315	-0.3929	0.443	0.4026	0.1142	0.2005	0.1966
0.0167	-0.1113	-0.1294	-0.1681	-0.1644	-0.4316	-0.2033	-0.1404
0.0200	0.1131	0.1246	-0.4638	-0.4562	-0.2027	-0.5499	-0.4805
0.0233	0.3254	0.3369	-0.1696	-0.1213	0.155	0.1684	0.1053
0.0267	-0.1019	-0.1213	0.1298	0.199	0.4377	0.4719	0.4889
0.0300	-0.3504	-0.3506	0.4579	0.455	0.1845	0.1537	0.1156
0.0333	-0.131	-0.1181	-0.158	-0.1209	-0.4936	-0.0724	-0.1005

Table 3-5. Sample relative orientation functions along fish body

Relative orientation between two segments (rad)	Function
θ_1	0
θ_2	$-0.174\cos(2\pi ft) - 0.078\sin(2\pi ft)$
θ_3	$-0.164\cos(2\pi ft) - 0.191\sin(2\pi ft)$
θ_4	$-0.114\cos(2\pi ft) - 0.154\sin(2\pi ft)$
θ_5	$0.297\cos(2\pi ft) - 0.048\sin(2\pi ft)$
θ_6	$0.252\cos(2\pi ft) - 0.124\sin(2\pi ft)$
θ_7	$0.275\cos(2\pi ft) - 0.043\sin(2\pi ft)$
θ_8	$0.195\cos(2\pi ft) - 0.301\sin(2\pi ft)$
Span-wise length (mm)	0.4

3.3. FSI interaction simulation with *OpenFOAM & MBDyn*

As described at the beginning of the chapter, the simulation of the zebrafish larvae motion can be categorized as an FSI (fluid-structure interaction) problem, involving prescribed solid body deformation-induced self-propelled forward motion and resultant surrounding fluid effects. At the beginning, an overview of the FSI algorithm is explained. **Fig. 3-3** depicts the structure of the present FSI tool. *OpenFOAM* was used to solve the fluid dynamics, including fluid force exerted on body surface and internal mesh motion induced by body surface motion; and the solid body dynamics were tackled with *MBDyn* including body forward motion data and internal muscle forces and moments. The extracted relative orientation equations along zebrafish body with *MATLAB* played the role as input in the solid body solver *MBDyn*. These inputs were used in *MBDyn* to calculate the internal forces and moments which can perform the desired trajectory constrained by the inputs.

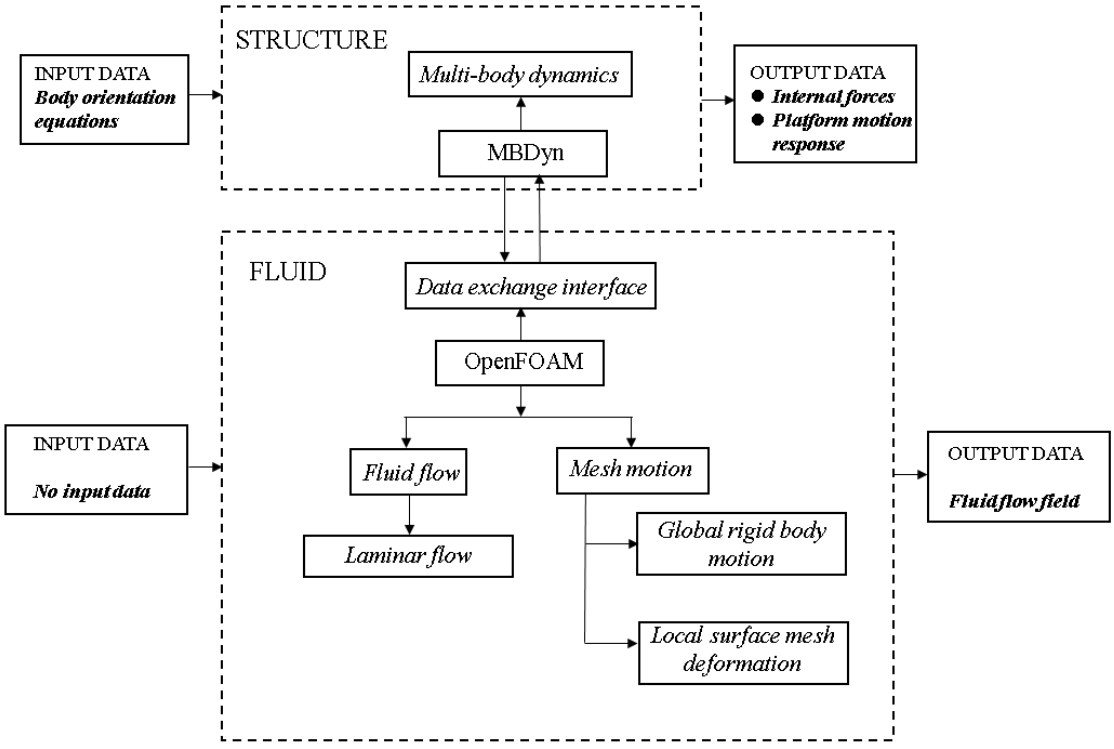

Figure 3-3. Structure of the fully coupled FSI analysis tool for zebrafish larvae

3.3.1. Zebrafish larva CFD model

In this study, the 3-D zebrafish larva model used in *OpenFOAM* was built with 51 ellipses extracted from the real fish silhouette and controlled by nine deformation equations. Due to the 2-6mm body length of zebrafish larvae, the absolute swimming velocity is much lower than larger fish, therefore, length-specific swimming speed is much more important. The fish model is shown in **Fig. 3-4** and normalized with fish body length. Each ellipse was specified with chord length, height and the position along fish body length. To simplify the model, the eyes and fin fold were not included. The final CFD model is shown with top and side view of zebrafish larvae in **Fig. 3-5**, the continuous fish body were divided into several segments to mimic the muscle contributions along the fish body, as shown in **Fig. 3-6**. The body segments are shown as blocks with different colours. In all cases, the entire fish body was divided into nine sections, and the influences on the number of segmentation will be discussed in the validation chapter. Details of the segmentation will be explained in the following sections regarding multibody dynamics toolbox *MBDyn* (https://www.mbdyn.org/). The mass density of the fish was assumed to be uniform along the body and the same as water, which is 996kg/m^3 [104], averaged body parameters such as body segments' mass and length listed in **Table 3-6** were used for all fish in the CFD simulation.

The flow field was numerically simulated using the open-source CFD toolbox *OpenFOAM* version 3.0.x. The 3-D computational domain was twenty times of the fish body length in the longitudinal (x) direction, ten times of fish body length in transverse (y) direction and four times of fish body length in perpendicular (z) direction as shown in **Fig. 3-7**. The overall fluid domain was assumed to be at rest initially, which means there is no incoming flow. In the simulation, the medium was water at 27°C; therefore, the kinematic viscosity of the fluid is $0.854*10^{-6} m^2/s$. Pressure boundary conditions were taken as zero gradient for all boundaries except the front and back plane, which were set as symmetry, velocity boundary conditions for the fish model were considered as '*movingWallVelocity*' for all body segments and fixed value for the remaining patches

to mimic the physical environment of the experiment (Petri dish). The *movingWallVelocity* is a particular boundary condition applied in *OpenFOAM* transient simulations, and it is used for moving mesh cases where the velocity of the wall changes with time, and sets the velocity to the desired value for moving walls. In this case, the boundary condition can impose a non-slip condition on the wall. In our case, the entire domain consisted of unstructured mesh only to tolerate large internal mesh deformation during self-propelled forward motion of the fish model. For ellipses with high aspect ratio at the tail region, the mesh was specially refined to ensure that enough cells were used to precisely capture the vortex detached at the tail tip. Also, a particular region was built behind the fish to keep cell density higher than other regions to increase the mesh resolution (shown in **Fig. 3-7**). Reynolds number was defined as $\frac{vL}{\upsilon}$, v stands for forward swimming velocity, L is the body length of fish larva, and υ represents the kinematic viscosity mentioned above. For the entire simulation, Reynolds number was estimated to be 340 according to the desired forward velocity of zebrafish larvae, which stands for intermediate flow regime, this is consistent with the real fluid property of zebrafish larvae.

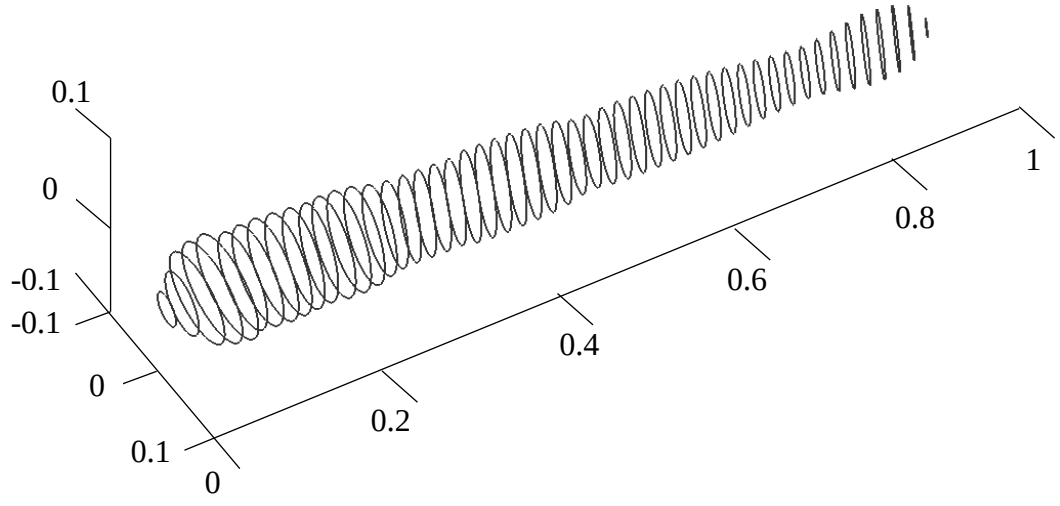

Figure 3-4. Zebrafish model approximated with outlines of the body at each of the 51 transverse sections along the body.

Figure 3-5. Top and side view of the zebrafish model used in OpenFOAM.

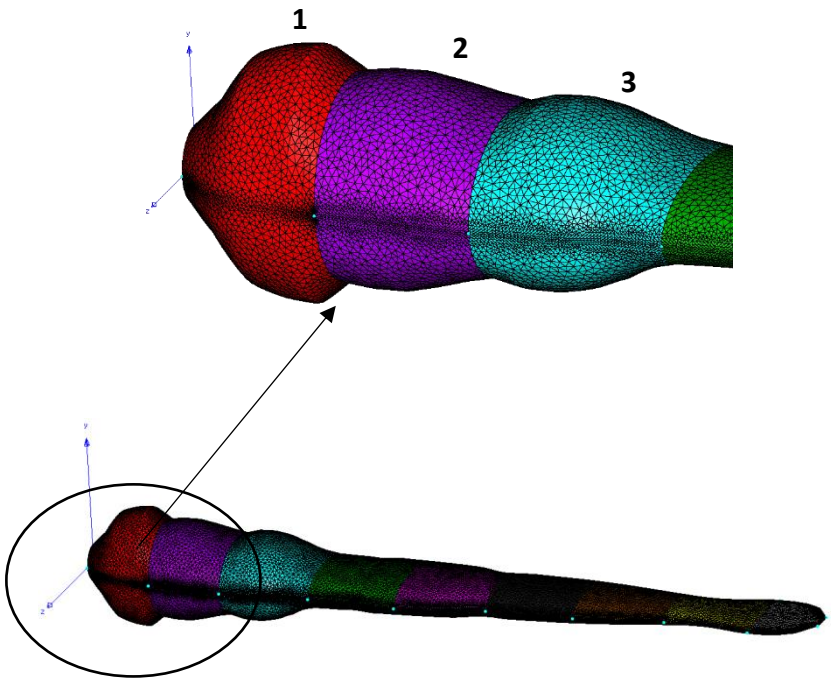

Figure 3-6. CFD model of zebrafish larvae.

3.3.2. Solid zebrafish larvae body dynamics

As described above, the FSI forward motion simulation involved two parts. The solid-body dynamics were solved with *MBDyn*, which is a multibody dynamics analysis software used as a general tool to address multidisciplinary simulation of multibody system, including rigid and flexible bodies subject to kinematic constraints. *MBDyn* is released under the GNU's General Public License (GPL) 2.1, it can be used and

distributed freely with its source code available to the public just like *OpenFOAM*. The software can solve the initial value problem in the form of Differential-Algebraic Equations (DAE), integrated in time domain using A/L-stable multistep integration schemes [121]. Constraints can be added independently in *MBDyn*, both for rigid and flexible body with six degrees of freedom.

Table 3-6. Mass and length for each body segment numbered from 1 to 9

Body section number	Mass (mg)	Length (mm)
1	0.0385	0.4
2	0.0553	0.4
3	0.0425	0.48
4	0.0308	0.48
5	0.0212	0.48
6	0.019	0.48
7	0.011	0.48
8	0.009	0.48
9	0.003	0.32
Total	0.23	4

To mimic the vertebrate muscle structure of zebrafish larvae, a continuous multi-segments fish model was built, consisting of several rigid body segments, it is convenient to use *MBDyn* to add multiple constraint equations to control the body deformation. A schematic diagram for the zebrafish model is displayed in **Fig 3-8.** In *MBDyn*, mass and moment of inertia of each body segment were specified, body's position and orientation were expressed by a particular unit *'node'*, and this unit has six degrees of freedom. It contains position and orientation information shown as a black point in the figure. The location of node and body can be different, also, the position of node can be expressed with a reference point by specifying the relationship between node and reference point.

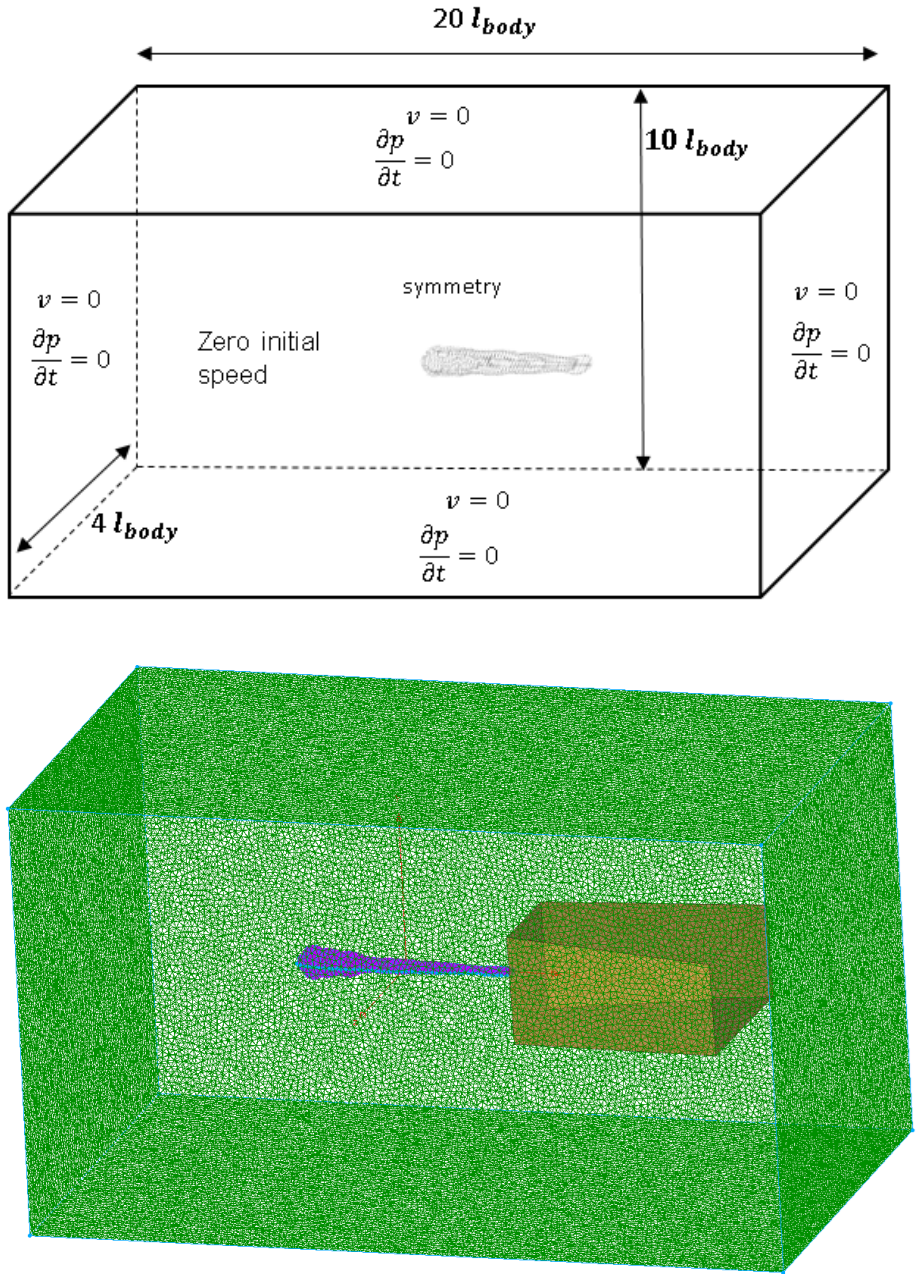

Figure 3-7.Fluid domain of zebrafish larva and mesh refinement behind zebrafish body with a yellow colour column.

Equilibrium equations were established considering both external and internal forces as well as moments. External force and moments were integrated over each body segment, if there exists reference point, the information would be translated to the corresponding node. Constraint was expressed by another unit *'joint'* shown in **Fig. 3-8**, it can connect

nodes and may have internal degrees of freedom (the reaction force). Internal forces and moments were evaluated at joints and they are related to the geometrical strains and curvatures via the constitutive law specified in **Eqn 3.3**, where F_x is the axial force component, F_y and F_z are the shear force components; M_x is the torsional moment component; M_y and M_z are the bending moment components; ε_x is the axial strain component, γ_y and γ_z are the shear strain components; κ_x is the torsional curvature component; κ_y and κ_z are the bending curvature components; the dot operator above a variable denotes its derivative to time; f is an arbitrary function defining the constitutive law.

Depending on the types of *joint*, functions are different. For instance, spherical joint acts like a sphere between the two nodes and constrains the relative position but frees the relative orientation. Dashed lines between nodes and joint indicate that distance between node and joint can be variable or even coincident. Both of them can be expressed globally and locally, and the initial position and orientation of the *node* and *joint* can be set up with a reference frame to simplify the relationships among those elements.

$$\begin{pmatrix} F_x \\ F_y \\ F_z \\ M_x \\ M_y \\ M_z \end{pmatrix} = f\left[\begin{pmatrix} \varepsilon_x \\ \varepsilon_y \\ \varepsilon_z \\ \kappa_x \\ \kappa_y \\ \kappa_z \end{pmatrix}, \begin{pmatrix} \dot{\varepsilon}_x \\ \dot{\varepsilon}_y \\ \dot{\varepsilon}_z \\ \dot{\kappa}_x \\ \dot{\kappa}_y \\ \dot{\kappa}_z \end{pmatrix}\right] \tag{3.3}$$

Differential algebraic equations (DAE) of the two adjacent nodes are written in the form of Newton-Euler equations, constrained by Lagrange's multipliers λ :

$$\begin{aligned} \mathbf{M}(\mathbf{x})\dot{\mathbf{x}} &= \mathbf{q} \\ \dot{\mathbf{q}} + \phi^{\mathrm{T}}{}_{/\mathbf{x}}\lambda &= \mathbf{f}(\mathbf{x}, \dot{\mathbf{x}}, \mathbf{t}) \\ \phi(\mathbf{x}, \mathrm{t}) &= 0 \end{aligned} \tag{3.4}$$

where **x** represents the vector of the generalized coordinates including both translational and rotational parameters in the global reference frame; **M(x)** is the mass matrix, **q** summarizes the momentum vector of the body containing both linear and angular components, and **f** summarizes the generic force including pressure and viscous force. ϕ is a set of kinematic constraints applied on the body and $\phi^T{}_{/x}$ represents the Jacobian of ϕ with respect to the generalized coordinates vector **x**. The dot operator above a variable denotes its derivative with respect to time.

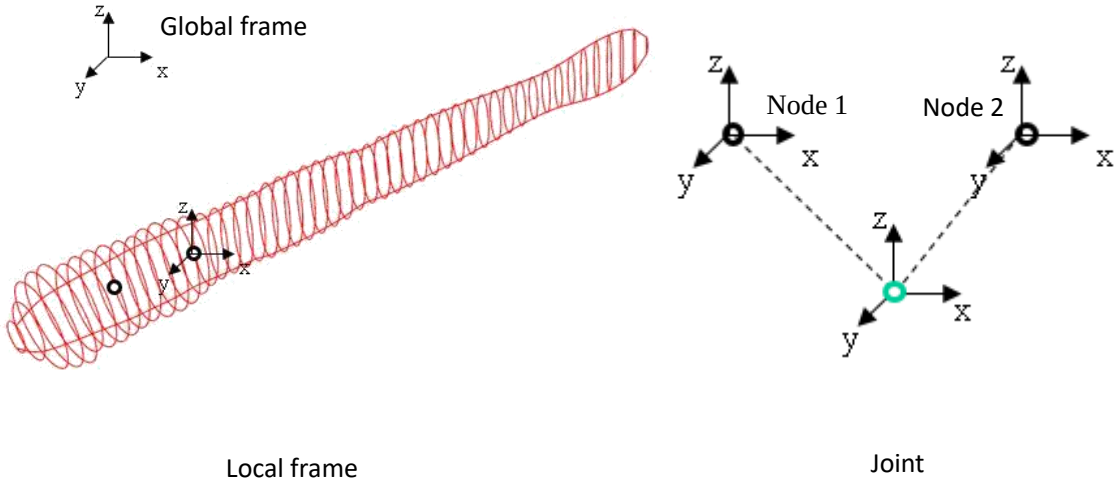

Figure 3-8. Schematic diagram for fish model in MBDyn. A 3-D zebrafish model is shown in the left picture, indicating the expressions of position and orientation of the node, which represents the fish body. The relationship between node and joint is shown in the right figure, and the dashed line suggests that the position of node and joint can be coincident and the orientation can be different depending on the reference frame selected.

The DAEs were integrated with implicit A/L stable linear multistep integration schemes, and a prediction-correction approach was used [122]. In the current case, each body segment was represented by one node in *MBDyn*. Except the ground node was set as 'static' type, all of the body nodes were dynamic type, and each two adjacent nodes were constrained by a deformation equation fitted with *MATLAB* curve-fitting toolbox.

As a solid body motion analysis software, *MBDyn* can provide position and orientation information for its peer solver, i.e. *OpenFOAM*. As *MBDyn* receives force information

from its peer solver, the solution procedure of updated motion data was achieved based on the following equation according to Newton's Second Law:

$$M_i\ddot{\vec{x}}_i = \vec{F}_{Di} + \vec{F}_{Mi} \tag{3.5}$$

In this equation, M_i refers to the mass of node i, $\ddot{\vec{x}}_i$ represents the acceleration vector of node i; $\vec{F}_{Di}$ is the drag force exerted on node i, and $\vec{F}_{Mi}$ is the inertia force. Assuming that we know the information including position x_t, velocity $\dot{x}_t$, and acceleration $\ddot{x}_t$of a node at current time step$t$, the updated data at time step $t + \Delta t$ is calculated with Newmark Beta Method [123]. In this case, the kinematic data at time $t + \Delta t$ is expressed as:

$$\begin{aligned}
\vec{x}_{t+\Delta t} &= \vec{x}_t + \Delta t\dot{\vec{x}}_t + \frac{\Delta t^2}{2}[(1-2\beta)\ddot{\vec{x}}_t + 2\beta\ddot{\vec{x}}_{t+\Delta t}] \\
\dot{\vec{x}}_{t+\Delta t} &= \dot{\vec{x}}_t + \Delta t[(1-\gamma)\ddot{\vec{x}}_t + \gamma\ddot{\vec{x}}_{t+\Delta t}] \\
\ddot{\vec{x}}_{t+\Delta t} &= \frac{1}{\beta\Delta t^2}(\vec{x}_{t+\Delta t} - \vec{x}_t - \Delta t\dot{\vec{x}}_t - \frac{\Delta t^2}{2}(1-2\beta)\ddot{\vec{x}}_t)
\end{aligned} \tag{3.6}$$

Where Δt is the increment of time between two consecutive time steps, γ and β are coefficients of the Newmark Beta method ($0 \ll \gamma \ll 1$ and $0 \ll \beta \ll 0.5$), which can be determined based on the desired stability and accuracy of this implicit method and are normally set to 0.5 and 0.25, respectively [124].

If we assume that $\Delta\vec{x} = \vec{x}_{t+\Delta t} - \vec{x}_t$, the above equation can be simplified as:

$$\begin{aligned}
\vec{x}_{t+\Delta t} &= \vec{x}_t + \Delta\vec{x} \\
\dot{\vec{x}}_{t+\Delta t} &= \frac{\gamma}{\beta\Delta t}\Delta\vec{x} - \left(\frac{\gamma}{\beta} - 1\right)\dot{\vec{x}}_t - \Delta t(\frac{\gamma}{2\beta} - 1)\ddot{\vec{x}}_t \\
\ddot{\vec{x}}_{t+\Delta t} &= \frac{1}{\beta\Delta t^2}\Delta\vec{x} - \frac{1}{\beta\Delta t}\dot{\vec{x}}_t - (\frac{1}{2\beta} - 1)\ddot{\vec{x}}_t
\end{aligned} \tag{3.7}$$

As force applied to nodes corresponds to kinematics, **Eqn 3.5** can be rewritten as:

$$M\ddot{\vec{x}}_{t+\Delta t} = \vec{F}(\vec{x}_{t+\Delta t}, \dot{\vec{x}}_{t+\Delta t}, \ddot{\vec{x}}_{t+\Delta t}) \tag{3.8}$$

Substituting **Eqn 3.7** into **Eqn 3.8**, we have:

$$\vec{H}(\Delta\vec{x}) = \frac{M}{\beta\Delta t^2}\Delta\vec{x} - \frac{M}{\beta\Delta t}\dot{\vec{x}}_t - M\left(\frac{1}{2\beta} - 1\right)\ddot{\vec{x}}_t - \vec{F}(\Delta\vec{x}) = 0 \tag{3.9}$$

The implicit equation regarding $\Delta\vec{x}$ is solved with Newton-Raphson method based on iterative method:

$$\Delta\vec{x}^{i+1} = \Delta\vec{x}^{i} - \frac{\vec{H}(\Delta\vec{x}^{i})}{\vec{H'}(\Delta\vec{x}^{i})} \tag{3.10}$$

Where the subscripts i and $i+1$ indicates ith and (i+1) th iterations in solving $\Delta\vec{x}$; in this case, for every iteration, node kinematics are updated. The convergence criteria is $\left|\Delta\vec{x}^{i+1} - \Delta\vec{x}^{i}\right| < \varepsilon$, where ε is the tolerance specified in MBDyn.

3.3.3. Hydrodynamic solver

Numerical simulation of fluid flow was performed with the Open-source CFD toolbox *OpenFOAM,* which offers free access to the source code so that people can modify and build their own code to meet specific requirements. As we intended to simulate the forward fish motion with prescribed deformation equation inside an immovable domain, we were focusing on dealing with dynamic internal mesh motion around the zebrafish model. We have built an in-house dynamic solver to handle the internal mesh with large deformation induced by zebrafish larvae swimming behaviors. In *OpenFOAM, PimpleDyMFoam* solver was used to solve the transient, incompressible and single-phase Newtonian fluids. It is a combination of *SIMPLE* and *PISO* algorithm to address

pressure-velocity coupling [125]. The incompressible conservation equations for mass and momentum are written in **Eqn 3.11** by deriving the general governing equation.

$$\underset{\text{Time accumulation}}{\frac{\partial}{\partial t}\rho\phi} = \underset{\text{Convection}}{-\nabla\cdot(\rho\vec{U}\phi)} + \underset{\text{Diffusive transport}}{\nabla\cdot(D\nabla\phi)} + \underset{\text{Source terms}}{S_\phi}$$

$$\nabla\cdot U = 0 \tag{3.11}$$

$$\frac{\partial\vec{U}}{\partial t} = -\nabla\cdot(\vec{U}\vec{U}) + \nabla\cdot(\upsilon\nabla\vec{U}) - \frac{1}{\rho}\nabla p$$

The first equation is the general governing equation. As the mass is not transferred by diffusion and there is no source term, by substituting ϕ with 1, we can get the mass conservation equation. As the transport of momentum is determined by shear rate tensor υ, and the source terms are pressure force if we neglect the gravitational acceleration, by substituting ϕ with $\vec{U}$ and replace the shear rate tensor based on Laplace Equation, we can get the momentum conservation equation.

In the momentum conservation equation, time derivatives used 2nd order implicit discretization scheme: CrankNicolson, and the pressure source term used cell-limited Gauss interpolation scheme to limit interpolated face values to improve boundedness and stability. Diffusion of transport used Gauss linear for interpolation of the diffusivity, and the convection term applied reconCentral interpolation scheme. In *OpenFOAM*, velocity is stored at the cell centre, and values need to be interpolated to the face centres linearly. ReconCentral interpolates the value in a different way that uses extrapolated gradient-based correction from both sides onto the face, using 1/2 weighting to increase stability for large deformation.

Zebrafish larva swims extremely fast with high tail beat frequency and amplitude, to mimic the forward motion of zebrafish larvae, the CFD solver needs to have both acceptable accuracy and high stability, and the internal mesh motion needs to be appropriately maintained.

The fish body consists of several connected segments, and there exists relative orientation between each two segments, surface meshes in the middle region need to be dealt with appropriately; otherwise, the internal mesh quality around body surface cannot be guaranteed. A schematic diagram depicting the body curvature at the intersection part between two body segments is shown in **Fig. 3-9** (the body curvature before optimization is not available as the solver blows up immediately, only curvature after optimization is shown).

Initial state of the body shape is shown in **Fig. 3-9A**, initially, expressed with four body segments locally, zebrafish body was straight. When the two adjacent body segments moved under constraint equation, the spatial location of intersection point I was determined by the spatial location of Body 1. However, it also belongs to Body 2, which could cause two different coordinates at one spatial location. To solve the problem, a weighting method was applied to determine the surface point spatial location on one body segment with two segments' information. By assuming that surface points on Body 1 and Body 2 were fully determined with point A and B's spatial location, P_A and P_B, we have equation $P_i = (1-\omega)P_A + \omega P_B$, where ω is the weighted parameter represented by the distance between a randomly selected surface point on Body 1 and point A relative to the distance between point A and point B. As the equation involves all the surface points on Body 1, points close to the intersection region could be influenced as well. Farther the surface point is to point A, the less influence point A has on surface deformation, this is reasonable on the intersection point of the two body segments, at this moment, ω equals 1, if the point was assumed to be on Body 1, the surface point is fully controlled by point B. It can be seen in **Fig. 3-9B** that the intersection region is smoothly curved. After the optimization, the body surface is continuous with no overlapping regions to ensure the body volume is conserved between two time steps.

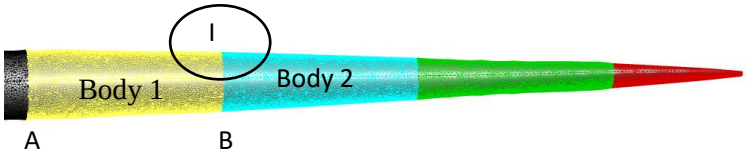

(A)

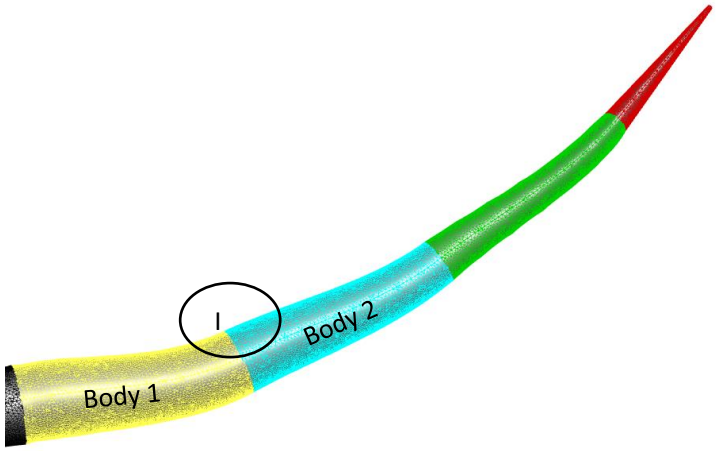

(B)

Figure 3-9. Schematic diagram of the relationship between two body segments. (A) Initial state of local body curvature. (B) Optimized body curvature in the intersection region after the body segments change locations

To keep the accuracy and stability of our results, following modifications have been made for discretization schemes and equation solvers

- 2nd order discretization scheme for time derivative
- Strong Coupling between *OpenFOAM* and *MBDyn*, i.e. inner iterations within one time step
- *ReconCentral* interpolation scheme for velocity
- Minimize relaxation factor for pressure
- BiCGStab solver for velocity equation

3.3.4. Coupling Strategy

Coupling between *OpenFOAM* and *MBDyn* was achieved using communication primitives provided by *MBDyn*. When a fully coupled simulation was performed, both *OpenFOAM* and *MBDyn* ran simultaneously as individual computer processes. Inter-process communication was built with Transmission Control Protocol (TCP) socket. The schematic diagram for fluid and zebrafish larva motion coupling is shown in **Fig. 3-10.** At the start of the simulation, *MBDyn* created a TCP/IP socket, while *OpenFOAM* connected to the socket, establishing a two-way communication. An external force element in *MBDyn* allows to communicate positions and orientations of a set of nodes, and the corresponding linear and angular velocities with *OpenFOAM*. In general, within one time step, there were approximately 20 inner iterations to exchange data between *OpenFOAM* and *MBDyn*, which has ensured that the two CFD solvers were fully coupled and the results were converged and accurate. The fluid force and moments integrated in the CFD solver for every patch were transmitted to *MBDyn*. Using the force data, *MBDyn* calculated the structural response of the system, i.e., the kinematics of the geometric nodes and the nodes containing information of body were sent back to *OpenFOAM*. Once *OpenFOAM* received kinematic information, the information was stored in the Centre of rotation (CoR) of each body segment to determine the surface points' information. Internal mesh deformation values were interpolated based on the surface points, forces and moments were calculated based on the updated positions and orientations of current and previous iterations implicitly and transmitted back to *MBDyn*. *MBDyn* received these data and updated to the new positions and orientations. Once the convergence criteria set in *OpenFOAM* were satisfied, the transmission came to an end and jumped to the next time step until reaching the final step to end the entire simulation.

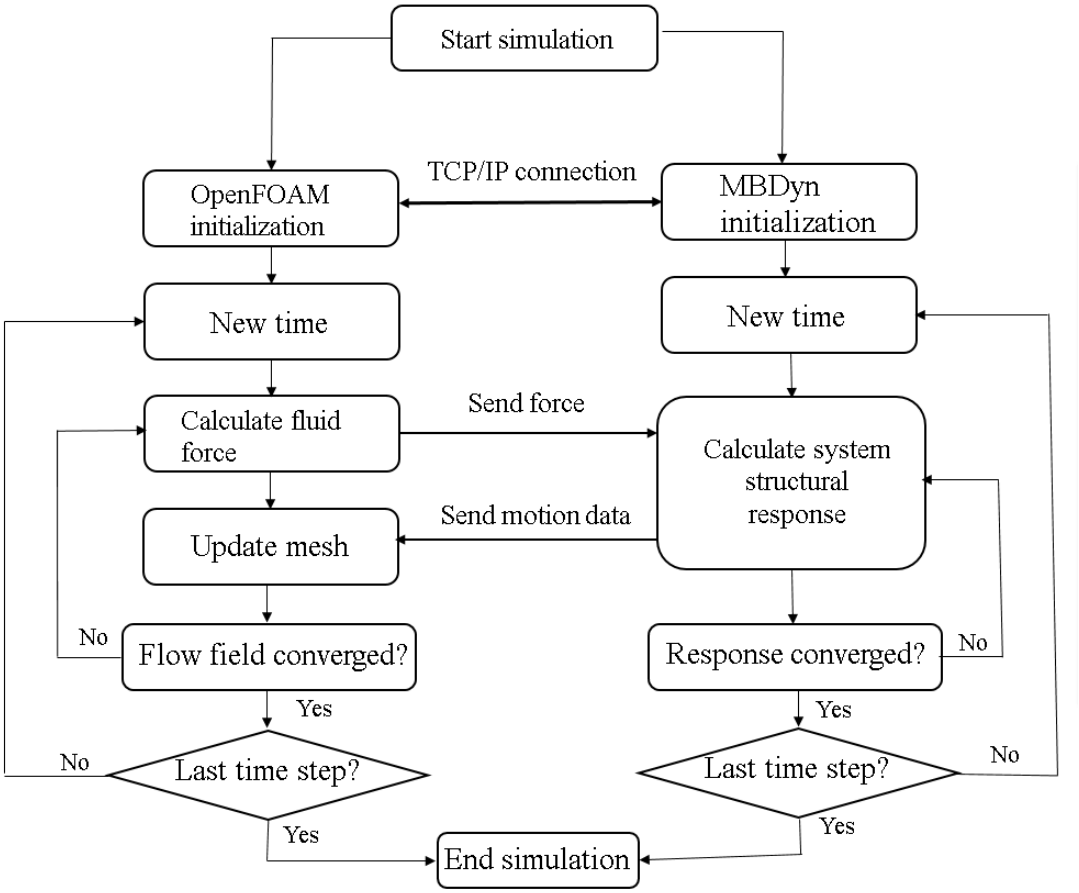

Figure 3-10. Flow chart describing the data transmission between OpenFOAM and MBDyn

3.4. Concluding remarks

In this chapter, a novel zebrafish larva model used to simulate the experimentally observed zebrafish larvae locomotion under various drug applications is presented based on a fully coupled numerical tool developed under CFD-MBD framework. The various experimental and numerical methods are discussed in detail. The experimental measurements start from video recordings on real zebrafish larvae locomotion and followed by extractions on zebrafish larvae motion equations with in-house *MATLAB* code. This part provides the most straightforward and credible data for zebrafish locomotion under different conditions.

The open-source CFD toolbox *OpenFOAM* is utilized to model fluid flow around zebrafish larvae during the forward motion. The surrounding boundary conditions are

set to be consistent with the real experimental environment of zebrafish larvae. The open-source solid body dynamics tool *MBDyn* is employed for calculating structural responses of rigid components in a multi-body system. The input data originates from the extracted data with in-house *MATLAB* code from experiments. The two separate solvers *OpenFOAM* and *MBDyn* are coupled via an interface library implemented to exchange force and motion data.

4 Numerical Validations

The methodology we have developed needs to be validated. In the present thesis, we have divided the validation contents into two parts, the first part is the validation of numerical coupling of *OpenFOAM* and *MBDyn,* and the second part is the validation of the simulation based on real data observed from the experiment and post-processed with in-house *MATLAB* code. As the zebrafish model is three-dimensional (3-D), our validation started with a two-dimensional (2-D) multi-body structure and followed by a 3-D validation. The following sections will include the mandatory validations.

4.1. Validation case for flow solver

The numerical methodology included a strong coupling technique between *OpenFOAM* and *MBDyn* to solve the typical FSI interactions of a self-propelled zebrafish larva model and the surrounding fluid. Validation on multi-body structure was firstly made. We have chosen a multi-body structure inspired by jellyfish provided by Wilson [126]. Wilson has extracted a 2-D multi-body model based on the real silhouette of jellyfish, which is depicted in **Fig. 4-1A**. The black dot indicates secants used to divide the centreline of jellyfish body and the body segments are expressed with mutually buoyant rigid elliptical bodies shown as **Fig. 4-1B**. In this figure, the relative angle between each two ellipses is prescribed from a sequence of snapshots of the outline of this jellyfish body over two contraction cycles. The captured values are depicted in **Fig. 4-1C**, based on those points, sinusoidal functions have been fitted and expressed with **Eqn 4.1**. The unit of time and theta are second and rad, respectively. Left-right symmetry is required for the structure and the prescribed kinematics, therefore, only half of the body information is required. By specifying relative orientation equations between each two segments, the jellyfish model can move upwards with alternant contraction and refilling. To scale the coordinates, an effective length L was defined as the arc length from the orifice lip to the inner most hinge (hinge 3). As shown in **Fig. 4-1B**, H and D denotes

the height and diameter of the model, respectively. Based on the two parameters, during contraction and refilling movements, additional two length scales were defined: the mean height of the bell, where $H/L{\sim}0.67$, and the maximum diameter of the bell, D_{max}, where $\frac{D_{max}}{L}{\sim}2.1$. The values for mean height and maximum diameter of bell were determined during the simulation [127]. As the case for zebrafish forward swimming did not include passive joint, fully prescribed constraints on hinges with kinematic Reynolds number equivalent to 140 were selected for comparison. The definition of Reynolds number is based on the prescribed hinge kinematics including the maximum diameter and undulation period, expressed as $\frac{D^2 max}{T\upsilon}$, where υ is the fluid kinematic viscosity. In *OpenFOAM*, mesh around jellyfish model was fully unstructured depicted in **Fig. 4-1D**. As the jellyfish model is two dimensional, the length in z direction is set as 1.

$$\begin{aligned}\theta_1 &= -0.147\cos(6.538t) - 0.325\sin(6.538t) + 0.7551\\ \theta_2 &= -0237\cos(6.456t) + 0.164\sin(6.456t) + 0.3472\\ \theta_3 &= -0.082\cos(6.427t) + 0.041\sin(6.427t) + 0.4511\end{aligned} \tag{4.1}$$

For the simulation on jelly fish longitudinal motion, there were approximately 100000 cells in total in the fluid domain, with a time step size of 1/1000 T. Numerical schemes used for the case have been stated in the methodology chapter, 2nd order time discretisation scheme has provided good accuracy for the simulation. Comparison of kinematic performance of jellyfish motion was carried out including the longitudinal centroid position and velocity. Here, both of the parameters were non-dimensionalized with the mean height, expressed as $\frac{Y_C}{\bar{H}}$ and $\frac{V_C T}{\bar{H}}$, respectively. As shown in **Fig. 4-2A**, the longitudinal centroid position of jellyfish is moving upwards as time evolves, and the longitudinal centroid velocity is gradually increasing towards a constant state after approximately four periods of time (shown as **Fig. 4-2B**). Both of the comparisons are slightly different from the past studies, these are most likely to be caused by the different hinge kinematics extracted from the scattered points depicted in **Fig. 4-1C.**

Depending on various curve fitting toolbox and methods, the fitted sinusoidal functions can be slightly different. Unfortunately previous data used by the author is not accessible.

Besides, the required input hinge power was compared, which mimics the muscle power provided by relative angle orientation function applied on hinges to power jellyfish's longitudinal motion. Power required to activate hinges should be equal to the sum of power resulting from the rate of change of kinetic energy of the system of bodies and rate of change of energy stored and released as they are deflected minus the work done by the fluid to the system of bodies, which is $W_h = \dot{E}_S + \dot{E}_b - \dot{W}_f$. The deflecting power was calculated with the sum of power of all the hinges, which is $\dot{E}_S = \sum_{i=1}^{n-1} k_i(\theta_i - \theta_{e_i})\dot{\theta}_i$, *n-1* is the number of hinges and k_i is the stiffness of hinge *i* .The power of the system of bodies was calculated with $\dot{E}_b = \sum_{i=1}^{n} (A_i(\dot{x}_i \cdot \ddot{x}_i) + J_i\dot{\alpha}_i\ddot{\alpha}_i)$, where A_i is the area of body *i* and J_i is the polar moment of inertia of body *i*. **Fig. 4-2C** depicts the comparison of required input power of hinges between validation paper and our simulated results. The component has been normalized by the mean input power to the actuators, it can be seen from the figure that the curve matches well with the previous result but only a slight increase for the wave crest and trough values for our simulated results. In addition, a comparison of vorticity at 140 Reynolds number has been made (depicted in **Fig. 4-2D**). The figure illustrates vorticity contours during bell contraction at t/T=2.3 for fully active swimmers. A developing starting vortex is attached to the lip of the orifice on each side, followed by a pair of fully developed vortices downstream. Due to the low Reynolds number, the vorticity diffuses quickly downstream, thus only one pair of vortices is captured in the simulated case.

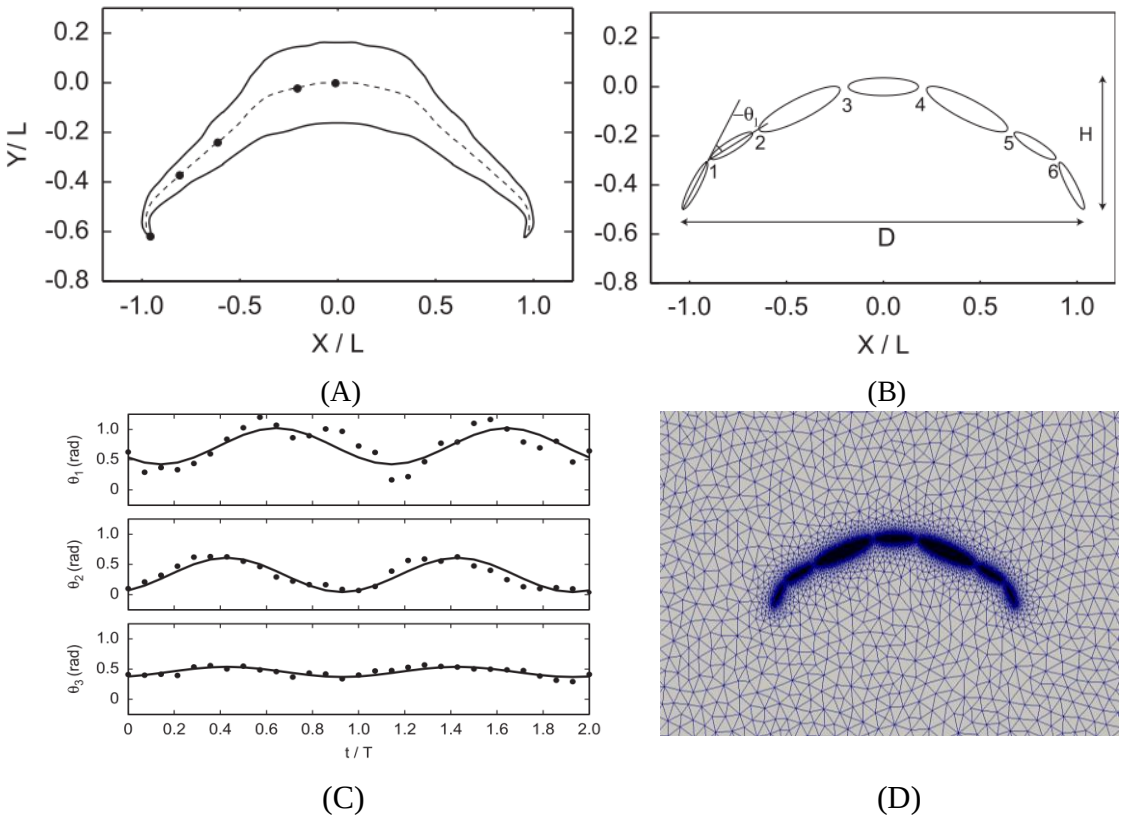

Figure 4-1. (A) Extracted jellyfish body model from real outline. (B) Divided jellyfish body expressed with mutually buoyant ellipses. (C) Fitted sinusoidal curves used to extract relative orientations equations of two adjacent ellipses based on jellyfish contraction and refilling motion.(D) Jellyfish model in OpenFOAM [126]

A sketch of vorticity development is shown in **Fig. 4-3** to further describe the jellyfish model longitudinal motion. In this figure, a total of three cycles are illustrated, and each column represents one period of time. In each cycle, the jellyfish swimming consists of a bell contraction phase and relaxation phase. During the contraction phase, the bell pushes inward, and the water is expelled from the bell cavity to push the entire body moving forward. A starting vortex is attached to each lip of the orifice, accompanied with a pair of vortices downstream in the wake. When the model is fully contracted, the attached vortices on the lip are moving downstream away from the body. During relaxation phase, a pair of stopping vortices are formed inside the bell cavity, and the directions are opposite to the starting vortex formed in the contraction phase. When the bell is fully relaxed, the new cycle starts with another contraction phase, and the stopping vortex in the previous relaxation phase still exists for a while, and will interact

with the starting vortex in the current cycle to form vortex with larger volume.

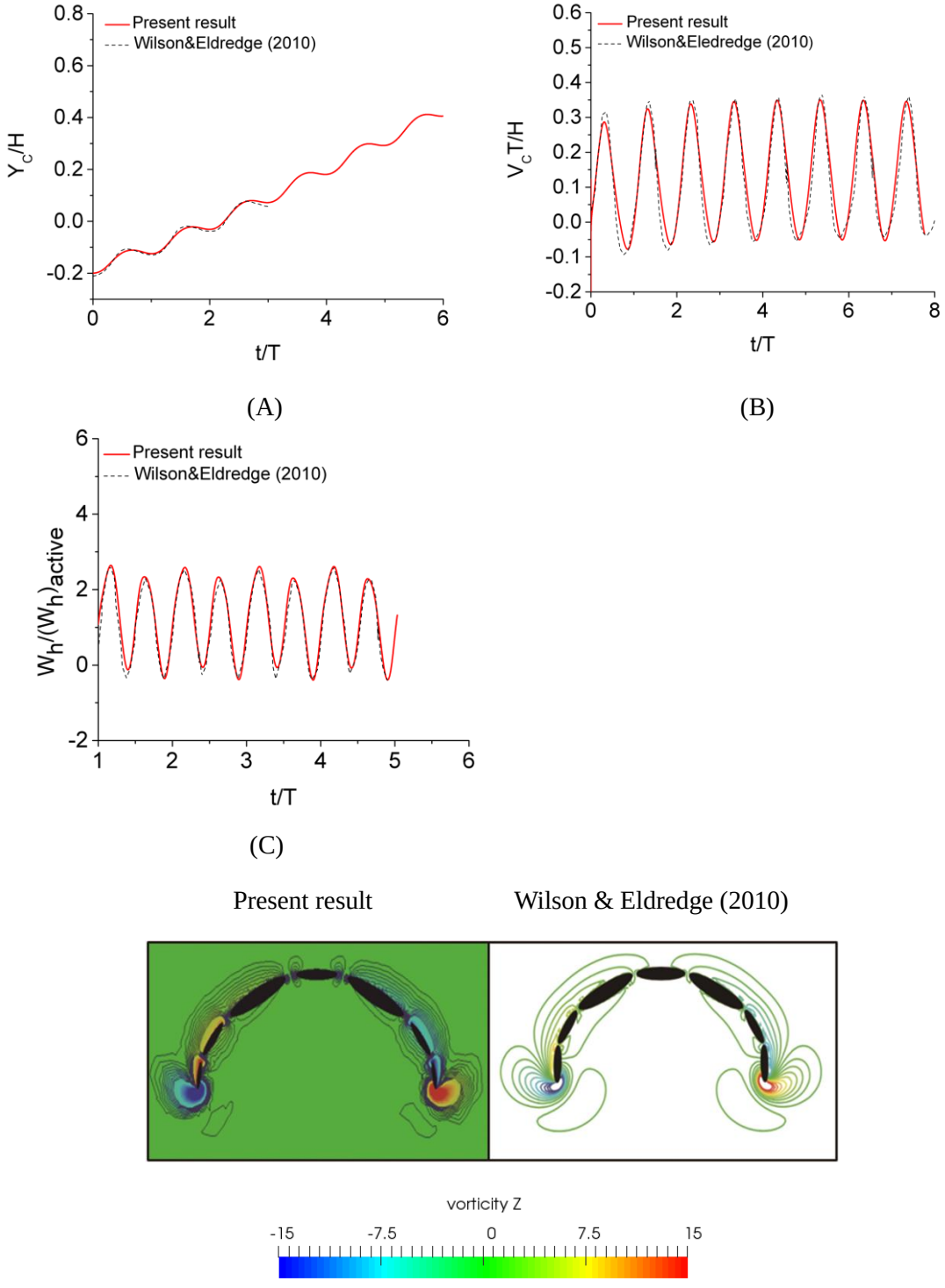

Figure 4-2. Kinematic and dynamic results comparisons between current simulation and validation paper at Re = 140. (A) Longitudinal centroid position (B) longitudinal centroid velocity (C) Required input power (D) vorticity contour comparison with Wilson & Eldredge's results at t/T = 2.3 [126].

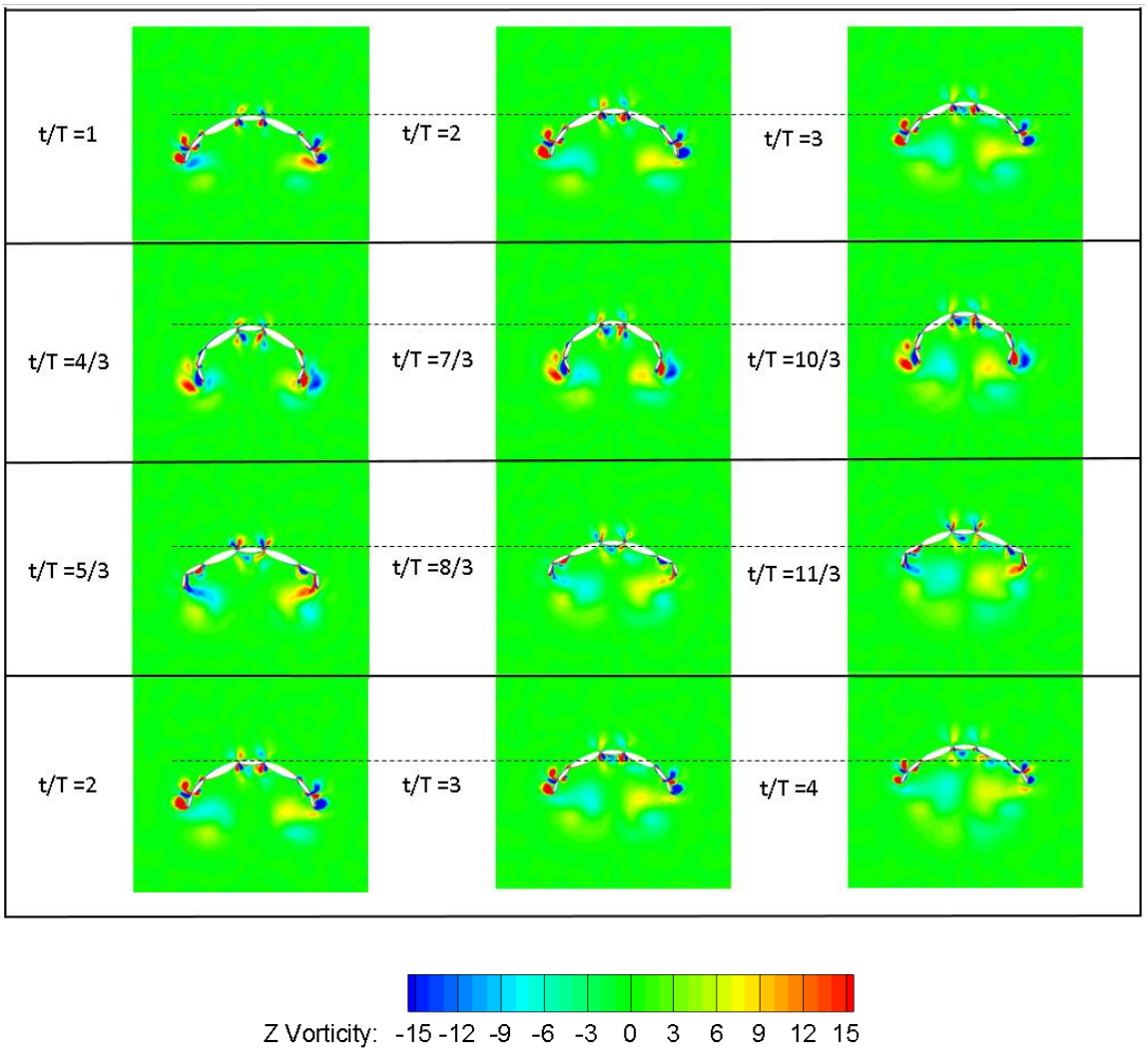

Figure 4-3. Vorticity development first three cycles at Re = 140. Left-most column indicates first cycle, and right-most column indicate third cycle. Dashed lines describe relative motions among three cycles.

4.2. Zebrafish larvae forward motion validation

4.2.1. Validation on forward motion kinematics

To validate whether the numerical methodology could simulate the real forward motion of zebrafish larvae, we have compared the kinematic performance of zebrafish larvae model with the real fish locomotion observed with high-speed camera. The zebrafish larvae body deformation equations were provided as inputs for *OpenFOAM* solver and the equations we have used is shown in **Table 4-1**. This is only a set of equations used for validation in this chapter, different equations have been extracted for different

zebrafish samples to exclude the individual effects in chapter 5. In this case, the fish larva generates a body wave travelling down its body at a near constant rate, therefore, frequency for all equations was assumed to be constant.

The real zebrafish larvae forward velocity was calculated with the changing positions of centre of mass obtained from *MATLAB* post-processing toolbox, and fitted to a sinusoidal curve. As the equations can only specify the relative orientations of two adjacent body segments, the angle variation of the first (head) and last (tail) body segments are not prescribed, therefore, we compared the head and tail angle first between experiments and numerical simulation. In **Fig. 4-4(A-B)**, the black curve indicates the simulated head and tail angle, as the fish is moving cyclically, the resulting head and tail angle values should evolve like a sinusoidal curve with time. The captured head and tail angle data (shown as red dot) at some specific frames from the recorded videos supports the result, showing that the experimental data fits well with the simulated angle curve. In **Fig. 4-4C**, we have depicted 8 midlines of zebrafish larvae for approximately two tail beat cycles. The midlines were extracted from binary images selected with relatively large tail beat amplitudes. X and Y coordinates were normalized with fish body length to express the distance travelled more straightforward.

As can be seen from the figure, the fish is moving forward almost parallel to X axis (with a slight angle deviation less than 10 degree). In the anterior part of the curve (approximately 20%), the bending is not significant, supporting the assumption that the anterior part is too stiff to undergo bending, expressed as zero relative orientation between the first two segments shown in **Table 4-1**. **Fig. 4-4D** shows comparisons of forward velocity. In *OpenFOAM*, the forward velocity was calculated with the centre of mass (COM) of simulated fish model.

Table 4-1. Zebrafish larvae body deformation equations

Relative orientation between two segments (rad)	Function $2\pi f = 397.9$
θ_1	0
θ_2	$-0.1465\cos(2\pi ft) + 0.1346\sin(2\pi ft)$
θ_3	$-0.1245\cos(2\pi ft) + 0.1327\sin(2\pi ft)$
θ_4	$-0.1542\cos(2\pi ft) + 0.1294\sin(2\pi ft)$
θ_5	$0.1565\cos(2\pi ft) + 0.2264\sin(2\pi ft)$
θ_6	$0.1723\cos(2\pi ft) + 0.2724\sin(2\pi ft)$
θ_7	$0.2123\cos(2\pi ft) + 0.184\sin(2\pi ft)$
θ_8	$0.2458\cos(2\pi ft) + 0.2673\sin(2\pi ft)$
Span-wise length (mm)	0.4

As shown in **Eqn 4.2**, the position vector P_{COM} was calculated by dividing the sum of the product of each body segment m_i and position vector P_i. The total fish body mass is expressed with m_{body}, and the simulated zebrafish model forward swimming speed is approximately $17.25 l_{body}/s$, and the experimentally observed speed is about $19 l_{body}/s$. The slight difference between experiment and CFD simulation on forward velocity, which is about 10%, can be caused by the slight discrepancies in morphology. Also, insufficient accuracy of the fish midline extraction might lead to slight inconsistency in certain captured points along the body, and this could influence the Fourier series curve fitting, or most likely, due to the fact that the real fish changes its body wave shape instantly during each tail beat cycle, leading to small changes in swimming speed, which will not occur in the prescribed cyclic swimming of the CFD fish model [104]. To make the swimming speed value more persuasive, we have collected the simulated results for ten zebrafish larvae and made comparisons in **Fig. 4-4E**. Besides, from **Fig. 4-4C**, it is also possible to estimate the experimentally observed swimming speed to be around $19 l_{body}/s$.

$$P_{COM} = \frac{\sum m_i P_i}{m_{body}} \tag{4.2}$$

Zebrafish larvae tend to swim in an intermediate flow regime with Reynolds number ranging from 10 to 1000, and it has been studied that larvae fish always require higher Strouhal number than adult fish [113]. To validate the simulation, Strouhal number was calculated for simulated CFD results. The Strouhal number (St) is a dimensionless number describing oscillating flow mechanisms and is defined as $\frac{Af}{U}$ in swimming animals, where A is the tail beat peak-to-peak amplitude, f is the tail beat frequency and U is the averaged swimming velocity. In the simulation, the Strouhal number was approximately 0.8. Considering the desired Reynolds number, our result is in reasonable range between 0.69 and 1.07 stated in Li's paper [79], suggesting that the simulation meets the requirements of a real zebrafish larvae. Besides, comparison on the gestures of fish swimming between CFD simulated motions and experimentally observed motion were made, together with the detached vortices in **Fig. 4-5**, the figure depicts the vorticity iso-surfaces formed based on Q Criterion behind a swimming normal zebrafish larva at different instants in time within one time period and the dorsal view for vorticity iso-surfaces. Here, Q can describe the wake topology and defines vortices as positive second invariant of velocity gradient in region where vorticity magnitude is greater than strain-rate magnitude [128].

As seen from the left-most and right-most column of **Fig. 4-5**, flow patterns behind the fish are represented by detached vortices and shown as translucent green fragments. Vortices start to form in the vicinity of the head, transmit downstream to tail and detach at the tail, which are consistent with the fish tail motion; when the lateral displacement of the tail reaches the highest amplitude, vortices start to shed at the tail tip, the already formed vorticity in the wake are mixed with the newly formed vorticity at tail tip. The right-most column also displays a 3-D view of the vortex rings generated behind the fish to understand formation of flow patterns better. To validate the numerical methodology, **Fig. 4-5** also compares the body curvatures of CFD model and the real

fish in the recorded experiment video. As can be seen, two sets of results match very well in terms of body shape at all specific time within a period, indicating that our CFD model is able to imitate the self-propelled swimming of zebrafish larva and its interactions with surrounding fluid.

4.2.2. Grid independence & sensitivity test

Under the consideration of economic cost in calculation, a grid independence test is necessary to be carried out on a self-propelled zebrafish with fully prescribed deformation under two mesh sizes, medium and fine mesh. In addition, the time step influence is also tested, e.g. Case 1: Medium mesh (M) with 83200 total cells and time step of T/650, Case 2: Medium mesh & smaller time step (MS) of 83200 cells and time step of T/1300, and Case 3: Fine mesh (F) of 166400 cells and time step of T/650. The size of the fluid domain and body deformation equations remain the same for three cases. Details of the kinematic input data is shown in **Table 4-1**.

To exclude mesh resolution and time step size influences on simulation results, we have compared the forward velocity and total force of zebrafish larvae in E3 medium and the results are shown in **Fig. 4-6(A-B)**. Computational results for three cases including kinematic performance and fluid domain calculation show close results. To save computational time and keep accuracy, we used the mesh formation and time step size the same as Case 1 for the entire following calculation.

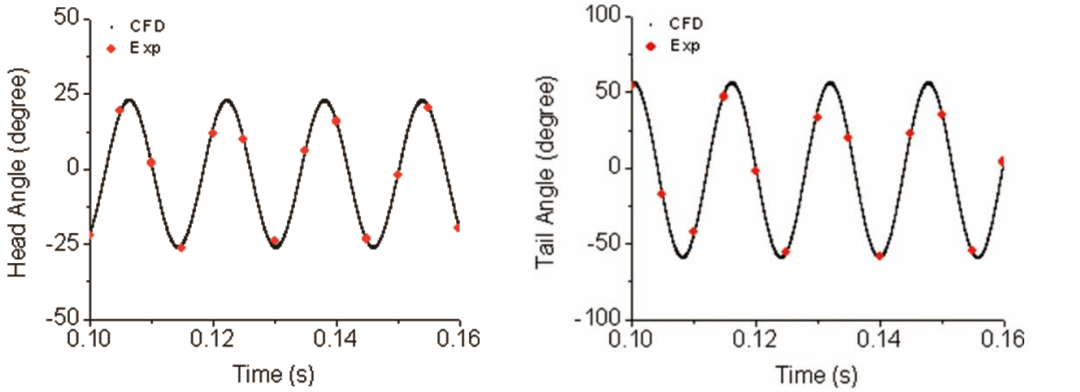

(A)

(B)

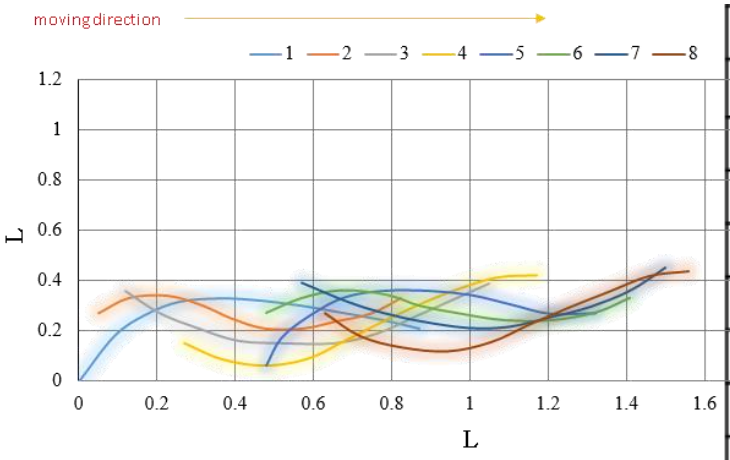

Backbone	Record time
1	2.44ms
2	7.25ms
3	12.16ms
4	16.98ms
5	22.02ms
6	27.13ms
7	32.34ms
8	38.46ms

(C)

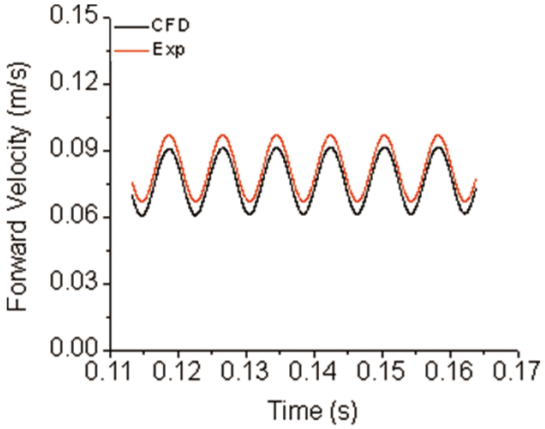

(D)

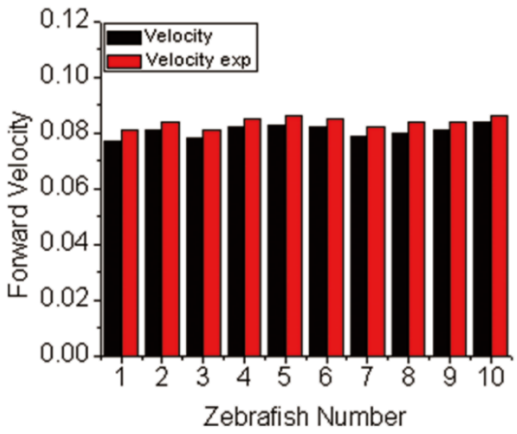

(E)

Figure 4-4. Comparison results beteween experiments and CFD simulation. (A) Head angle (B)Tail angle (C) Zebrafish midline for two full tail beat cycles derived from high speed camera of 500 fps, and normalized with body length L. (D) Forward velocity(E) Velocity comparison for 10 different zebrafish larvae.

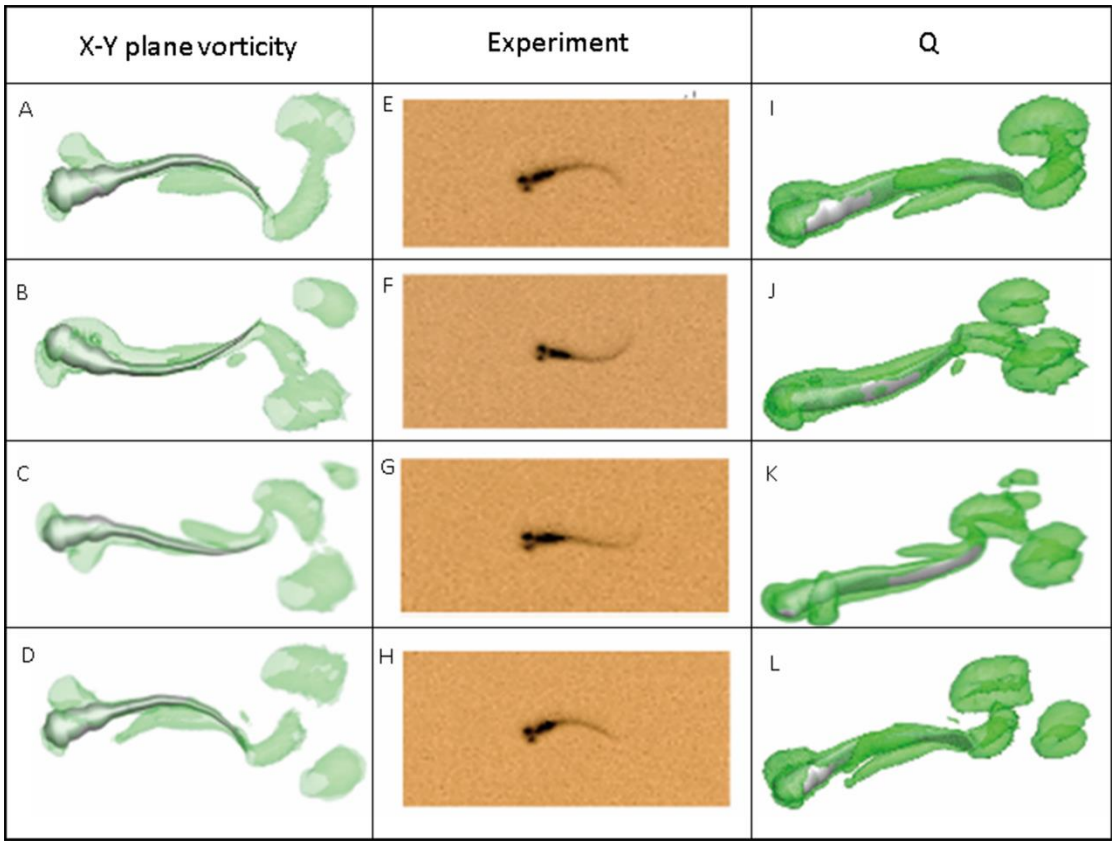

Figure 4-5. Vortex rings behind zebrafish larva for Q=0.5 at different time step within one period of time and the corresponding video record for the experiment. X-Y plane vorticity is a 2-D view of the 3-D vortices which can compare the body curvature with experiment results easier. From A-D, E-H and I-L, time steps are 0, T/3, 2T/3 and T for each column. T represents one period of time.

In addition, the sensitivity of the results to body segments of zebrafish larvae model has been tested with CFD simulation. Considering the accuracy and efficiency for body segmentation, we have divided the body trunk into 5, 10 and 15 segments, respectively. By capturing the body deformation with *MATLAB* toolbox and simulate the forward motion with CFD toolbox, we have compared the forward velocity and total hydrodynamic force in **Fig 4-6(C-D),** indicating that the simulation results are not sensitive to the number of body segments ranging from 5 to 15.

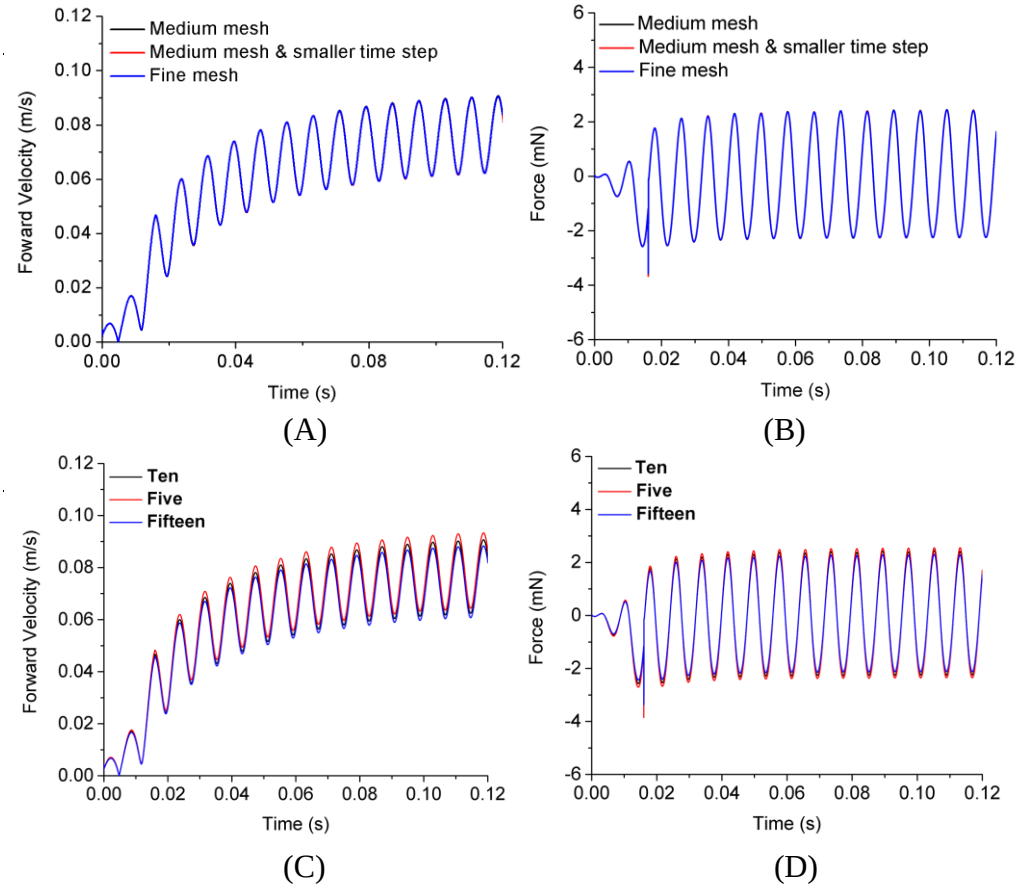

Figure 4-6. Grid independence test with acetic acid treated zebrafish larva sensitivity study. (A) Forward velocity for three levels of grid. (B) Total force in the moving direction for three levels of grid. (C) Forward velocity for three numbers of segmentations. (D) Total hydrodynamic force for three numbers of segmentations.

4.3. Concluding remarks

In this chapter, the present in-house code involving numerical methodology and *MATLAB* post-processing is validated through a jellyfish inspired multibody structure and experiments. Kinematic and dynamic performances of a 2-D jellyfish inspired structures are compared, including displacement, velocity, and input power, etc. The present simulation results agree well with those from literature. Additionally, the sensitivities of the present flow solver to some parameters (e.g. grid density and time step) are checked in this chapter. It is concluded that with sufficiently dense grid and small time step, good convergence can be achieved by the present CFD code.

Besides, parameters such as velocity and tail beat angle calculated from the numerical simulation are compared with those accessible from real experiments. Validations on these consistency are fulfilled from different aspects. The initial visual similarities are presented with fish body curvature changes during one period of time, and these similarities are quantified with head and tail beat angle and forward velocity. Moreover, the forward velocity is calculated in various methods, including experiments and numerical simulations based on COM, and straightforward mathematical calculation from time and body curve displacement. Results agree well between experiment and numerical simulation.

In summary, the validation and sensitivity studies of the present FSI solver are carried out in this chapter. It can be concluded that the present FSI solver has acceptable order of accuracy to investigate FSI applications related to experiments on zebrafish larvae.

5 Numerical Analysis of Drug Influences on Zebrafish Locomotion

5.1. Comparisons of kinematic and energetics with drug treatment

5.1.1. 0.01% acetic acid effects due to nociceptive responses

Nociception study on fish is becoming more and more dominant in the current research field. As acetic acid has been validated to be able to trigger nociceptive responses, we intend to study kinematic and dynamic performances of zebrafish larvae under 0.01% acetic acid induced nociceptive responses. Choice of the acetic acid concentration was determined based on previous work indicating that 0.01% acetic acid can to some extent stimulate zebrafish larvae swimming [72]. Detailed experimental setup has been stated in the methodology chapter, here we will focus on the numerical simulation results.

The influences from 0.01% acetic acid on kinematic performances of 5 dpf zebrafish larvae were firstly studied. Extracted body curvature equations after acid treatment have higher averaged frequency compared with those of control group. This is quite reasonable as acetic acid treated zebrafish might accelerate quicker to reach the maximum speed and escape the acid environment [88]. As depicted in **Fig. 5-1**, comparisons on the trajectory of COM for control and acetic acid treated groups are presented. COM displacement in x direction represents the forward distance moved by zebrafish larva within recorded time, and it is evident that after 0.01% acetic acid treatment, within same time range, the zebrafish larva tends to swim longer distance. Also the slope of the lines reach a constant value for both control group and acid treated group, suggesting that velocity is constant. COM displacement in y direction describes the deflection in y direction during forward motion. This might be sensitive to many factors including body deformation equations, thus results can be different. From **Fig. 5-1(B)**, it is evident to find that after approximately ten full tail beat cycles, the y direction deviations for both control group and acid treated zebrafish are less than 10%

of body length, leading to an acceptable 6 degree deviation angle. Besides, the head and tail angle and forward velocity have been compared respectively before and after 0.01% acetic acid treatment. There is a slight increase in maximum tail beat angle after treated with acetic acid, but the head turning angle does not show any significant changes. This might be due to the assumption that the anterior part of zebrafish larvae (approximately 20% of body length) is stiffer than the other part, therefore, the changes of head region curvature due to nociceptive stimuli might not be as obvious as the tail region. Considering the tail beat angle, there is an approximately 7 degrees' of variation before and after acid treatment. The value cannot be regarded as significant, whereas considering the forward velocity, the increment is much more significant, which suggests that to reach higher speed, increasing tail beat frequency would be more effective than increasing tail beat amplitude. This assumption has already been studied by other researchers with similar conclusions [76, 114]. Muller added new ideas based on his research on different ages' zebrafish larvae [129], suggesting that for younger larvae, tail beat frequency is the primary method to reach higher speeds, whereas for older zebrafish larvae, both frequency and amplitude contribute to the increase of forward velocity. This is quite reasonable as our simulation has revealed that both frequency and tail beat amplitude have increased, resulting higher forward speed.

In addition, comparisons on body moment of inertia J_{body} and body angular velocity ω_{body} were carried out. For the zebrafish model, the body moment of inertia was calculated with **Eqn 5.1** and body angular velocity was derived from the momentum equation **Eqn 5.2** and calculated with **Eqn 5.3**. In **Eqn 5.1**, the mass of body segment i is expressed with m_i, and the position vector of the body segment centre in the fish reference frame is expressed with $r_{mov,i}$ and equals $r_i - r_{com}$. In **Eqn 5.2**, $J_{com,i}$ is the moment of inertia of i^{th} body with respect to centre of mass and is calculated with **Eqn 5.4**, J_i is the moment of inertia about the vertical central line of each body segment. In this case, we assumed each body segment as ellipsoid, thus the moment of inertia about the vertical Z-axis was approximated as $\frac{1}{5}m_i(a^2 + b^2)$, where a and b is

the radius of other two elliptical planes. Angular velocity $\omega_{com,i}$ can be calculated by dividing the cross product of $r_{mov,i}$ and $\dot{r}_{mov,i}$ by $r^2{}_{mov,i}$. As the fish model locomotion in the direction perpendicular to forward motion was constrained (which is consistent with the real zebrafish larvae cyclic swimming) [75], the angular velocity can be calculated with **Eqn 5.5**. As can be seen from **Fig. 5-1(E-F)**, the calculated maximum body angular velocity after 0.01% acetic acid shows a slight increase, the change is probably due to increased body lateral displacement and frequency. Whereas the averaged body moment of inertia value does not change significantly as the deflection angles of the forward motion relative to the x axis for both control and acid group are similar. To better quantify the kinematic characteristics, comparisons on the angle in global frame of each body segment before and after 0.01% acetic acid treatment were made in the following section.

$$J_{body} = \sum_i J_i + m_i r^2{}_{mov,i} \tag{5.1}$$

$$J_{body}\omega_{body} = \sum_i J_{com,i}\omega_{com,i} \tag{5.2}$$

$$\omega_{body} = \frac{\sum_i J_{com,i}\omega_{com,i}}{J_{body}} \tag{5.3}$$

$$J_{com,i} = J_i + m_i r^2{}_{mov,i} \tag{5.4}$$

$$\omega_{com,i} = \frac{\dot{r}_{ymov,i} r_{xmov,i} - \dot{r}_{xmov,i} r_{ymov,i}}{r^2{}_{mov,i}} \tag{5.5}$$

In order to better understand the changes of kinematic characteristics after 0.01% acetic acid treatment on zebrafish, angles of all body segments were compared within one period of time (shown as **Fig. 5-2**). For the anterior part of the body, the angles tend to keep constant after acid treatment, whereas for middle and posterior region, the angles tend to increase after acid treatment, which are consistent with our findings in the previous paragraphs.

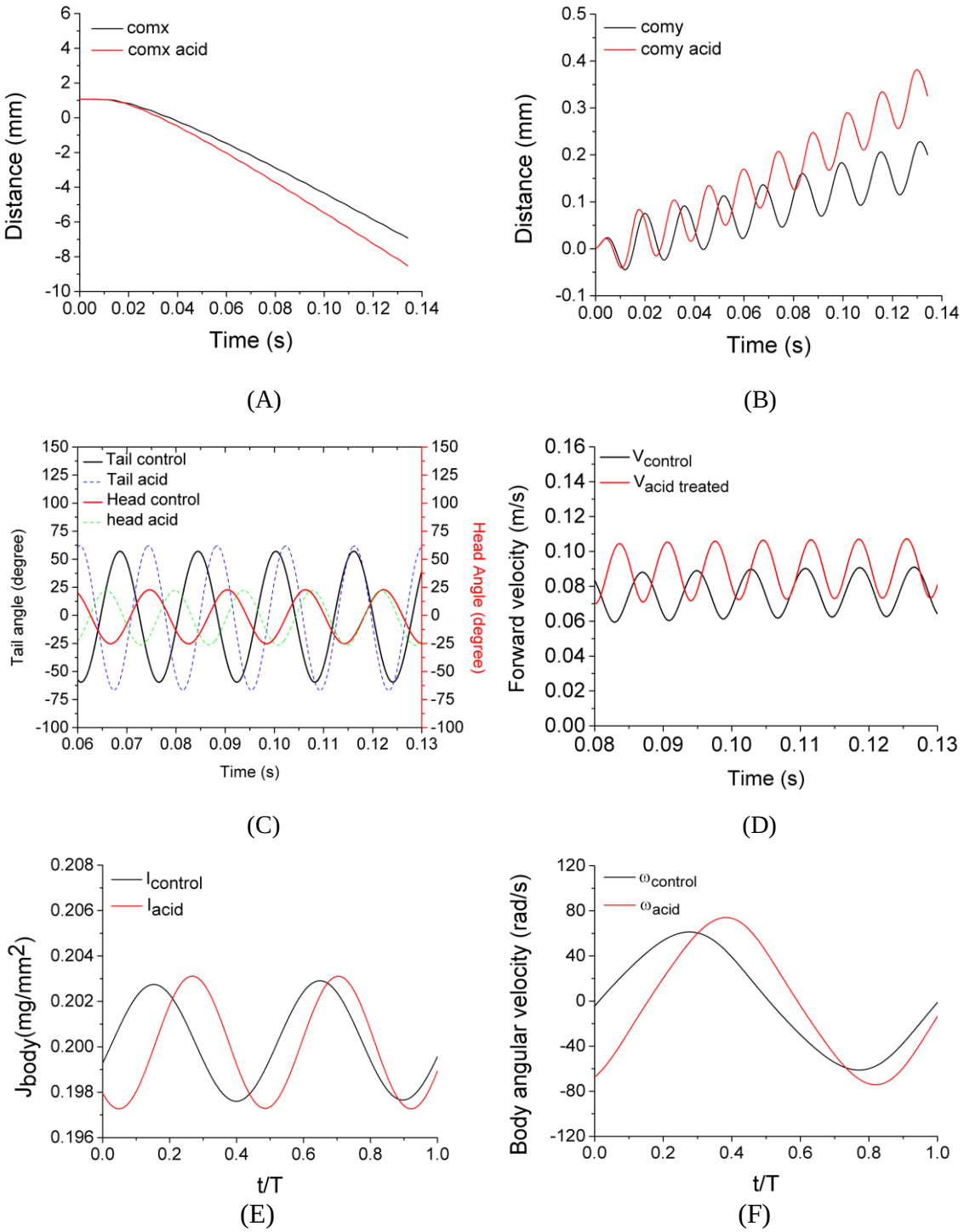

Figure 5-1. Kinematic performance before and after 0.01% acetic acid treatment. (A) COM in x direction comparison. (B) COM in y direction comparison. (C) Head and tail angle comparison (D) Forward velocity comparison during cyclic swimming, the image does not include the startle stage. (E) Body moment of inertia comparison before and after 0.01% acetic acid treatment. (F) Body angular velocity comparison before and after 0.01% acetic acid treatment.

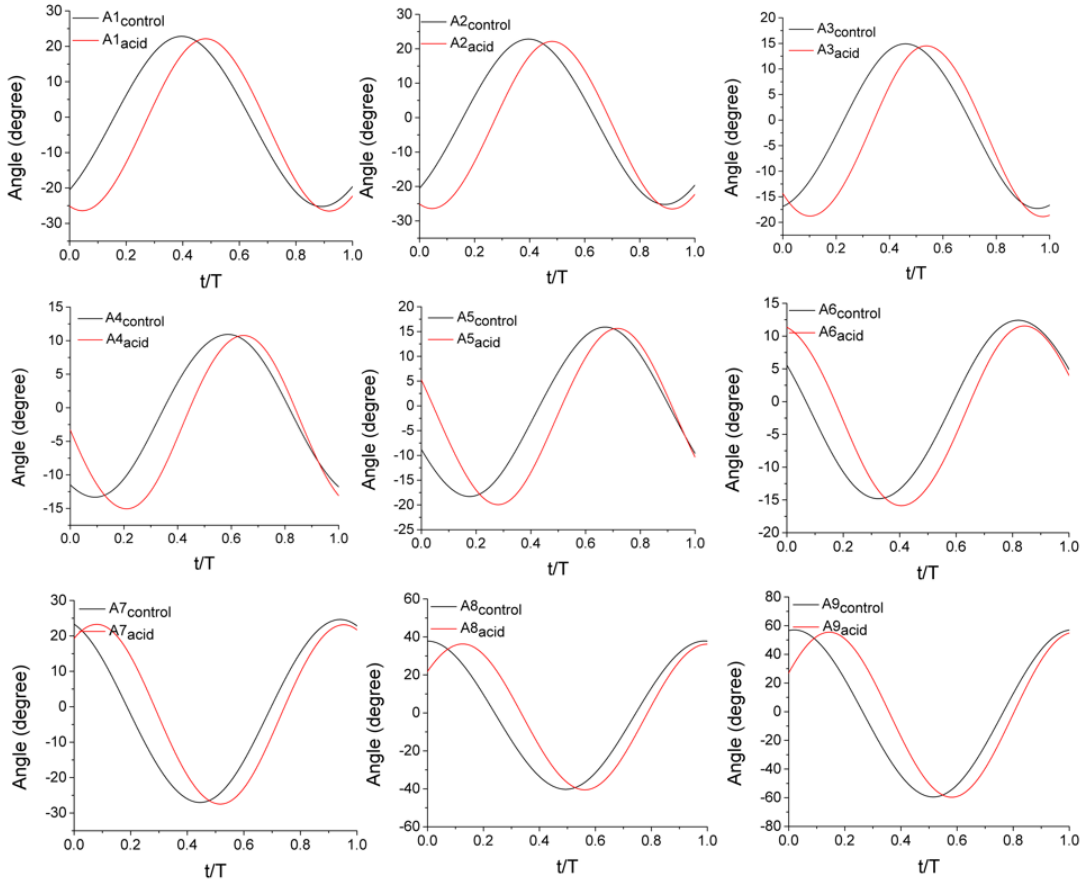

Figure 5-2. Angle of all body segments relative to the global frame comparisons before and after 0.01% acetic acid treatment within one period of time. Angles for all body segments are expressed as A1-A9.

Compared to kinematic characteristics, dynamic performances including force and power are not that straightforward as they can be hardly acquired with direct observations or camera recordings. In this chapter, hydrodynamic and mechanical power consumption during self-propelled forward motion will be studied. As the movement of each two neighbouring body segments was constrained with a prescribed deformation equaiton except for fish head and tail, mechanical power contribution along fish body can be approximated by power generated by vitual joint between each two body segments. During muscle contraction, fish body bends, energy is generated and transmitted into the water, and the bended body interacts with the surrounding fluid, a thrust force generates and pushes the fish moving forward. Within this process, Approximately 20% of the energy (depending on fish species, the percentage can float dramatically) [130] generated by muscle contraction is consumed due to the viscous

dissipation of fish body tissues, and the remaining energy is transmitted into the water. In our model, viscous dissipations of fish body tissues were neglected to simplify the simulation. During cyclic swimming, as a continuous fish body, the total kinetic energy expressed as **Eqn 5.6** is zero, therefore, all the effective mechanical energy generated by fish muscle is used to balance the external energy (shown as **Eqn 5.7 and 5.8**). The mechanical power generated from fish muscle includes the translational power due to linear motion and the rotational power due to body rotation, in this case, all the other terms are cancelled out except for the rotational power. Therefore, the mechanical power was estimated with the cross product of torque and angular velocity expressed with **Eqn 5.9**, and the total power transmitted into the water is expressed with **Eqn 5.10**.

$$W_{internal(fish\_to\_fish)} + W_{external(fluids\_to\_fish)} = \Delta E_{fish\_kinetic} = 0 \quad (5.6)$$

$$W_{internal(fish\_to\_fish)} = -W_{external(fluids\_to\_fish)} \quad (5.7)$$

$$P_{internal(fish\_to\_fish)} = -P_{external(fluids\_to\_fish)} \quad (5.8)$$

$$P_{internal(fish\_to\_fish)} = \sum_i M_i \cdot \omega_i \quad (5.9)$$

$$P_{external(fluids\_to\_fish)} = \sum_j -F_j \cdot V_j - M_j \cdot \omega_j \quad (5.10)$$

In the above equations, $\Delta E_{fish\_kinetic}$ represents total kinetic energy, mechanical energy and power are expressed with $W_{internal(fish\_to\_fish)}$ and $P_{internal(fish\_to\_fish)}$, and fluid energy and power exerted on fish body are expressed with $W_{external(fluids\_to\_fish)}$ and $P_{external(fluids\_to\_fish)}$. M_i is the internal torque for the i^{th} joint caculated by *MBDyn* in the global frame, ω_i represents the angular velocity for the i^{th} joint. F_j is the hydrodynamic force acting on the j^{th} body and V_j is the velociy of j^{th} body. M_j and ω_j have similar meaning to M_i and ω_i, but the target is body segment instead of virtural joint.

As the hydrodynamic power derives from forces, comparisons of fluid forces exerted on body segments are going to be made first. The subsection will focus on forces

exerted on fish body parallel to the x axis, which contribute to the forward motion. As shown in **Fig. 5-3**, a detailed hydrodyanmic force oscillations within one period of time on each body segment are depicted. The time period is based on control group zebrafish larvae, thus it is apparent that the force evolves more than one period for acetic acid treated group. In the group of figures, postive force value indicates thrust, and negative force value indicates drag. It is straightforward to deduce from the figures that drag force is generated mainly in the anterior part, whereas thrust force is generated mainly in the posterior part. Details will be discussed in the following subsections.

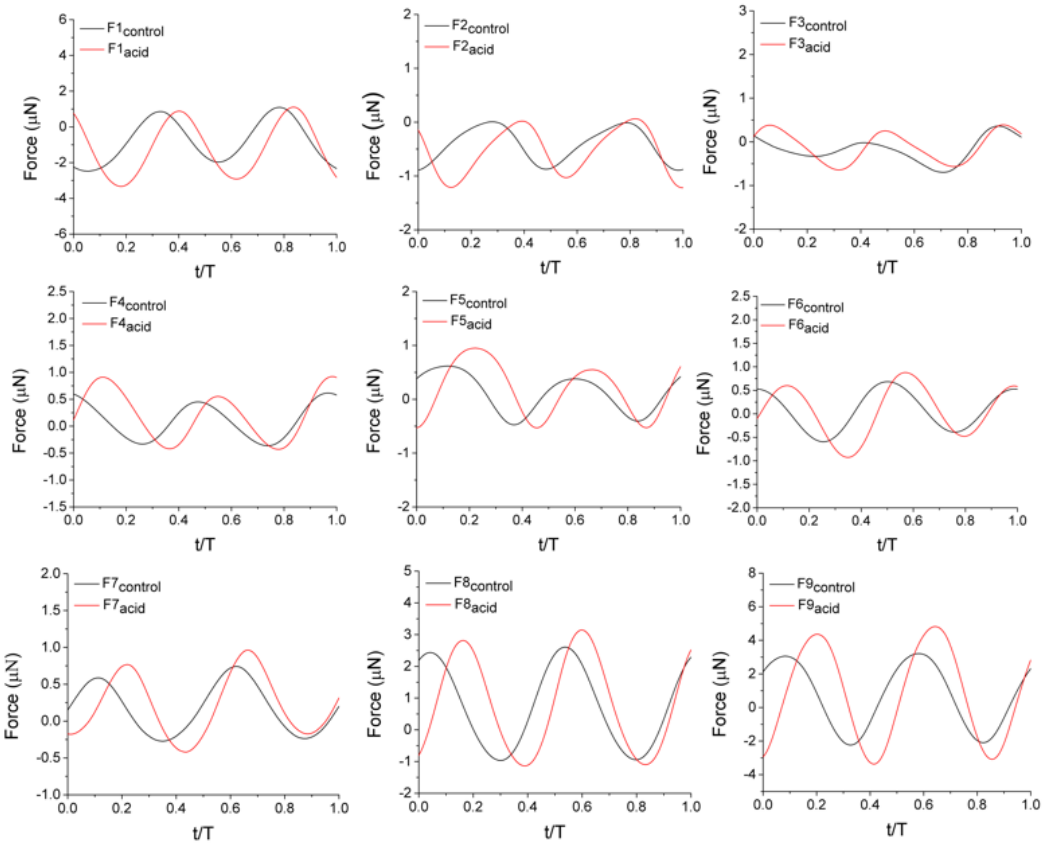

Figure 5-3. Total force exterted on all body segements in forward motion direction. The forces are expressed with F1-F9 for nine body segments.

Comparison of averaged power between control group and acid treated group is shown in **Fig. 5-4(A)**, as the absolute value of hydrodynamic power equals the mechanical power, only hydrodynamic power comparison will be displayed. Acetic acid treated zebrafish larvae generate higher power than control group, this is consistent with the

velocity tendency as the power variation is correlated with force and velocity. A further comparison on hydrodynamic power against tail beat frequency of ten zebrafish larvae siblings is shown in **Fig. 5-4(B)**. It can be seen that for control group zebrafish, the tail beat angular velocity values are distributed around $400\,rad/s$, and for acetic acid treated zebrafish, the tail beat angular velocity values are distributed around $450\,rad/s$. We have also calculated the cost of transport for two groups of zebrafish. The cost of transport is defined as energy spent to travel unit distance per unit mass, which is expressed as $\frac{P_m}{U}$, P_m is the power per unit mass, and U is the averaged forward velocity. The resulting values for cost of transport is $81.73\mu J/m\cdot kg$ and $96.24\mu J/m\cdot kg$ for control group and acetic acid treated group, respectively. These values are similar to those reported by Li et al (from $105\mu J/m\cdot kg$ to $50\mu J/m\cdot kg$) in [79] on larvae zebrafish. The increment of speed and tail beat frequency in the intermediate flow regime ($10<Re<10^3$) increase the energy dissipation, resulting in higher cost of transport, which agrees with previous study [104] .

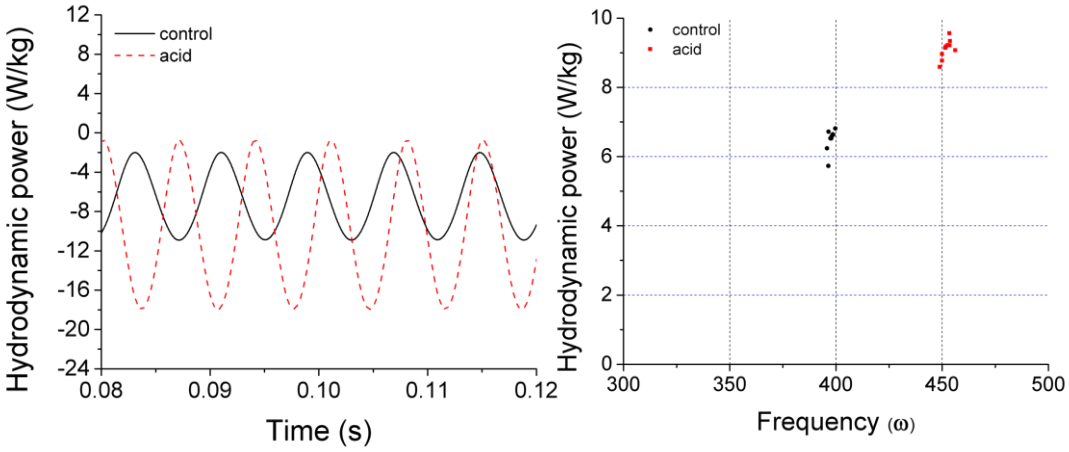

(A) (B)

Figure 5-4. (A) Total hydrodynamic and mechanical power comparison before and after 0.01% acetic acid treatment. (B) Frequency distribution of control group and 0.01% acetic acid treated group and corresponding total hydrodynamic power.

To further understand the different power generated at different locations along the fish body, variations of kinematic and dynamic performance along fish body were evaluated. Starting from regional analysis, we have selected three typical points of control group

zebrafish larvae (shown in **Fig. 5-5(A)**) along fish body to represent head region, middle region and tail region, respectively. Time history of force and velocity were compared and depicted in **Fig. 5-5(B-C)**. The trajectory is not completely parallel to x axis in global frame (about 6 degrees), therefore, forece and velocity are pointnig towards the real moving direction of zebrafish. A full body length distribution of forward component of body force is also depicted in **Fig. 5-5D,** as the fish body is divided into nine consecutive segments, forces distributed along the body are expressed with nine discrete averaged values to represent hydrodynamic forces acting on each body segment. The force shows negative value from head to approximately 30% of body length (which is roughly anterior to centre of mass), suggesting net drag generation in this region. Posterior to COM, the force value is mainly positive except near zero (slightly negative) value at 60% of body length, indicating that the posterior part mainly generate thrust force to power the forward motion. However, as the fish model is not a flexible continuous body, the force distribution is only an approximation of averaged value. For exampe, force distribution around 60% of body length could be more complex instead of an averaged near zero value, our results only provides tendency of force distribution along zebrafish body to better interpret the drag and thrust generations.

Although the absolute value of averaged hydrodynamic power equals the mechanical power, the distribution along fish body might differ. Therefore, hydrodynamic and mechanical power distributions along the body have been calculated and displayed in **Fig. 5-6**. In **Fig. 5-6(A-B)**, the hydrodyanmic power distribution of five fish samples were compared to show the tendency, and in **Fig. 5-6(C-D)**, a statistical analysis of power distribution for all twenty fish is evaluated and expressed with mean and standard deviation.

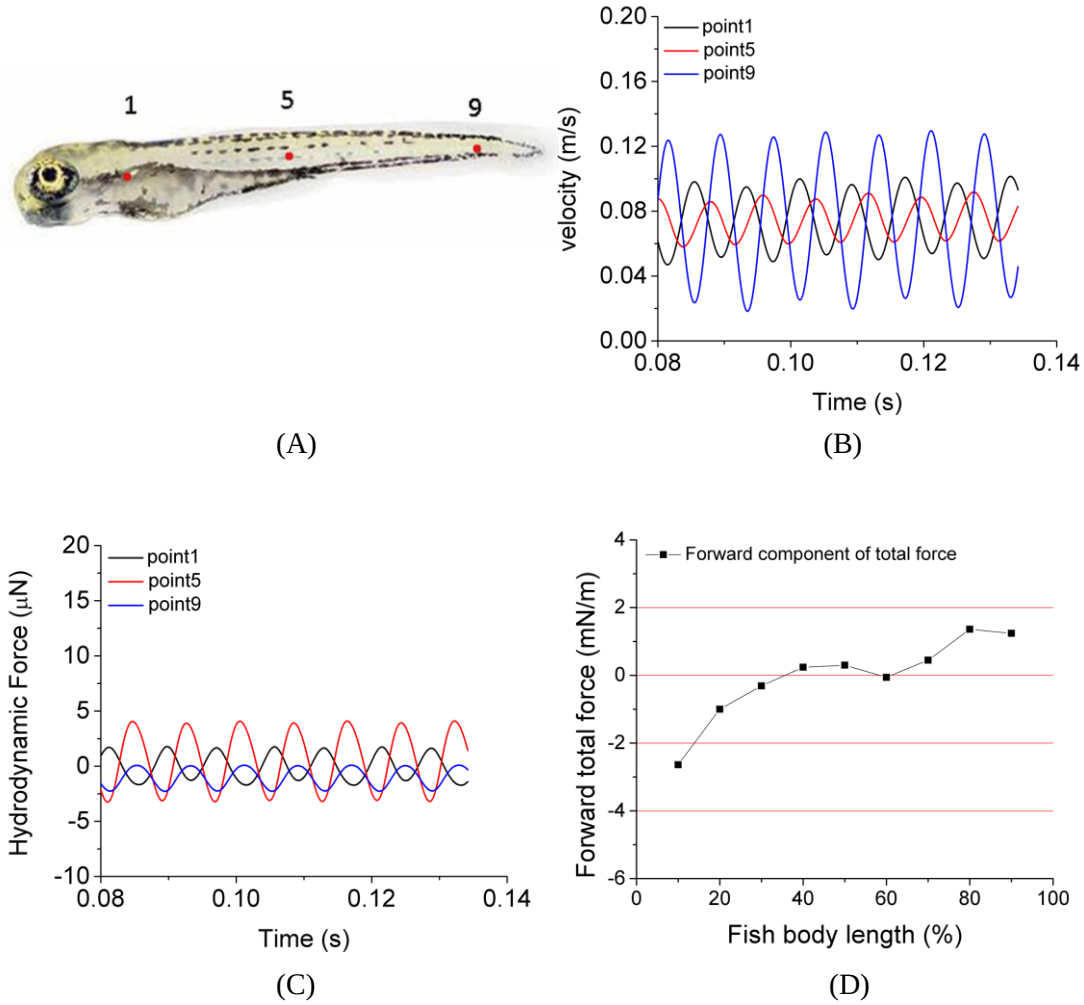

Figure 5-5. Velocity and force distribution along zebrafish body (A) Real zebrafish picture with three typical points along the body (B) Global velocity of the three points (C) Hydrodynamic force of the three points (D) Forward component of total force distribution along the body.

A more detailed mechanical and hydrodynanmic power and an approximation of cost of transport were summarised in **Table 5-1**. The unit for both hydrodynamic and mechanical power is μW. Based on our results the hydrodynamic power generation shows an increase starting from the centre of mass and a deep increase in the rear region starting from 75% of body length. According to motion equations, this region has the largest motion amplitude along the body in global frame, resulting in larger fluid force, thus more hydrodynamic power. Ideally, the consumption of muscle power requires a study of muscle strain and electromyography (EMG) patterns for muscle function at

specific positions along the body. However, the extremely small body size of larval fish makes it impossible to place receivers on the body. Constraints added in our fish model provide energy to move forward from static state, which perform as muscle fibre in real fish to provide mechanical power. The examined mechanical power shows a steep increase towards the tail from the middle region and then a steep decrease in the tail region. This might suggest that the main power generated by muscle to support steady forward swimming exists in the entire body but concentrates in the middle and posterior region. The conclusion seems to be inconsistent with the previous viewpoint that most power is generated in the anterior region, while the posterior region performs like a transmitter [131]. However, this previous work has used Saithe and Mackerel, which are different species from our model. The author provided an assumption of lengthened posterior muscle which can do negative work to support their viewpoint that posterior muscle behaves like transmitter; nevertheless, experiment on scup, which is a similar species to Satithe and Mackerel, was carried out with isolated muscle study [132]. And this experiment has drew a conclusion different from Saithe and Mackerel that muscle power is mainly generated in the middle and posterior region. also, with isolated muscle experiments, shortening of posterior muscle was observed on Scup, which is contradictory to the assumption made on Satithe and Mackerel. Therefore, with simialr caudal fin swimming mode, the influences from different species cannot be excluded before experiements are made.

Based on the equations set up in our model, the anterior region equations have smaller curvature, implying that the simulated muscle in this region has smaller strain when it is constracted, thus less positive work is done. Moreover, during steady swimming state, red muscle dominates the swimming motion, if the main muscle power is generated in the anterior part, loss of energy in the form of heat occurs in the process of force transmission towards the tail, which might increase the burden of red muscle as it powers the entire steady swimming process [132]. Whereas given that muscle functions vary among different species, the results need to be further tested with the help of muscle isolation analysis

In **Fig. 5-7**, the vorticity on x-y plane of the 3-D fish model is compared. By comparing them in one period of time, it can be seen that the vortex detached from the tail tip is faster for acid treated group compared with control group fish. The earlier detached vortex has been labelled with black circles in the right column, indicating larger distance travelled within one period of time, i.e., higher velocity. The vorticity results for control and acetic acid treated group are consistent with velocity comparisons depicted in **Fig. 5-1B**. However, the variations observed from vorticity is not that apparent compared to quantified results, and for different types of drugs, influences might be too small to be captured with vorticity changes; therefore, in this case, quantification of kinematic and enegetic performance is quite necessary.

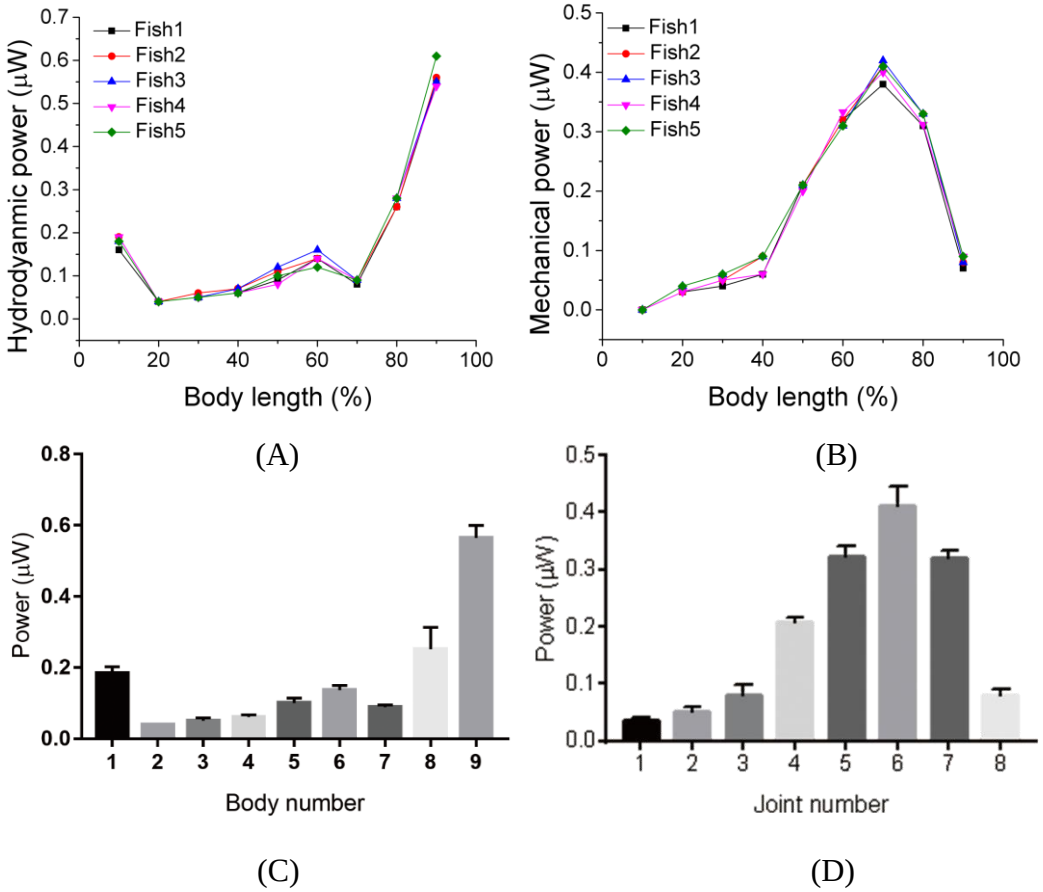

Figure 5-6. Hydrodynamic (A) and mechanical (B) power distribution of five fish. Statistical analysis of hydrodynamic (C) and mechanical (D) power distribution along the body with mean ±sd for twenty fish of each group.

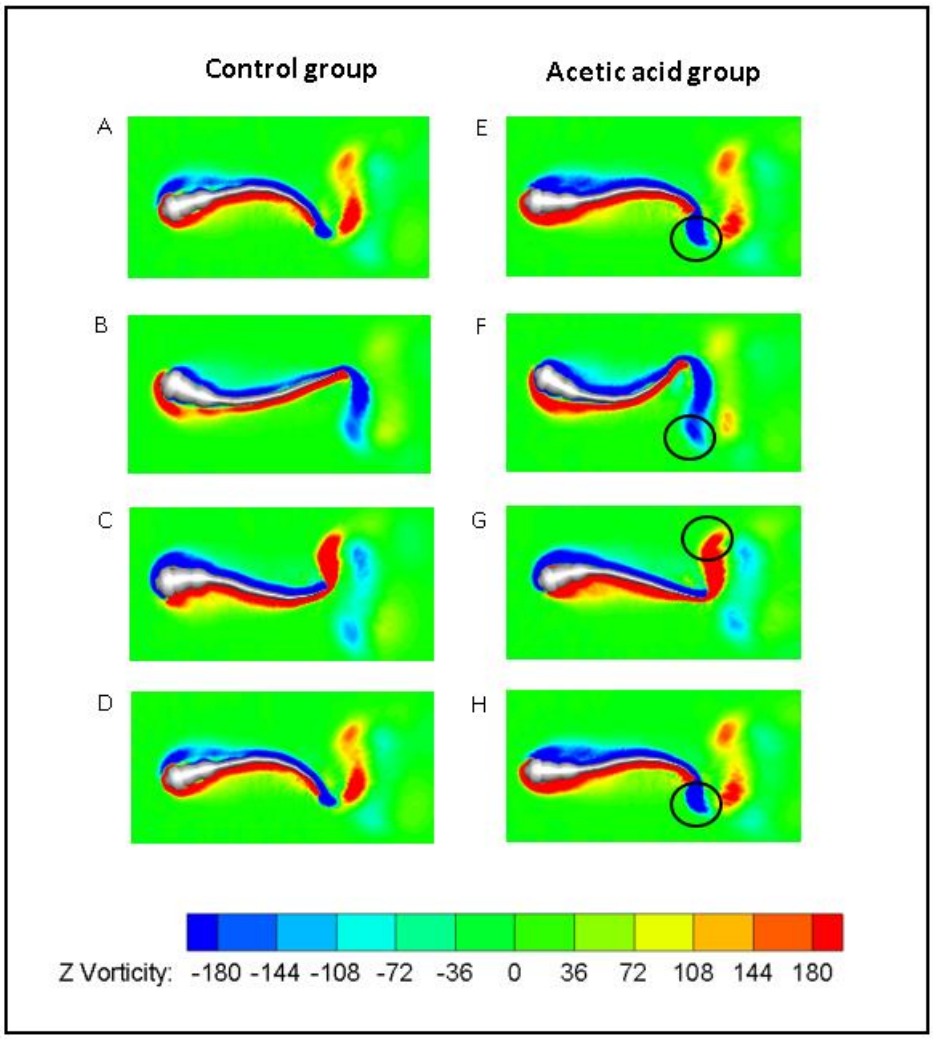

Figure 5-7. Vorticity comparisons in x-y plane between control group zebrafish and drug treated groups within one period of time. For A-D. E-H, time steps are 0, T/3, 2T/3 and T for each column. T represents one period of time.

5.1.2. Neuro-active drug effects

Administration of neuroactive drugs is an effective method to test animal's nervous system functions [133]. As neuroactive drugs acting on different neural pathways could cause different behavioural phenotypes, it is possible to study how the nervous system affects locomotion behaviors by applying different neuroactive drugs [23]. Zebrafish larva model was studied with same drugs used in adults and mammalians and showed similar behavioural responses, suggesting that zebrafish larvae are sensitive to neuroactive drugs. Therefore, in the following part, statistical analysis of the kinematic

and dynamic performance variations before and after treatment will be presented for two commonly used neuroactive drugs, diphenylhydantoin (DPH) and yohimbine.

Table 5-1. Detailed hydrodynamic and mechanical power of 10 fish and cost of tranport

		S1	S2	S3	S4	S5	S6	S7	S8	S9	cost of transport μJ/m
fish1	Hyd	0.16	0.04	0.05	0.06	0.09	0.14	0.08	0.26	0.55	79.97
	Mec	0.00	0.03	0.04	0.06	0.21	0.32	0.38	0.31	0.07	
fish2	Hyd	0.17	0.04	0.03	0.05	0.08	0.12	0.08	0.26	0.51	78.78
	Mec	0.00	0.03	0.04	0.06	0.20	0.31	0.36	0.30	0.07	
fish3	Hyd	0.19	0.04	0.06	0.07	0.11	0.14	0.09	0.26	0.56	84.33
	Mec	0.00	0.03	0.05	0.09	0.21	0.32	0.41	0.33	0.08	
fish4	Hyd	0.23	0.04	0.05	0.06	0.12	0.15	0.10	0.08	0.63	90.57
	Mec	0.00	0.04	0.06	0.12	0.22	0.37	0.49	0.34	0.08	
fish5	Hyd	0.18	0.04	0.05	0.07	0.12	0.16	0.09	0.28	0.55	80.64
	Mec	0.00	0.04	0.06	0.09	0.21	0.31	0.42	0.33	0.08	
fish6	Hyd	0.19	0.04	0.05	0.06	0.08	0.14	0.09	0.28	0.54	77.61
	Mec	0.00	0.03	0.05	0.06	0.20	0.33	0.40	0.31	0.08	
fish7	Hyd	0.18	0.04	0.06	0.06	0.10	0.14	0.09	0.28	0.59	85.56
	Mec	0.00	0.04	0.06	0.09	0.22	0.31	0.42	0.33	0.10	
fish8	Hyd	0.18	0.04	0.05	0.06	0.10	0.13	0.09	0.27	0.55	79.66
	Mec	0.00	0.04	0.04	0.07	0.20	0.32	0.41	0.31	0.08	
fish9	Hyd	0.18	0.04	0.05	0.06	0.10	0.13	0.09	0.27	0.55	79.18
	Mec	0.00	0.03	0.05	0.06	0.21	0.32	0.42	0.30	0.08	
fish10	Hyd	0.18	0.04	0.05	0.06	0.10	0.12	0.09	0.28	0.61	81.01
	Mec	0.00	0.04	0.06	0.09	0.21	0.31	0.41	0.33	0.09	

Compared to acetic acid, the two neuroactive drugs are more sensitive to concentrations and ages [25, 134, 135], different concentrations and lighting conditions can lead to reversed results for same drug. For instance, for 5 dpf zebrafish larvae, 10mg/L yohimbine will increase the locomotion activity of fish larvae, whereas 200mg/L yohimbine decreases the activity. In the current study, two specific drug concentrations were selected based on previous research to test the influences with our 5 dpf zebrafish model. Similar kinematic and dynamic comparisons to acetic acid for neuroactive drugs are presented in the following sections.

COM displacement was compared and illustrated in **Fig. 5-8**. It can be seen from **Fig. 5-8(A)** that for DPH treated zebrafish, the travelling distance expressed with COM displacment in x direction is significantly smaller than other groups within same time range, and for yohimbine treated zebrafish larvae, the distacne travelled is almost the same as control group. **Fig. 5-9(A-B)** depict the averaged head and tail comparisons between control group and neuroactive drugs treated groups. As the drugs will influence swimming frequencies and initial angles, phase differences exist among those groups in head and tail angle, respectively. From those figures, there are no significant differences for the amplitude of head and tail angle, but only different tail beat frequencies. An illustration of forward swimming speed comparisons among control group and drug treated groups are presented in **Fig. 5-9C**. The results are similar between control group and 100mg/L yohimbine treatd group, but the condition differs for 500 μM DPH solution, and is manifested as an apparent decrease of velocity compared to control group, similar tendencies are discovered in hydrodynamic power comparison (**shown as Fig. 5-9D**). The results on velocity comparisons imply that the influences of neuroactive drugs on velocity could possibly be attributed to changes in tail beat frequency instead of tail beat amplitude.

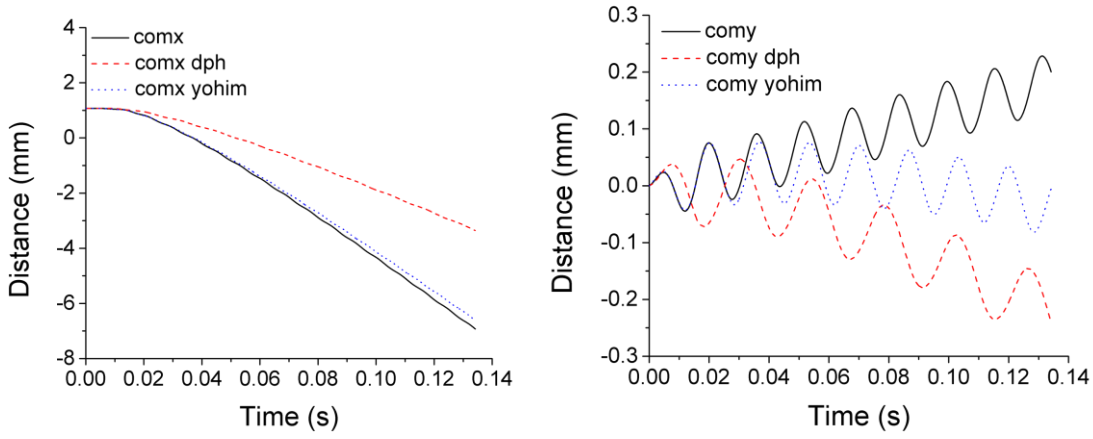

(A) (B)

Figure 5-8. Centre of mass displacement comparison between control group and drug treated group (A) COM in x direction displacemnent (B) COM in y direction displacement.

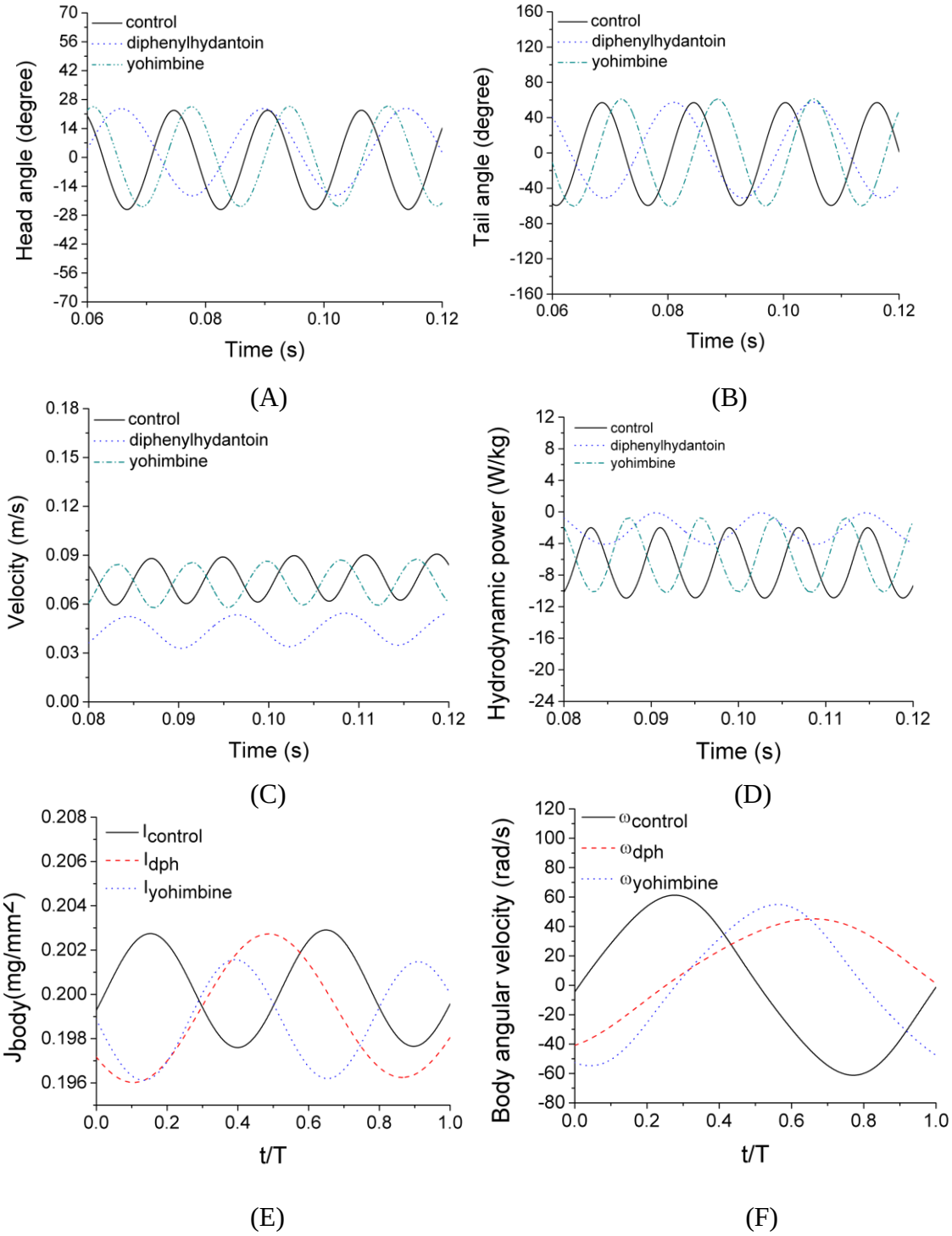

Figure 5-9. Kinematic and dynamic performance comparisons of zebrafish larvae among control groups and neuroactive drugs treated groups. (A) Head angle (B) Tail angle (C) Forward velocity (D) Hydrodynamic power. (E) Body moment of inertia. (F) Body angular velocity.

In **Fig.5-9(E-F)**, comparisons of body moment of inertia and body angular velocity are depicted and it is apparent that there is no significant differences for body moment of inertia between control group and DPH treated group, but a lower averaged value for yohimbine treated group. This is consistent with y direction displacement of COM depicted in **Fig. 5-8(B)** as the deviation angle for yohimbine treated group is significantly smaller than other two groups. For the body angular velocity, the tendency is similar to velociy comparison, showing a smaller maximum value for DPH treated group compared to other two groups.

A sketch of forward component of total force distribution comparison among three tested groups is shown in **Fig. 5-10**. The three groups share a similar tendency on force distribution along the body. Forces exerted on all body sections are assumed to be distributed evenly, which means the value can be averaged with length of each body segment. It is apparent that the averaged forward force values for DPH treated group are smaller than other two groups along the whole body length. Considering the smaller tail beat frequency, it is evident that DPH treated zebrafish larvae are less active than other two groups. To be more specific, comparisons of detailed force evolution within one period of time were made on all body segments among three groups (shown in **Fig. 5-11**). The force values are real values without any normalizations to express the real hydrodynamic characteristics of zebrafish larvae locomotion. It is apparent that for DPH treated group, there exists only one wave crest compared to two crests on other two groups, suggesting nearly half of the tail beat frequency compared to other two groups.

In addition, hydrodynamic and mechanical power distribution comparisons among control group and neuroactive drugs treated groups were presented (shown as **Fig. 5-12**), followed by a statistical analysis on velocity and hydrodynamic power as it is more prudent to compare differences between control group and drug treated group. As shown in **Fig. 5-13**, the velocity and hydrodynamic power relationships between control group and yohimbine treated group is ‘not significant’, implying that 100mg/L

yohimbine does not have influences on zebrafish locomotion. Whereas such relationship behaves as '****' between control group and DPH treated group, which suggests that there is a significant difference exists between results from control and 500 μM DPH groups.

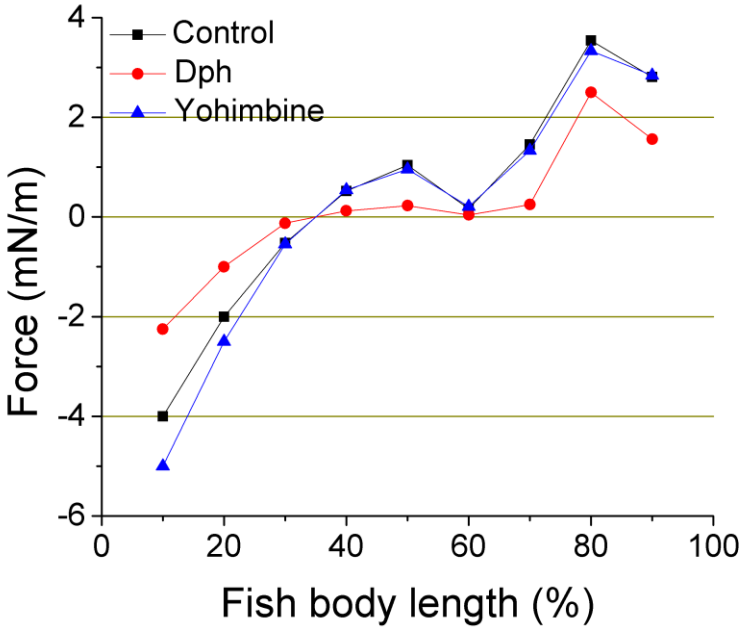

Figure 5-10. Comparisons of forward component of total force distribution for three groups. Each point represents force exerts on one body segment, points are connected with broken lines to display the trend.

To justify 0.01% acetic acid influences, acetic acid group was added in the figure and the results complies with the previous findings. Finally, vorticity between control group and neuroactive drugs treated group was compared (shown as **Fig. 5-14**). For DPH treated group, within the same one period of time, the evolution of vorticity is much shorter than other groups, approximately half of other groups, suggesting that only half of the distance travelled by DPH treated group compared with control group. For yohimbine treated group, vorticity patterns are similar to those in control group. All of the vorticity results for drug treated groups are consistent with velocity comparisons depicted in **Fig. 5-13.**

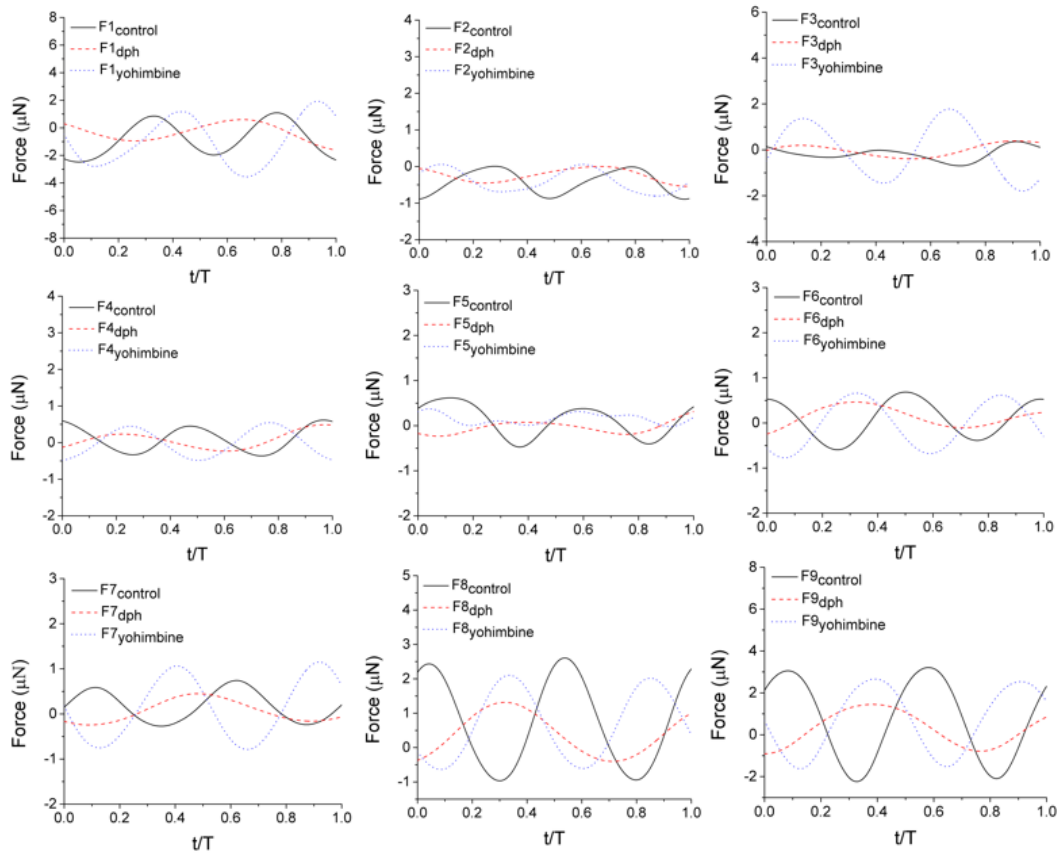

Figure 5-11. Total force exerted on each body segment in forward motion direction comparison for control group and drug treated groups. Forces are expressed with F1-F9 for nine body segments.

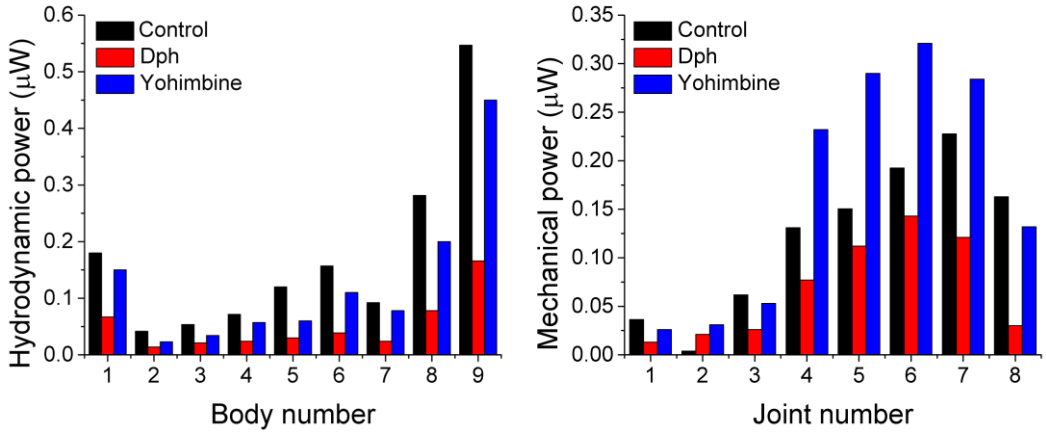

(A) (B)

Figure 5-12. Comparisons of hydrodynamic power (A) and mechanical power (B) distribution along fish body for control group and two neuro-drug treated groups.

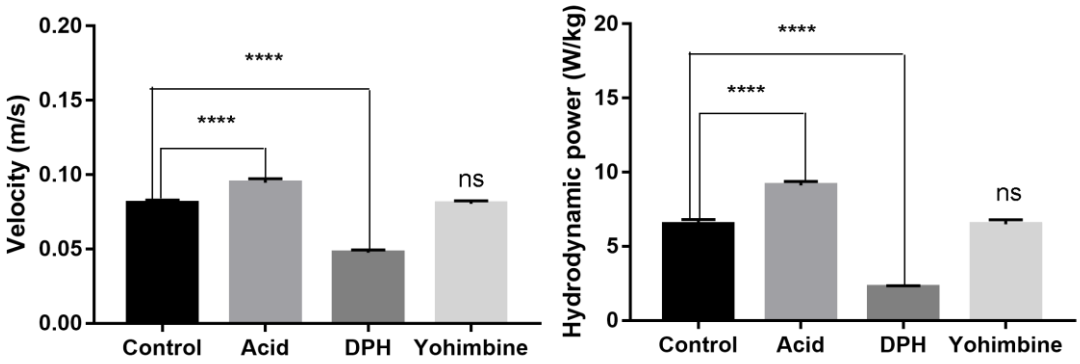

(A) (B)

*Figure 5-13. Statistical analysis on forward velociy (A) and hydrodynamic power (B) among control group and three types of drugs treated group with one-way ANOVA for totally twenty fish, expressed in mean ±sd; for P<0.0001, the significance level is expressed with ****, ns represents not significant.*

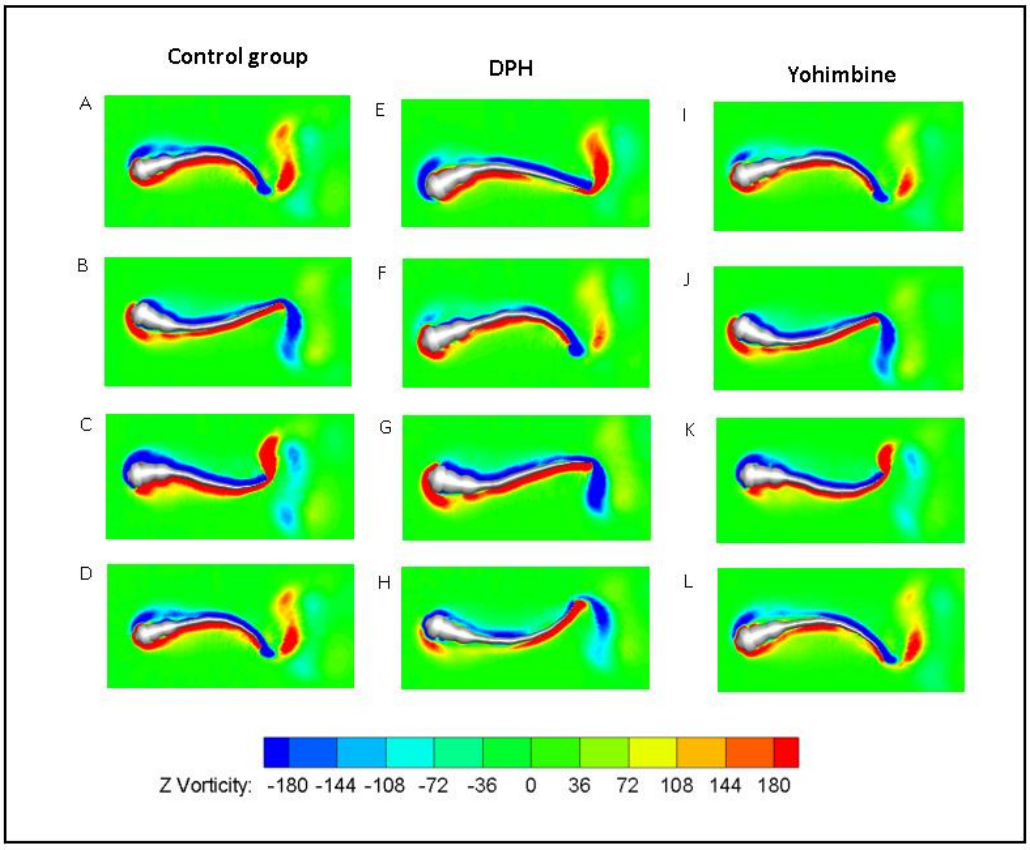

Figure 5-14. Vorticity comparison among control group, yohimbine and DPH treated groups. From A-D, E-H and I-L, time steps are 0, T/3, 2T/3 and T for each column. T represents one period of time.

All of the aforementioned results related to acetic acid, yohimbine and DPH have

evaluated the effects of drugs on zebrafish swimming systematically in both kinematic and energetic performance, also, part of the kinematic results have reflected behavioral changes which are similar to previous biological observations [25, 134], indicating that the method has the ability to replicate neuroactive drug influences on zebrafish larvae locomotion behaviours. The effect of exposure to acid on zebrafish swimming behaviour has been studied for different substances including acetic acid and citric acid at different zebrafish developmental stages [88, 136]. However, these studies are limited to the nociceptive responses of zebrafish larvae on stress, fear or anxiety, i.e. environment influences. Furthermore, the observed data mainly focused on the total distance fish has travelled in a period of time or the time spent in active status [72, 88]. To some extent, the tool introduced in the thesis can mimic the mutual interactions of real fish with the surrounding fluid and thus allows investigation of the relationship between fish body mechanical force and torque and its swimming behaviours. Using this approach, the future work would focus on evaluating potential analgesic drugs for pain relief and neuroactive drug effects on fish behaviours, which might help to understand functions of nervous system.

5.2. Assistance of CFD simulation on the evaluation of Gypenoside protection

5.2.1. Gypenosides protection effects against aceetic acid

Gypenosides have been shown to have a range of effects, including antioxidation, antilipidemia, neuroprotection and inflammation [95]. Although the possible protective effects of GYP on zebrafish have been discussed on the oxidative stress associated with retinal degeneration [96], protection of GYP against pain in zebrafish has been investigated only rarely. In the current study, the protective action of GYP against the toxic effects of 0.1% acetic acid is tested by examining the effects of exposure to these substances on zebrafish larva locomotion and on the expression of ant-oxidative and proinflammatory genes.

As mentioned in the previous chapter, muscle contractions are driven by motoneurons

in the spinal cord, and these contractions control the fish locomotion activity [137], therefore, muscle status can be reflected in activity level of the fish [81]. Comparisons are made for the time spent by each group in three different swimming conditions based on experimental data: Inactive (when the fish is at rest or shows only a subtle tail beat with no obvious displacement in the water), Active 1 (when the fish swims cyclically for a relatively long period of time) and Active 2 (when the fish is swimming for a short period of time including acceleration with large tail curvature followed by a quick de-acceleration). As shown in **Fig. 5-15A**, compared with control group, the GYP-treated group has not shown any obvious changes with regard to the percentage of time spent in active swimming, indicating that 5 μg/ml GYP does not appear to be toxic to 5 dpf zebrafish larvae. Exposure to acetic acid resulted in the fish being inactive for 80% of the time. Inactivity decreases to approximately 50% of the time following GYP treatment of fish exposed to acetic acid, suggesting an alleviatory effect of GYP solution on the muscle inflammation caused by the acid. Cyclic swimming occurs randomly in 5 dpf zebrafish larvae [76]; in the current study an increase of only 3% in time spent for cyclic swimming was observed after GYP treatment. However, for short time swimming, a significant increase of approximately 25% in total time is shown after GYP treatment, indicating increased enthusiasm. No obvious differences (less than 5% in total time) exist between the GYP group and the GYP+Acid group, suggesting that the GYP solution has an alleviatory effect on the muscle inflammation caused by 0.1% acetic acid.

Based on the simulated results from *OpenFOAM* such as position and orientation for each segment, the forward velocity of the fish larva was calculated from COM of the fish body. The COM was derived from the position of each segment at each time step using a mass-averaged method [129]. **Fig. 5-15B** shows a mean velocity comparison for all groups. The mean velocity of cruising in the acetic acid treated group is significantly lower than that in each of the other three groups, while the GYP+Acid group has displayed a similar mean velocity to the GYP and the control group.

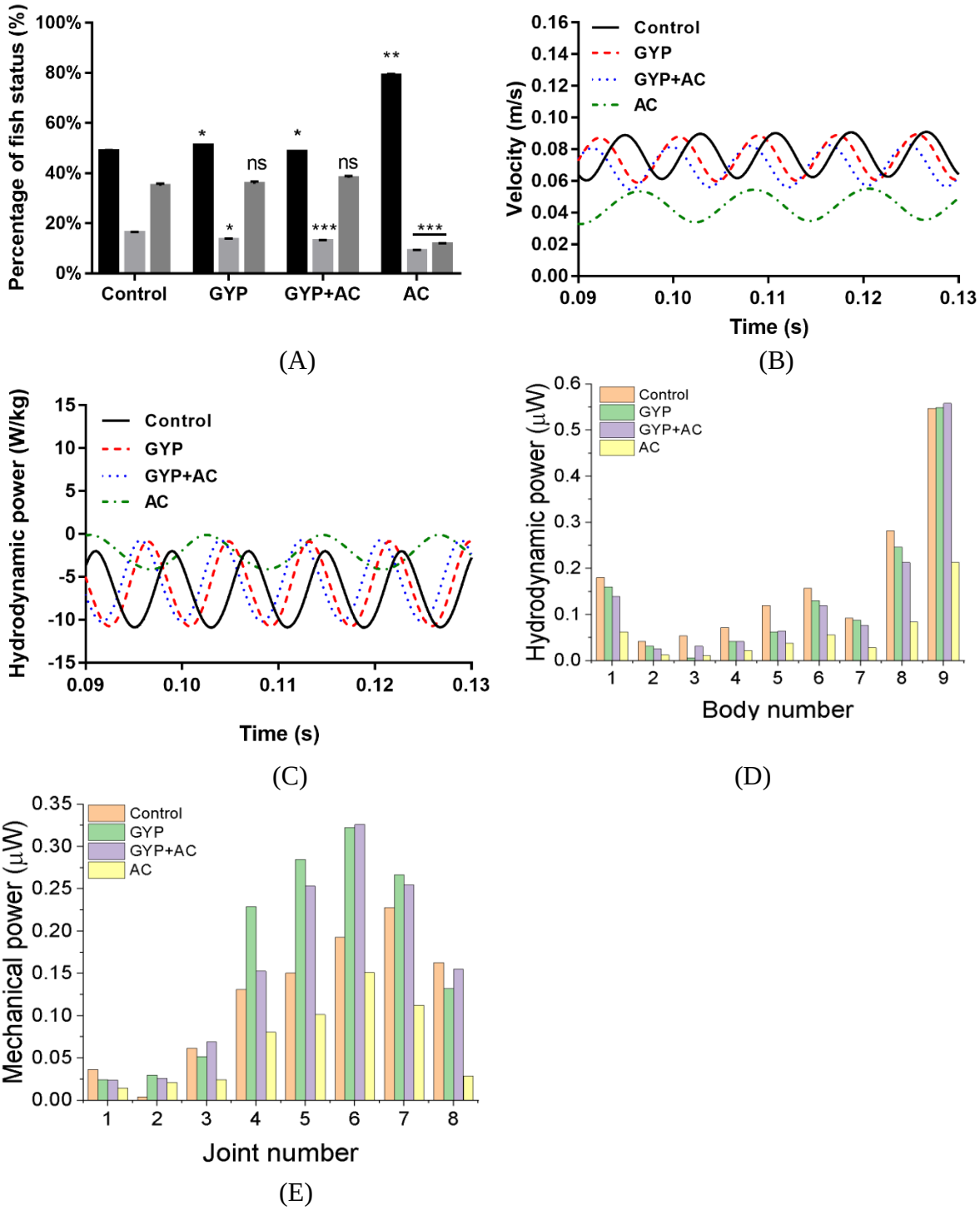

*Figure 5-15. (A) Comparisons of swimming status for each treatment group. AC: 0.1% acetic acid; GYP: Gypenosides Inactive (black column): Active 1: cyclic swimming (light grey) Active 2 (dark grey): short time swimming. *p<0.05, **p<0.01, ***p<0.001, **** p <0.0001 (B) Velocity comparison for four groups. (C) Hydrodynamic power comparison for four groups. (D) Hydrodynamic power distribution along fish body. (E) Mechanical power distribution along the fish body.*

The statistical analysis in **Fig. 5-16A** indicates that mean velocities of GYP and GYP+Acid groups are significantly higher than that of the Acid group, suggesting that the effect on forward velocity of exposure to 0.1% acetic acid is alleviated by 5μg/ml GYP. **Fig. 5-15C** compares the hydrodynamic power of the control group with the drug-treated groups. It is not surprising that the tendency is similar to forward velocity as the hydrodynamic power is calculated based on the forward velocity of the fish. As we expected, 5 μg/ml GYP could alleviate the influences on power generation, allowing the muscle of the zebrafish larvae to generate greater power, producing larger body deformation and larger hydrodynamic power compared with the 0.1% acetic acid treated group. The statistical analysis of hydrodynamic power shown in **Fig. 5-16B.** makes the conclusion more persuasive. There is a significant difference in hydrodynamic power before and after GYP treatment with acetic acid; as the muscle correlates with the power supply, it is prudent to deduce that GYP treatment could to some extent protect fish muscle from inflammation caused by acetic acid. Unlike many biomechanical situations in which the propulsive system is separated from the main body, zebrafish larvae undulate their entire body to swim forward [138], therefore, the whole body contributes to generation of thrust and drag during the tail beat cycle, although the contribution from each might differ. In **Fig. 5-15D** and **Fig. 5-15E**, the distribution of hydrodyanmic power and mechanical power along the fish body are presented to quantify the differences of force and power for different groups. Given that the fish larvae were submerged in the solution, the whole body would have been exposed, therefore we assumed that the axial muscle along the entire body would be affected by exposure to acetic acid and GYP. Although the total power was kept balanced during cruising, the power distribution is different for the internal muscle and body surface. The averaged hydrodyanmic power for the fish larvae in different groups in **Fig. 5-15D** showes a significant higher value starting from approximately 75% of body length. According to motion equations, this region has the largest shape change along the body in global frame, resulting in larger fluid force and more hydrodynamic power. In **Fig. 5-15E**, the mechanical power generated along the body shows an increase towards the tail and a steep decrease at the tail. Higher mechanical power starts

from approximately joint number 4, located at the centre of the body, indicating that the main power is generated in the posterior half of the body. In the posterior region, the larger body curvature indicates higher muscle strain, thus indicating that more strenuous work is done by this part of the body. Among the different groups, the group treated with 0.1% acetic acid displays significantly lower hydrodynamic power and mechanical power. After treatment with GYP, the power increases to a level close to that of the control group. For all body segments, both mechanical and hydrodynamic power follow the tendency of the total hydrodynamic power, suggesting that exposure influences the entire axial muscle system. In this part of the study, the internal muscle power has been quantified to provide a better understanding of the beneficial effects of GYP.

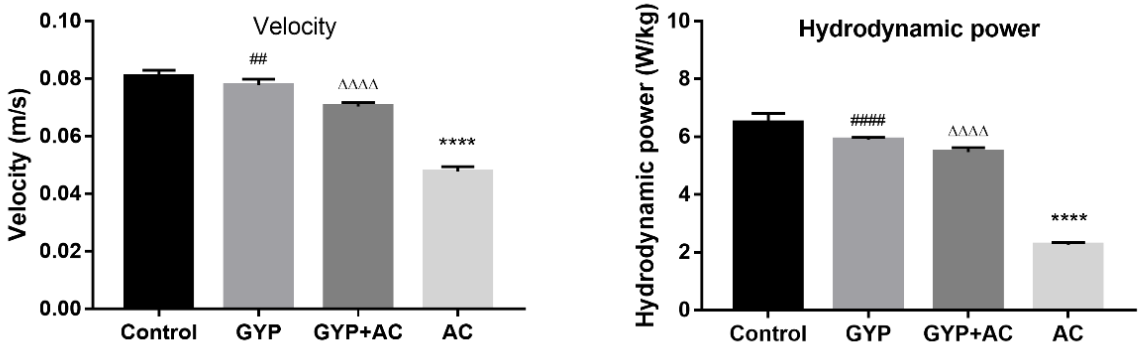

(A) (B)

*Figure 5-16. Statistical analysis for all tested groups on velocity (A) and Hydrodynamic power (B) with mean±. s.d. *p<0.05, **p<0.01, ***p<0.001, **** p <0.0001. Control vs GYP is expressed with '#' to represent significant differences between groups. Control vs Acid is expressed with '*', and GYP+Acid vs Acid is expressed with 'Δ'.*

Statistical analysis of hydrodynamic and mechanical power at different body sections and virtual joints were carried out to clarify if the effects of GYP protection vary along the zebrafish body (shown as **Fig. 5-17**). For hydrodynamic power, the overall tendency along the body of power generated remains the same with total body hydrodynamic power shown in **Fig. 5-16B**. It is obvious that the zebrafish larvae exposed to 0.1% acetic acid generates lower hydrodynamic power. When comparing GYP and GYP+Acid group, it is possible that at some body sections the GYP+Acid group

zebrafish can generate higher hydrodynamic power than that of GYP group. This might be casued by minor side effects of GYP, together with stimulation by acetic acid, as the effect of GYP could vary at different body sections due to different organs and different absorbing abilities. However, similar circumstance should not affect mechanical power, which directly reflects power generated with muscle contractions.

5.2.2. Gypenosides effects against oxidative stress and inflammation

Oxidative stress and inflammation play an important role in the development of pain [139]. Previous work showed that the natural product quercetin inhibited inflammatory pain by increasing glutathione (GSH) generation and decreasing the production of inflammatory mediators [140]. Another natural product, diosgenin, demonstrated a capacity to ameliorate the neuropathic pain associated with diabetes mellitus. Diosgenin treatment in streptozotocin-induced diabetic rat inhibited production of IL-1β and TNF-α in serum, enhanced catalase and SOD activities in serum, sciatic nerve and dorsal root ganglion, and restored nociceptive thresholds [141]. Our previous work demonstrated that GYP restored antioxidative capacity and inhibited proinflammatory cytokine production in H_2O_2-treated retinal pigment epithelial (RPE) cells [96].

In the present study, whether GYP mediated oxidative stress and inflammation in acetic acid-treated zebrafish larvae is presented. QRT-PCR data demonstrated that expression of antioxidant genes, including SOD1, SOD2 and GPX1, was significantly decreased in acetic acid-treated zebrafish compared to untreated control zebrafish and that co-treatment with GYP resulted in a marked increase in expression of these three genes (**Fig. 5-18A**).

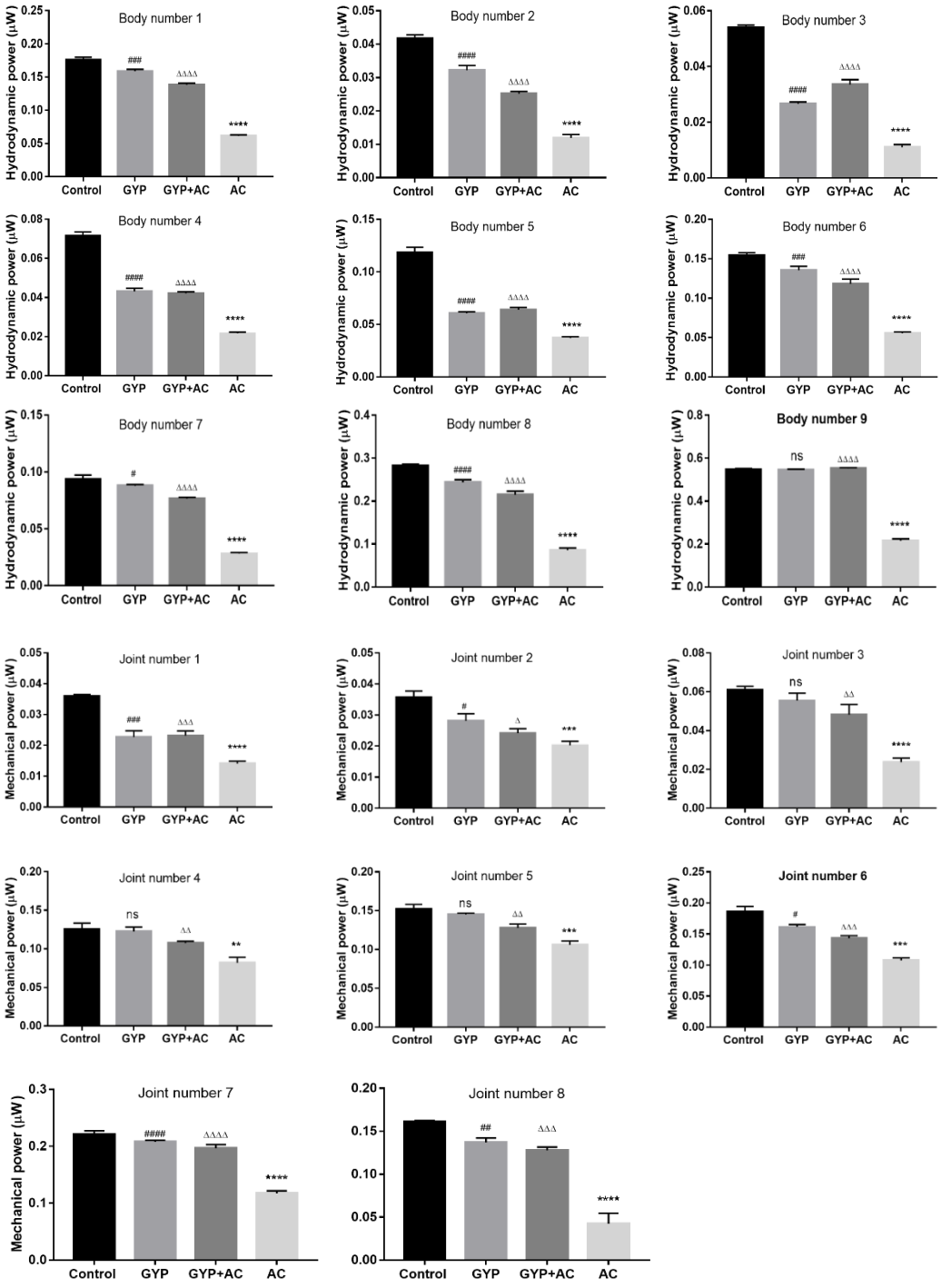

*Figure 5-17. Statistical analysis on hydrodynamic and mechanical power along the body. Body sections numbering from 1 to 9 depict hydrodynamic power comparisons among treated groups. Virtual joints numbering from 1 to 8 display mechanical power comparisons among treated groups. For all groups, ns, no significance; *p<0.05, **p<0.01, ***p<0.001, **** p <0.0001. Control vs GYP is expressed with '#' to represent significant differences between groups. Control vs Acid is expressed with '*', and GYP+Acid vs Acid is expressed with 'Δ'.*

Acetic acid treatment caused significantly increased expression of inflammatory cytokine genes IL-1β, IL-6 and TNF-α when compared to untreated control zebrafish; co-treatment with GYP reversed the acetic acid-induced effects (**Fig. 5-18B**). Intraperitoneal injection of diluted acetic acid has been widely used to induce pain in rodent models [140, 142]. Acetic acid induced production of inflammatory cytokines such as IL-1β, IL-8 and TNF-α, which mediated writhing response in mice [142]. Acetic acid has been applied to induce pain and nociception in zebrafish (larvae or adults) via introduction to zebrafish water or by local injection [72, 84, 86, 88, 143, 144]. Studies on functional consequence of acetic acid exposure in zebrafish have mainly been focused on zebrafish locomotion activity and behaviour. Here effects of acetic acid on oxidative stress and inflammation in zebrafish (**Fig. 5-18**) have also been examined. Most importantly, a novel approach to evaluate the therapeutic potential of GYP for neuropathic pain has been developed.

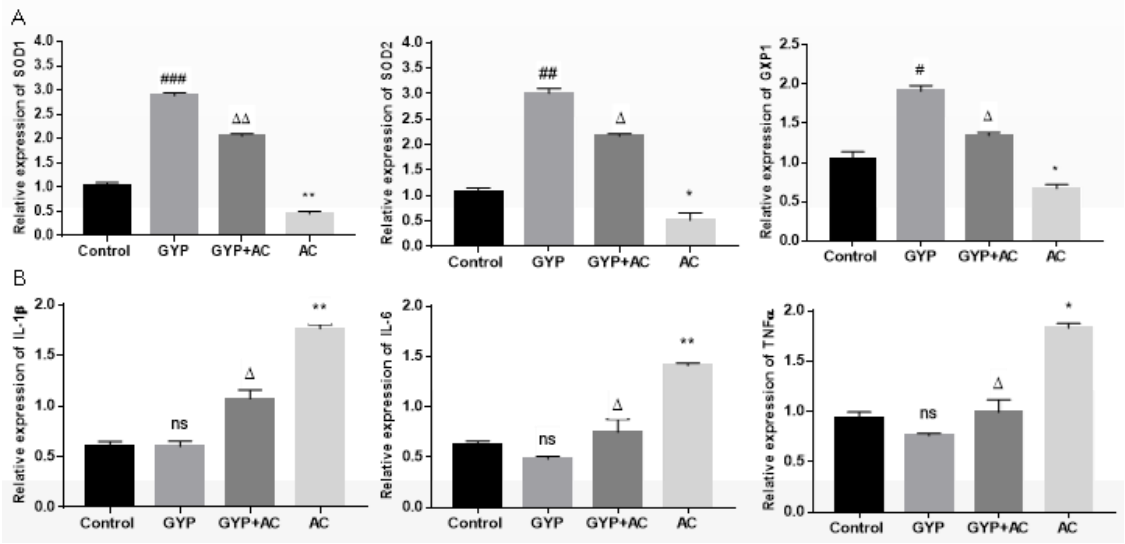

*Figure 5-18. GYP regulated expression of antioxidant and proinflammatory genes. (A) Expression of antioxidant genes in untreated and treated zebrafish larvae. (B) Expression of proinflammatory genes. Experiments were repeated three times. Data were presented as means± standard error (SE). ns, no significance; *p<0.05, **p<0.01, ***p<0.001. Control vs GYP is expressed with '#' to represent significant differences between groups. Control vs Acid is expressed with '*', and GYP+Acid vs Acid is expressed with 'Δ'.*

5.3. Concluding remarks

In this chapter, based on the methodology described in chapter 3, the influences of different types of drugs on zebrafish larvae locomotion, including nociceptive drug acetic acid, neuroactive drugs DPH and yohimbine, and analgesic drug Gypenosides are studied both experimentally and numerically. Kinematic and dynamic comparisons are firstly made before and after treatment with 0.01% acetic acid. In conclusion, the low concentration acetic acid can induce nociceptive responses on zebrafish larvae and stimulated the locomotion activity. An increase of tail beat amplitude and frequency have been discovered after acid treatment, and the increased forward velocity can be attributed to these two parameters. Body moment of inertia is determined by the deviation of swimming path in y direction, and body angular velocity is more related to the body oscillating frequency and amplitude.

In addition, the force and power distribution along fish body are compared. There exists a significant higher maximum and averaged force value for acid treated group compared to control group along the body. Detailed forces exerted on body segments have been compared for each body segment separately within same time range. The sign of force values have been specified to indicate whether they are drag or thrust forces. Based on our results, the anterior part (approximately 20% of fish body and close to the calculated centre of mass) mainly experiences drug forces, and the posterior part (after centre of mass) mainly generate thrust forces. However, as the fish model is not a flexible continuous body, the force distribution is only an approximation of averaged value. For example, force distribution around 60% of body length could be more complex instead of an averaged near zero value, our results only provides tendency of force distribution along zebrafish body to better interpret the drag and thrust generation.

The hydrodynamic and mechanical power distributions are different from force distribution. The hydrodynamic power shows an increase starting from the center of mass and a deep increase in the rear region starting from 75% of body length. This is consistent with the body motion equations. The examined mechanical power shows a steep increase towards the tail from middle region and then a steep decrease in the tail region, suggesting that the main power generated by muscle to support steady forward swimming exists in the entire body and concentrate in the posterior part. The anterior part is too stiff to bend (smaller muscle strain), and thus generate less muscle power. Also, cost of transport, which is a functional parameter to describe the swimming efficiency qualitatively is examined. Low power and speed might always lead to low cost of transport, but not high swimming efficiency [79]. Finally, vorticity generated behind the fish for both control group and acid group are compared. Faster detach of vortex happens on acid treated group, suggesting larger swimming velocity. However, the variations are too difficult to capture; therefore, it is necessary to do more quantifications on kinematic and energetic performances. For neuroactive drugs DPH and yohimbine, comparisons are similar to 0.01% acetic acid, but with diverse performances. Compared to positive activation of 0.01% acetic acid, 500 μM DPH drug works negative towards zebrafish locomotion, and 100mg/ml yohimbine does not have any significant influences on zebrafish activity. In addition, we have studied the protection of Gypenosides on zebrafish from high concentration acetic acid. We have combined CFD simulations on zebrafish locomotion to study the effects on zebrafish behaviors and internal muscle mechanics. As a high concentration of acetic acid is known to cause pain/damage to zebrafish larvae muscle and has been tested extensively, we choose to investigate the protective effects of of 5 $\mu g/mL$ GYP against exposure to 0.1% acetic acid and have observed the alleviation of muscle inflammation after GYP treatment. The conclusions have been confirmed by both QRT-PCR data and CFD simulated results, showing that our computational method could assist in evaluating the protective effect of GYP against acetic acid and other harmful substances. In addition, quantification of the internal muscle mechanics are made, which can partially reflect the effects of medicine on muscle status, and the data is difficult to acquire from

standard experiments. Considering the cheaper cost and faster preparations of CFD simulation compared to QRT-PCR analysis, our method could potentially be used to evaluate the effects of drugs on zebrafish behaviors and thus support the development of therapeutic drugs for neuropathic pain.

6 Conclusions and Recommendations

The work has introduced a novel methodology to quantify the drug influences on zebrafish larvae locomotion kinematics and energetics both experimentally and numerically. For experimental study, five dpf zebrafish larvae are selected as a target for the drug treatment experiment. The experiment is carried out with observations of zebrafish larvae locomotion behaviors under different drug treatments. Drugs such as acetic acid, diphenylhydantoin (DPH), yohimbine and Gypenosides (GYP) have been selected to study influences of both analgesic and neuroactive drugs on zebrafish larvae locomotion, nociceptive induced responses, for example. The locomotion behaviors are recorded with high-speed camera and stored in the computer for further analysis. We have developed an in-house *MATLAB* code that can, but is not limited to post-processing the recorded zebrafish larvae videos. Literally, the code can extract and analyze most of the swimming kinematic characteristics of zebrafish larvae such as forward swimming speed, tail beat angle, total distance travelled, etc. The current study focuses on extraction of zebrafish larvae body curvature equations from the relative angle orientation along the body at each time step. The extracted data has been employed as input data for numerical simulation. Due to different purposes, part of the zebrafish larvae have also been post-processed with total RNA isolation and cDNA synthesis for the quantitative real-time polymerase chain reaction (qRT-PCR). The qRT-PCR analysis is required for the determination of influences of drugs on zebrafish larvae from the perspective of specific gene expression.

For numerical simulation, a fully coupled numerical tool based on CFD-MBD framework has been developed. We have built a continuous 3-D zebrafish larvae model consisting of several rigid body segments, which are extracted from the outline of real zebrafish larvae. The open-source CFD software *OpenFOAM* is applied in the research to simulate fluid dynamics of zebrafish locomotion, which is a typical FSI case. An in-

house dynamic solver is built in *OpenFOAM* to handle dynamic mesh motion around zebrafish larva model. *OpenFOAM* is coupled with an open-source multibody dynamic software *MBDyn* to solve the FSI problem. The previously extracted body curvature data of zebrafish larvae is used as input data for *MBDyn* to provide the most straightforward and authentic data for zebrafish larvae locomotion simulation under various conditions induced by drug treatments. In return, the numerical simulation provides data and analysis on external and internal dynamics and muscle mechanisms that could not be acquired with only biological experiments. These quantified data can not only provide insights into influences of drugs on zebrafish locomotion from a different aspect, but also assist the results acquired from biological experiments.

Numerical methodology is validated with past research articles about a jelly-fish like multibody structure and experiments. Kinematic performances of zebrafish larvae such as head and tail beat angle and forward velocity are compared with experimentally measured results, comparisons present good quantitative agreement. Gestures of recorded real zebrafish larvae locomotion and simulated results are compared within one period of time to support this quantitative agreement.

Quantification of drug influences on fish larvae locomotion is carried out in two steps. The first step includes study of nociceptive and neuroactive drugs' influences on fish larvae locomotion. Reasonable comparison results have been supplied, 0.01% acetic acid has s positive influences on 5 dpf zebrafish locomotion, when it comes to 500 μM DPH, the influence turns into negative, and the 100mg/mL yohimbine does not bring any significant variations on swimming behaviors. Changes in kinematics have been supported by vorticity generation as well. Moreover, estimation of the Strouhal number value has been made, which is approximately 0.8. The value is much higher than optimal streamlined fish swimming value of 0.5. This can be explained with the fact that zebrafish larvae swim in intermediate flow regime where viscous force dominant. Therefore, overcoming such viscous effect requires more thrust and thus higher Strouhal number is needed.

Different from previous researches related to drug influences on zebrafish larvae focusing more on kinematic behaviors, the current study has quantified the hydrodynamic performance and internal muscle mechanics. Based on the results, the hydrodynamic power generation shows an increase starting from the centre of mass and a steep increase in the rear region. Constraints added in our fish model provide energy to move forward from static state, which perform as muscle fibres in real fish to provide mechanical power. Mechanical power distribution shows a steep increase towards the tail from the middle region and then a steep decrease in the tail region. This might suggest that the main power generated by muscle to support steady forward swimming exists in the entire body. The conclusion seems to be inconsistent with the previous viewpoint that most power is generated in the anterior region, while the posterior region performs like a transmitter. However, based on the equations set up in our model, the anterior region equations have smaller curvature, implying that the simulated muscle in this region has smaller strain when it is contracted, thus less positive work is done. Moreover, during steady swimming state, red muscle dominates the swimming motion; if the main muscle power is generated in the anterior part, loss of energy in the form of heat occurs in the process of force transmission towards the tail, which might increase the burden of red muscle as it powers the entire steady swimming process. Given that muscle functions vary among different species, our results need to be further tested with the help of biological analysis. To some extent, the developed tool can mimic the mutual interactions of real fish with the surrounding fluid and thus allows investigation of the relationship between fish body mechanical force and torque and its swimming behaviours. Using this approach, the future work would focus on evaluating potential analgesic drugs for pain relief and neuroactive drug effects on fish behaviours, which might help to understand functions of nervous system.

The second part includes statistical and numerical analysis on protection of GYP against acetic acid damage on zebrafish larvae. Our quantifications of kinematics and internal muscle mechanics assist the real-time PCR results on this protection. Specifically, the

qRT-PCR data we have gathered demonstrates that GYP mediated oxidative stress and inflammation in acetic acid-treated zebrafish larvae through increasing the expression of antioxidant genes and inflammatory cytokine genes. With numerical analysis, we have quantified the protection of GYP against acetic acid with comparisons of velocity, locomotion activity and power consumption along fish body and comply with biological results. Considering part of the results are difficult to acquire from standard experiments, together with the cheaper cost and faster and more flexible preparations of CFD simulation, it is confident to say that the current method could potentially be used to evaluate the effects of drugs on zebrafish behaviours prior to any biological experiments to assist the evaluation and development of therapeutic drugs for neuropathic pain.

For future work, another possible factor that might influence the accuracy of the results is considered, the fish body stiffness, which has not been taken into account in the present research. Previous studies on stiffness include the flexural stiffness of superficial neuromasts [145] used for detections of surrounding fluid, and fish body visco-elastic property predictions and related muscle mechanical behaviour based on continuous beam model [130]. The body stiffness of aquatic animals could be adjusted at specific positions in order to optimize their swimming performance such as the maximum forward speed and minimum energy cost [146], and subtle changes in fish model can have a significant impact on the swimming performance [79]. However, the distribution of visco-elastic properties, i.e. stiffness and damping coefficients along the fish body, are difficult to measure precisely, thus the mutual contributions from visco-elastic properties to the optimized swimming performance cannot be determined individually. Moreover, it is technically difficult to observe subtle body curvature changes. Different fish species may have different stiffness and damping characteristics for different purposes, such as for acceleration/deceleration or cruising swimming [100]. Based on the current research, the study of passive contribution to fish forward swimming might give inspirations on some uncertainties, especially the mechanical power distribution, i.e. muscle power generation along the body. Considering the

importance of body stiffness for a better understanding of muscle functions in controlling fish swimming, in our future research, we intend to focus on the visco-elastic properties at some predicted positions with the help of muscle dissection. To be specific, muscle related adverse medical treatment may have effects on muscle tissues such as shortened or dissolved local muscle fibres [147]. By applying predicted stiffness and damping coefficients and comparing these with the live fish tissue properties at those locations, it might be possible to account for the influences on altered swimming behaviours.

7 References

1. Rainboth, W., *Inland fishes of India and adjacent countries.* Reviews in Fish Biology and Fisheries, 1994. **4**(1): p. 135-136.
2. Lieschke, G.J. and P.D. Currie, *Animal models of human disease: zebrafish swim into view.* Nat Rev Genet, 2007. **8**(5): p. 353-67.
3. Lawrence, C., *The husbandry of zebrafish (Danio rerio): A review.* Aquaculture, 2007. **269**(1-4): p. 1-20.
4. Markovich, M.L., N.V. Rizzuto, and P.B. Brown, *Diet affects spawning in zebrafish.* Zebrafish, 2007. **4**(1): p. 69-74.
5. Haffter, P., M. Granato, M. Brand, M.C. Mullins, M. Hammerschmidt, D.A. Kane, J. Odenthal, F.J.M. Van Eeden, Y.J. Jiang, C.P. Heisenberg, R.N. Kelsh, M. Furutani-Seiki, E. Vogelsang, D. Beuchle, U. Schach, C. Fabian, and C. Nüsslein-Volhard, *The identification of genes with unique and essential functions in the development of the zebrafish, Danio rerio.* Development, 1996. **123**: p. 1-36.
6. Mullins, M.C., M. Hammerschmidt, P. Haffter, and C. Nüsslein-Volhard, *Large-scale mutagenesis in the zebrafish: in search of genes controlling development in a vertebrate.* Current Biology, 1994. **4**(3): p. 189-202.
7. Gharedaashi, E., *Determination of median lethal concentration (LC50) of copper sulfate and lead nitrate and effects on behavior in Caspian sea kutum (Rutilus frisii kutum).* Journal of Toxicology and Environmental Health Sciences, 2013. **5**(1): p. 12-16.
8. Belyaeva, N.F., V.N. Kashirtseva, N.V. Medvedeva, Y.Y. Khudoklinova, O.M. Ipatova, and A.I. Archakov, *Zebrafish as a model system for biomedical studies.* Biochemistry (Moscow) Supplement Series B: Biomedical Chemistry, 2009. **3**(4): p. 343-350.

9. Parng, C., C. Seng Wl Fau - Semino, P. Semino C Fau - McGrath, and P. McGrath, *Zebrafish: a preclinical model for drug screening.* (1540-658X (Print)).
10. Cassar, S., I. Adatto, J.L. Freeman, J.T. Gamse, I. Iturria, C. Lawrence, A. Muriana, R.T. Peterson, S. Van Cruchten, and L.I. Zon, *Use of Zebrafish in Drug Discovery Toxicology.* Chem Res Toxicol, 2020. **33**(1): p. 95-118.
11. Caballero, M.V. and M. Candiracci, *Zebrafish as Toxicological model for screening and recapitulate human diseases.* Journal of Unexplored Medical Data, 2018. **3**(2).
12. Bretaud, S., S. Lee S Fau - Guo, and S. Guo, *Sensitivity of zebrafish to environmental toxins implicated in Parkinson's disease.* (0892-0362 (Print)).
13. Goolish, E.M., P. Okutake K Fau - Johnson, and P. Johnson, *The behavioral response of zebrafish to hypergravity conditions.* (1077-9248 (Print)).
14. Dai, Y.J., Y.F. Jia, N. Chen, W.P. Bian, Q.K. Li, Y.B. Ma, Y.L. Chen, and D.S. Pei, *Zebrafish as a model system to study toxicology.* Environ Toxicol Chem, 2014. **33**(1): p. 11-7.
15. Russell, W.M., *The development of the three Rs concept.* (0261-1929 (Print)).
16. MacArthur Clark, J., *The 3Rs in research: a contemporary approach to replacement, reduction and refinement.* (1475-2662 (Electronic)).
17. Wiley, D.S., S.E. Redfield, and L.I. Zon, *Chemical screening in zebrafish for novel biological and therapeutic discovery.* Methods Cell Biol, 2017. **138**: p. 651-679.
18. Tamplin, O.J., R.M. White, L. Jing, C.K. Kaufman, S.A. Lacadie, P. Li, A.M. Taylor, and L.I. Zon, *Small molecule screening in zebrafish: swimming in potential drug therapies.* Wiley Interdiscip Rev Dev Biol, 2012. **1**(3): p. 459-68.
19. Yu, P.B., C.C. Hong, C. Sachidanandan, J.L. Babitt, D.Y. Deng, S.A. Hoyng, H.Y. Lin, K.D. Bloch, and R.T. Peterson, *Dorsomorphin inhibits BMP signals required for embryogenesis and iron metabolism.* Nat Chem Biol, 2008. **4**(1): p. 33-41.

20. Babin, P.J., C. Goizet, and D. Raldua, *Zebrafish models of human motor neuron diseases: advantages and limitations.* (1873-5118 (Electronic)).

21. Cunha-Oliveira, T., A.C. Rego, and C.R. Oliveira, *Cellular and molecular mechanisms involved in the neurotoxicity of opioid and psychostimulant drugs.* Brain Research Reviews, 2008. **58**(1): p. 192-208.

22. d'Amora, M. and S. Giordani, *The Utility of Zebrafish as a Model for Screening Developmental Neurotoxicity.* Front Neurosci, 2018. **12**: p. 976.

23. Li, F., J. Lin, X. Liu, W. Li, Y. Ding, Y. Zhang, S. Zhou, N. Guo, and Q. Li, *Characterization of the locomotor activities of zebrafish larvae under the influence of various neuroactive drugs.* Ann Transl Med, 2018. **6**(10): p. 173.

24. Yang, X., J. Lin, X. Peng, Q. Zhang, Y. Zhang, N. Guo, S. Zhou, and Q. Li, *Effects of picrotoxin on zebrafish larvae behaviors: A comparison study with PTZ.* Epilepsy Behav, 2017. **70**(Pt A): p. 224-231.

25. Liu, X., J. Lin, Y. Zhang, X. Peng, N. Guo, and Q. Li, *Effects of diphenylhydantoin on locomotion and thigmotaxis of larval zebrafish.* Neurotoxicol Teratol, 2016. **53**: p. 41-7.

26. Howe, K., M.D. Clark, C.F. Torroja, J. Torrance, C. Berthelot, M. Muffato, J.E. Collins, S. Humphray, K. McLaren, L. Matthews, S. McLaren, I. Sealy, M. Caccamo, C. Churcher, C. Scott, J.C. Barrett, R. Koch, G.J. Rauch, S. White, W. Chow, B. Kilian, L.T. Quintais, J.A. Guerra-Assuncao, Y. Zhou, Y. Gu, J. Yen, J.H. Vogel, T. Eyre, S. Redmond, R. Banerjee, J. Chi, B. Fu, E. Langley, S.F. Maguire, G.K. Laird, D. Lloyd, E. Kenyon, S. Donaldson, H. Sehra, J. Almeida-King, J. Loveland, S. Trevanion, M. Jones, M. Quail, D. Willey, A. Hunt, J. Burton, S. Sims, K. McLay, B. Plumb, J. Davis, C. Clee, K. Oliver, R. Clark, C. Riddle, D. Elliot, G. Threadgold, G. Harden, D. Ware, S. Begum, B. Mortimore, G. Kerry, P. Heath, B. Phillimore, A. Tracey, N. Corby, M. Dunn, C. Johnson, J. Wood, S. Clark, S. Pelan, G. Griffiths, M. Smith, R. Glithero, P. Howden, N. Barker, C. Lloyd, C. Stevens, J. Harley, K. Holt, G. Panagiotidis, J. Lovell, H. Beasley, C. Henderson, D. Gordon, K. Auger, D. Wright, J. Collins, C. Raisen, L. Dyer, K. Leung, L. Robertson, K. Ambridge,

D. Leongamornlert, S. McGuire, R. Gilderthorp, C. Griffiths, D. Manthravadi, S. Nichol, G. Barker, S. Whitehead, M. Kay, J. Brown, C. Murnane, E. Gray, M. Humphries, N. Sycamore, D. Barker, D. Saunders, J. Wallis, A. Babbage, S. Hammond, M. Mashreghi-Mohammadi, L. Barr, S. Martin, P. Wray, A. Ellington, N. Matthews, M. Ellwood, R. Woodmansey, G. Clark, J. Cooper, A. Tromans, D. Grafham, C. Skuce, R. Pandian, R. Andrews, E. Harrison, A. Kimberley, J. Garnett, N. Fosker, R. Hall, P. Garner, D. Kelly, C. Bird, S. Palmer, I. Gehring, A. Berger, C.M. Dooley, Z. Ersan-Urun, C. Eser, H. Geiger, M. Geisler, L. Karotki, A. Kirn, J. Konantz, M. Konantz, M. Oberlander, S. Rudolph-Geiger, M. Teucke, C. Lanz, G. Raddatz, K. Osoegawa, B. Zhu, A. Rapp, S. Widaa, C. Langford, F. Yang, S.C. Schuster, N.P. Carter, J. Harrow, Z. Ning, J. Herrero, S.M. Searle, A. Enright, R. Geisler, R.H. Plasterk, C. Lee, M. Westerfield, P.J. de Jong, L.I. Zon, J.H. Postlethwait, C. Nusslein-Volhard, T.J. Hubbard, H. Roest Crollius, J. Rogers and D.L. Stemple, *The zebrafish reference genome sequence and its relationship to the human genome.* Nature, 2013. **496**(7446): p. 498-503.

27. Hwang, W.Y., D. Fu Y Fau - Reyon, M.L. Reyon D Fau - Maeder, S.Q. Maeder Ml Fau - Tsai, J.D. Tsai Sq Fau - Sander, R.T. Sander Jd Fau - Peterson, J.R.J. Peterson Rt Fau - Yeh, J.K. Yeh Jr Fau - Joung, and J.K. Joung, *Efficient genome editing in zebrafish using a CRISPR-Cas system.* (1546-1696 (Electronic)).

28. Doyon, Y., J.C. McCammon Jm Fau - Miller, F. Miller Jc Fau - Faraji, C. Faraji F Fau - Ngo, G.E. Ngo C Fau - Katibah, R. Katibah Ge Fau - Amora, T.D. Amora R Fau - Hocking, L. Hocking Td Fau - Zhang, E.J. Zhang L Fau - Rebar, P.D. Rebar Ej Fau - Gregory, F.D. Gregory Pd Fau - Urnov, S.L. Urnov Fd Fau - Amacher, and S.L. Amacher, *Heritable targeted gene disruption in zebrafish using designed zinc-finger nucleases.* (1546-1696 (Electronic)).

29. Bedell, V.M., Y. Wang, J.M. Campbell, T.L. Poshusta, C.G. Starker, R.G. Krug Ii, W. Tan, S.G. Penheiter, A.C. Ma, A.Y.H. Leung, S.C. Fahrenkrug, D.F. Carlson, D.F. Voytas, K.J. Clark, J.J. Essner, and S.C. Ekker, *In vivo genome*

editing using a high-efficiency TALEN system. Nature, 2012. **491**(7422): p. 114-118.

30. Widrick, J.J., M.S. Alexander, B.A.-O. Sanchez, D.E. Gibbs, G. Kawahara, A.H. Beggs, and L.M. Kunkel, *Muscle dysfunction in a zebrafish model of Duchenne muscular dystrophy.* (1531-2267 (Electronic)).
31. Bassett, D.I. and P.D. Currie, *The zebrafish as a model for muscular dystrophy and congenital myopathy.* Hum Mol Genet, 2003. **12 Spec No 2**: p. R265-70.
32. Guyon, J.R., L.S. Steffen, M.H. Howell, T.J. Pusack, C. Lawrence, and L.M. Kunkel, *Modeling human muscle disease in zebrafish.* Biochim Biophys Acta, 2007. **1772**(2): p. 205-15.
33. Newman, M., E. Ebrahimie, and M. Lardelli, *Using the zebrafish model for Alzheimer's disease research.* Front Genet, 2014. **5**: p. 189.
34. Newman, M., G. Verdile, R.N. Martins, and M. Lardelli, *Zebrafish as a tool in Alzheimer's disease research.* Biochim Biophys Acta, 2011. **1812**(3): p. 346-52.
35. Vaz, R.L., T.F. Outeiro, and J.J. Ferreira, *Zebrafish as an Animal Model for Drug Discovery in Parkinson's Disease and Other Movement Disorders: A Systematic Review.* Front Neurol, 2018. **9**: p. 347.
36. Makhija, D.T. and A.G. Jagtap, *Studies on sensitivity of zebrafish as a model organism for Parkinson's disease: Comparison with rat model.* (0976-500X (Print)).
37. Hoffman, E.P., R.H. Fischbeck Kh Fau - Brown, M. Brown Rh Fau - Johnson, R. Johnson M Fau - Medori, J.D. Medori R Fau - Loike, J.B. Loike Jd Fau - Harris, R. Harris Jb Fau - Waterston, M. Waterston R Fau - Brooke, L. Brooke M Fau - Specht, L. Specht, and et al., *Characterization of dystrophin in muscle-biopsy specimens from patients with Duchenne's or Becker's muscular dystrophy.* (0028-4793 (Print)).
38. van Eeden, F.J., M. Granato, U. Schach, M. Brand, M. Furutani-Seiki, P. Haffter, M. Hammerschmidt, C.P. Heisenberg, Y.J. Jiang, D.A. Kane, R.N. Kelsh, M.C. Mullins, J. Odenthal, R.M. Warga, M.L. Allende, E.S. Weinberg,

and C. Nusslein-Volhard, *Mutations affecting somite formation and patterning in the zebrafish, Danio rerio.* Development, 1996. **123**(1): p. 153.

39. Granato, M., F.J. van Eeden, U. Schach, T. Trowe, M. Brand, M. Furutani-Seiki, P. Haffter, M. Hammerschmidt, C.P. Heisenberg, Y.J. Jiang, D.A. Kane, R.N. Kelsh, M.C. Mullins, J. Odenthal, and C. Nusslein-Volhard, *Genes controlling and mediating locomotion behavior of the zebrafish embryo and larva.* Development, 1996. **123**(1): p. 399.
40. Schapira G Fau - Dreyfus, J.C., M. Dreyfus Jc Fau - Joly, and M. Joly, *Changes in the flow birefringence of myosin as a result of muscular atrophy.* (0028-0836 (Print)).
41. Voisin, T. and B. Vellas, *Diagnosis and treatment of patients with severe Alzheimer's disease.* (1170-229X (Print)).
42. Mueller, T. and M.F. Wullimann, *An evolutionary interpretation of teleostean forebrain anatomy.* (1421-9743 (Electronic)).
43. Wullimann, M.F., B. Rupp, and H. Reichert, *The brain of the zebrafish Danio rerio: an overview*, in *Neuroanatomy of the Zebrafish Brain: A Topological Atlas*, M.F. Wullimann, B. Rupp, and H. Reichert, Editors. 1996, Birkhäuser Basel: Basel. p. 7-17.
44. Nornes, S., M. Newman, S. Wells, G. Verdile, R. Martins, and M. Lardelli, *Independent and cooperative action of Psen2 with Psen1 in zebrafish embryos.* Experimental cell research, 2009. **315**: p. 2791-801.
45. Terman, G.W. and J.J. Bonica, *Spinal mechanisms and their modulation* Conference Proceedings, 2001.
46. Dubin, A.E. and A. Patapoutian, *Nociceptors: the sensors of the pain pathway.* J Clin Invest, 2010. **120**(11): p. 3760-72.
47. C.S.Sherrington, *Flexion-reflex of the Limb, Crossed Extension-Reflex, and Reflex Stepping and Standing* Journal of Physiology 1910.
48. Grubb, S. and G.W. Pasvankas, *Anatomy and Physiology: Mechanisms of Nociceptive Transmission*, in *Academic Pain Medicine: A Practical Guide to*

Rotations, Fellowship, and Beyond, Y. Khelemsky, A. Malhotra, and K. Gritsenko, Editors. 2019, Springer International Publishing: Cham. p. 1-7.

49. Vardeh, D. and J.F. Naranjo, *Anatomy and Physiology: Mechanisms of Nociceptive Transmission*, in *Pain Medicine: An Essential Review*, R.J. Yong, et al., Editors. 2017, Springer International Publishing: Cham. p. 3-5.
50. Müller-Schwefe, G., B. Morlion, K. Ahlbeck, E. Alon, S. Coaccioli, F. Coluzzi, F. Huygen, W. Jaksch, E. Kalso, M. Kocot-Kępska, H.-G. Kress, A.C. Mangas, C. Margarit Ferri, P. Mavrocordatos, A. Nicolaou, C.P. Hernández, J. Pergolizzi, M. Schäfer, and P. Sichère, *Treatment for chronic low back pain: the focus should change to multimodal management that reflects the underlying pain mechanisms.* Current Medical Research and Opinion, 2017. **33**(7): p. 1199-1210.
51. Daniel Le Bars, M.G., And Samuel W. Cadden, *Animal Models of Nociception.* Pharmacological Reviews, 2001. **53**: p. 56.
52. Bennett, G.J. and Y.K. Xie, *A peripheral mononeuropathy in rat that produces disorders of pain sensation like those seen in man.* (0304-3959 (Print)).
53. K.A.Sluka, *Stimulation of Deep Somatic Tissue with Capsaicin ProducesLong-Lasting Mechanical Allodynia and Heat Hypoalgesia that Depends on Early Activation of the cAMP Pathway.* The Journal of Neuroscience, 2002. **22**: p. 7.
54. Hargreaves, K., R. Dubner, F. Brown, C. Flores, and J. Joris, *A new and sensitive method for measuring thermal nociception in cutaneous hyperalgesia.* Pain, 1988. **32**(1): p. 77-88.
55. Stiles, J., C.N. Honda, S.G. Krohne, and E.A. Kazacos, *Effect of topical administration of 1% morphine sulfate solution on signs of pain and corneal wound healing in dogs.* Am J Vet Res, 2003. **64**(7): p. 813-8.
56. Radhakrishnan, R., S.A. Moore, and K.A. Sluka, *Unilateral carrageenan injection into muscle or joint induces chronic bilateral hyperalgesia in rats.* Pain, 2003. **104**(3): p. 567-77.

57. Schaeck, M., W. Van den Broeck, K. Hermans, and A. Decostere, *Fish as research tools: alternatives to in vivo experiments.* Altern Lab Anim, 2013. **41**(3): p. 219-29.

58. Newby, N.C. and E.D. Stevens, *The effects of the acetic acid "pain" test on feeding, swimming, and respiratory responses of rainbow trout (Oncorhynchus mykiss).* Applied Animal Behaviour Science, 2008. **114**(1-2): p. 260-269.

59. Sneddon, L.U., *The evidence for pain in fish: the use of morphine as an analgesic.* Applied Animal Behaviour Science, 2003. **83**(2): p. 153-162.

60. Sneddon, L.U., V.A. Braithwaite, and M.J. Gentle, *Do fishes have nociceptors? Evidence for the evolution of a vertebrate sensory system.* Proc Biol Sci, 2003. **270**(1520): p. 1115-21.

61. Leonard, R.B., *Primary afferent receptive field properties and neurotransmitter candidates in a vertebrate lacking unmyelinated fibers.* Prog Clin Biol Res, 1985. **176**: p. 135-45.

62. Snow, P.J., M.B. Plenderleith, and L.L. Wright, *Quantitative study of primary sensory neurone populations of three species of elasmobranch fish.* J Comp Neurol, 1993. **334**(1): p. 97-103.

63. Rose, J.D., *The Neurobehavioral Nature of Fishes and the Question of Awareness andPain.* Reviews in Fisheries Science, 2002.

64. Stevens, C.W., *Alternatives to the use of mammals for pain research.* Life Sci, 1992. **50**(13): p. 901-12.

65. Sneddon, L.U., *Anatomical and electrophysiological analysis of the trigeminal nerve in a teleost fish, Oncorhynchus mykiss.* Neuroscience Letters, 2002.

66. Sneddon, L.U., *Anatomical and electrophysiological analysis of the trigeminal nerve in a teleost fish, Oncorhynchus mykiss.* Neuroscience Letters, 2002. **319**(3): p. 167-171.

67. Malafoglia, V., B. Bryant, W. Raffaeli, A. Giordano, and G. Bellipanni, *The zebrafish as a model for nociception studies.* J Cell Physiol, 2013. **228**(10): p. 1956-66.

68. de Velasco, E.M.F., P.Y. Law, and R.E. Rodríguez, *Mu Opioid Receptor from the Zebrafish Exhibits Functional Characteristics as Those of Mammalian Mu Opioid Receptor.* Zebrafish, 2009. **6**(3): p. 259-268.

69. Lau, B., Y. Bretaud S Fau - Huang, E. Huang Y Fau - Lin, S. Lin E Fau - Guo, and S. Guo, *Dissociation of food and opiate preference by a genetic mutation in zebrafish.* (1601-1848 (Print)).

70. Norton, W. and L. Bally-Cuif, *Adult zebrafish as a model organism for behavioural genetics.* (1471-2202 (Electronic)).

71. Cachat, J., M. Canavello P Fau - Elegante, B. Elegante M Fau - Bartels, P. Bartels B Fau - Hart, C. Hart P Fau - Bergner, R. Bergner C Fau - Egan, A. Egan R Fau - Duncan, D. Duncan A Fau - Tien, A. Tien D Fau - Chung, K. Chung A Fau - Wong, J. Wong K Fau - Goodspeed, J. Goodspeed J Fau - Tan, C. Tan J Fau - Grimes, S. Grimes C Fau - Elkhayat, C. Elkhayat S Fau - Suciu, M. Suciu C Fau - Rosenberg, K.M. Rosenberg M Fau - Chung, F. Chung Km Fau - Kadri, S. Kadri F Fau - Roy, S. Roy S Fau - Gaikwad, A. Gaikwad S Fau - Stewart, I. Stewart A Fau - Zapolsky, T. Zapolsky I Fau - Gilder, S. Gilder T Fau - Mohnot, E. Mohnot S Fau - Beeson, H. Beeson E Fau - Amri, Z. Amri H Fau - Zukowska, R.D. Zukowska Z Fau - Soignier, A.V. Soignier Rd Fau - Kalueff, and A.V. Kalueff, *Modeling withdrawal syndrome in zebrafish.* (1872-7549 (Electronic)).

72. Lopez-Luna, J., Q. Al-Jubouri, W. Al-Nuaimy, and L.U. Sneddon, *Reduction in activity by noxious chemical stimulation is ameliorated by immersion in analgesic drugs in zebrafish.* The Journal of Experimental Biology, 2017. **220**(Pt 8): p. 1451-1458.

73. David, A. and K. Pancharatna, *Developmental anomalies induced by a non-selective COX inhibitor (ibuprofen) in zebrafish (Danio rerio).* 2009(1382-6689 (Print)).

74. Sneddon, L.U., *Evolution of nociception and pain: evidence from fish models.* Philos Trans R Soc Lond B Biol Sci, 2019. **374**(1785): p. 20190290.

75. Seth A.Budick and D. M.O'Malley, *locomotor repertoire of the larva zebrafish: swimming, turning and prey capture.* The Journal of Experimental Biology, 2000. **203**: p. 15.

76. Muller, U.K., *Swimming of larval zebrafish: ontogeny of body waves and implications for locomotory development.* The Journal of Experimental Biology, 2004. **207**(5): p. 853-868.

77. Müller, U.K., E.J. Stamhuis, and J.J. Videler, *How the body contributes to the wake in undulatory fish swimming: Flow fields of a swimming eel (Anguilla anguilla).* The Journal of Experimental Biology, 2001. **204**: p. 13.

78. Katz, S.L. and R.E. Shadwick, *Curvature of Swimming Fish Midlines as an Index of Muscle Strain Suggests Swimming Muscle Produces Net Positive Work.* Journal of Theoretical Biology, 1998. **193**(2): p. 243-256.

79. Li, G., U.K. Muller, J.L. van Leeuwen, and H. Liu, *Fish larvae exploit edge vortices along their dorsal and ventral fin folds to propel themselves.* J R Soc Interface, 2016. **13**(116).

80. Gehrig, J., G. Pandey, and J.H. Westhoff, *Zebrafish as a Model for Drug Screening in Genetic Kidney Diseases.* Front Pediatr, 2018. **6**: p. 183.

81. Correia, A.D., S.R. Cunha, M. Scholze, and E.D. Stevens, *A Novel Behavioral Fish Model of Nociception for Testing Analgesics.* Pharmaceuticals, 2011. **4**(4): p. 665-680.

82. Malafoglia, V., M. Colasanti, W. Raffaeli, D. Balciunas, A. Giordano, and G. Bellipanni, *Extreme thermal noxious stimuli induce pain responses in zebrafish larvae.* J Cell Physiol, 2014. **229**(3): p. 300-8.

83. Peter J. Steenbergen and N. Bardine, *Antinociceptive effects of buprenorphine in zebrafish larvae: An alternative for rodent models to study pain and nociception?* Applied Animal Behaviour Science, 2014. **152**: p. 92-99.

84. Taylor, J.C., L.S. Dewberry, S.K. Totsch, L.R. Yessick, J.J. DeBerry, S.A. Watts, and R.E. Sorge, *A novel zebrafish-based model of nociception.* Physiol Behav, 2017. **174**: p. 83-88.

85. Curtright, A., M. Rosser, S. Goh, B. Keown, E. Wagner, J. Sharifi, D.W. Raible, and A. Dhaka, *Modeling nociception in zebrafish: a way forward for unbiased analgesic discovery.* PLoS One, 2015. **10**(1): p. e0116766.

86. Steenbergen, P.J. and N. Bardine, *Antinociceptive effects of buprenorphine in zebrafish larvae: An alternative for rodent models to study pain and nociception?* Applied Animal Behaviour Science, 2013. **152**.

87. Bingham, S., P.J. Beswick, D.E. Blum, N.M. Gray, and I.P. Chessell, *The role of the cylooxygenase pathway in nociception and pain.* Semin Cell Dev Biol, 2006. **17**(5): p. 544-54.

88. Lopez-Luna, J., Q. Al-Jubouri, W. Al-Nuaimy, and L.U. Sneddon, *Impact of stress, fear and anxiety on the nociceptive responses of larval zebrafish.* PLoS One, 2017. **12**(8): p. e0181010.

89. Rana, N., A. Moond M Fau - Marthi, S. Marthi A Fau - Bapatla, T. Bapatla S Fau - Sarvepalli, K. Sarvepalli T Fau - Chatti, A.K. Chatti K Fau - Challa, and A.K. Challa, *Caffeine-induced effects on heart rate in zebrafish embryos and possible mechanisms of action: an effective system for experiments in chemical biology.* (1557-8542 (Electronic)).

90. Sanchez-Simon, F.M., F.J. Arenzana, and R.E. Rodriguez, *In vivo effects of morphine on neuronal fate and opioid receptor expression in zebrafish embryos.* Eur J Neurosci, 2010. **32**(4): p. 550-9.

91. Abdelkader, T.S., T.-H. Chang Sn Fau - Kim, J. Kim Th Fau - Song, D.S. Song J Fau - Kim, J.-H. Kim Ds Fau - Park, and J.H. Park, *Exposure time to caffeine affects heartbeat and cell damage-related gene expression of zebrafish Danio rerio embryos at early developmental stages.* (1099-1263 (Electronic)).

92. Santos, L.C., J. Ruiz-Oliveira, P.F. Silva, and A.C. Luchiari, *Caffeine Dose-Response Relationship and Behavioral Screening in Zebrafish*, in *The Question of Caffeine*. 2017.

93. Hsu, H.Y., J.S. Yang, K.W. Lu, C.S. Yu, S.T. Chou, J.J. Lin, Y.Y. Chen, M.L. Lin, F.S. Chueh, S.S. Chen, and J.G. Chung, *An experimental study on the*

antileukemia effects of gypenosides in vitro and in vivo. Integr Cancer Ther, 2011. **10**(1): p. 101-12.

94. Dong, S.Q., Q.P. Zhang, J.X. Zhu, M. Chen, C.F. Li, Q. Liu, D. Geng, and L.T. Yi, *Gypenosides reverses depressive behavior via inhibiting hippocampal neuroinflammation.* Biomed Pharmacother, 2018. **106**: p. 1153-1160.
95. Zhang, H.K., Y. Ye, Z.N. Zhao, K.J. Li, Y. Du, Q.M. Hu, and J.F. He, *Neuroprotective effects of gypenosides in experimental autoimmune optic neuritis.* Int J Ophthalmol, 2017. **10**(4): p. 541-549.
96. Alhasani, R.H., L. Biswas, A.M. Tohari, X. Zhou, J. Reilly, J.F. He, and X. Shu, *Gypenosides protect retinal pigment epithelium cells from oxidative stress.* Food Chem Toxicol, 2018. **112**: p. 76-85.
97. Li, L., B.H. Jiao L Fau - Lau, and B.H. Lau, *Protective effect of gypenosides against oxidative stress in phagocytes, vascular endothelial cells and liver microsomes.* (1062-8401 (Print)).
98. Quan, Y. and M.Z. Qian, *[Effect and mechanism of gypenoside on the inflammatory molecular expression in high-fat induced atherosclerosis rats]*. (1003-5370 (Print)).
99. Voesenek, C.J., R.P. Pieters, and J.L. van Leeuwen, *Automated Reconstruction of Three-Dimensional Fish Motion, Forces, and Torques.* PLoS One, 2016. **11**(1): p. e0146682.
100. Eric.D.Tytell, C.-Y. Hsu, and T.L. Williams, *Interactions between internal forces, body stiffness, and fluid environment in a neuromechanical model of Lamprey swimming.* Biophyics and Computational Biology, 2010. **107**.
101. McMillen, T. and P. Holmes, *An elastic rod model for anguilliform swimming.* J Math Biol, 2006. **53**(5): p. 843-86.
102. Voesenek, C.J., F.T. Muijres, and J.L. van Leeuwen, *Biomechanics of swimming in developing larval fish.* J Exp Biol, 2018. **221**(Pt 1).
103. Adrian, R.J., *Particle-Imaging Techniques for Experimental Fluid Mechanics.* Annual Review of Fluid Mechanics, 1991. **23**(1): p. 261-304.

104. Li, G., U.K. Muller, J.L. van Leeuwen, and H. Liu, *Body dynamics and hydrodynamics of swimming fish larvae: a computational study.* The Journal of Experimental Biology, 2012. **215**(Pt 22): p. 4015-33.

105. MÜLler, U.K., J. Smit, E.J. Stamhuis, and J.J. Videler, *HOW THE BODY CONTRIBUTES TO THE WAKE IN UNDULATORY FISH SWIMMING.* The Journal of Experimental Biology, 2001. **204**(16): p. 2751.

106. Tytell, E.D. and G.V. Lauder, *The hydrodynamics of eel swimming: I. Wake structure.* 2004(0022-0949 (Print)).

107. J. Lighthill, M., *Large-Amplitude Elongated-Body Theory of Fish Locomotion.* Proceedings of the Royal Society B, 1971. **179**: p. 125-138.

108. Wu, T.Y.-T., *Hydromechanics of Swimming of Fishes and Cetaceans*, in *Advances in Applied Mechanics*, C.-S. Yih, Editor. 1971, Elsevier. p. 1-63.

109. Liu, H., R. Wassersug, and K. Kawachi, *A computational fluid dynamics study of tadpole swimming.* The Journal of Experimental Biology, 1996. **199**(6): p. 1245.

110. Liu, H., R. Wassersug, and K. Kawachi, *The three-dimensional hydrodynamics of tadpole locomotion.* The Journal of Experimental Biology, 1997. **200**(22): p. 2807.

111. Carling, J., T.L. Willams, and G. Bowtell, *Self-propelled anguilliform swimming: simulations solution of the two-dimensional navier-stokes equations and newton's laws of motion.* The Journal of Experimental Biology, 1998. **201**: p. 24.

112. Kern, S. and P. Koumoutsakos, *Simulations of optimized anguilliform swimming.* The Journal of Experimental Biology, 2006. **209**(Pt 24): p. 4841-57.

113. Borazjani, I. and F. Sotiropoulos, *Numerical investigation of the hydrodynamics of carangiform swimming in the transitional and inertial flow regimes.* The Journal of Experimental Biology, 2008. **211**(Pt 10): p. 1541-58.

114. Borazjani, I. and F. Sotiropoulos, *Numerical investigation of the hydrodynamics of anguilliform swimming in the transitional and inertial flow regimes.* The Journal of Experimental Biology, 2009. **212**(Pt 4): p. 576-92.

115. Katumata, Y., U.K. MÜLler, and H. Liu, *Computation of Self-Propelled Swimming in Larva Fishes.* Journal of Biomechanical Science and Engineering, 2009. **4**(1): p. 54-66.

116. Li, G., H. Liu, U.K. Mu¨ller, and J.L. van Leeuwen, *Swimming Hydrodynamics and Maneuverability in C-Start of Zebrafish Larvae: An Integrated Computational Study*, in *ASME-JSME-KSME 2011 Joint Fluids Engineering Conference: Volume 1, Symposia – Parts A, B, C, and D*. 2011. p. 2059-2066.

117. Jia, L., R.K. Raghupathy, A. Albalawi, Z. Zhao, J. Reilly, Q. Xiao, and X. Shu, *A colour preference technique to evaluate acrylamide-induced toxicity in zebrafish.* Comp Biochem Physiol C Toxicol Pharmacol, 2017. **199**: p. 11-19.

118. Topic Popovic, N., I. Strunjak-Perovic, R. Coz-Rakovac, J. Barisic, M. Jadan, A. Persin Berakovic, and R. Sauerborn Klobucar, *Tricaine methane-sulfonate (MS-222) application in fish anaesthesia.* Journal of Applied Ichthyology, 2012. **28**(4): p. 553-564.

119. Sancho, G., D. Ma, and P. Lobel, *Behavioral observations of an upcurrent reef colonization event by larval surgeonfish Ctenochaetus strigosus (Acanthuridae).* Marine Ecology Progress Series, 1997. **153**: p. 311-315.

120. Najafov, A. and G. Hoxhaj, *Chapter 1 - Introduction*, in *PCR Guru*, A. Najafov and G. Hoxhaj, Editors. 2017, Academic Press. p. 1-6.

121. Li, Y., *Coupled Computational fluid dynamics/multibody dynamics method with application to wind turbine simulations.* Lowa Research online, 2014.

122. Masarati, P., M. Morandini, and P. Mantegazza, *An Efficient Formulation for General-Purpose Multibody/Multiphysics Analysis.* Journal of Computational and Nonlinear Dynamics, 2014. **9**(4): p. 041001.

123. Zhang, X., Z. Chen, and Y. Liu, *Chapter 3 - The Material Point Method*, in *The Material Point Method*, X. Zhang, Z. Chen, and Y. Liu, Editors. 2017, Academic Press: Oxford. p. 37-101.

124. Newmark, N.M., *A method of computation for structural dynamics*. 1959: American Society of Civil Engineers.

125. Liu, Y., Q. Xiao, A. Incecik, C. Peyrard, and D. Wan, *Establishing a fully coupled CFD analysis tool for floating offshore wind turbines.* Renewable Energy, 2017. **112**: p. 280-301.

126. Wilson, M.M. and J.D. Eldredge, *Performance improvement through passive mechanics in jellyfish-inspired swimming.* International Journal of Non-Linear Mechanics, 2011. **46**(4): p. 557-567.

127. Dabiri, J.O., S.P. Colin, J.H. Costello, and M. Gharib, *Flow patterns generated by oblate medusan jellyfish: field measurements and laboratory analyses.* The Journal of Experimental Biology, 2005. **208**(7): p. 1257.

128. Kolář, V., *Vortex identification: New requirements and limitations.* International Journal of Heat and Fluid Flow, 2007. **28**(4): p. 638-652.

129. van Leeuwen, J.L., C.J. Voesenek, and U.K. Muller, *How body torque and Strouhal number change with swimming speed and developmental stage in larval zebrafish.* J R Soc Interface, 2015. **12**(110): p. 0479.

130. Zhang, W., Y. Yu, and B. Tong, *Prediction of fish body's passive visco-elastic properties and related muscle mechanical performance in vivo during steady swimming.* Science China Physics, Mechanics and Astronomy, 2014. **57**(2): p. 354-364.

131. Videler, J.J. and F. Hess, *Fast Continuous Swimming of Two Pelagic Predators, Saithe (Pollachius Virens) and Mackerel (Scomber Scombrus): a Kinematic Analysis.* Journal of Experimental Biology, 1984. **109**(1): p. 209.

132. Lawrence C. Rome, Douglas Swank, and D. Corda, *How Fish Power Swimming.* Science, 1993. **261**.

133. Irons, T.D., R.C. MacPhail, D.L. Hunter, and S. Padilla, *Acute neuroactive drug exposures alter locomotor activity in larval zebrafish.* Neurotoxicology and Teratology, 2010. **32**(1): p. 84-90.

134. Li, Q., J. Lin, Y. Zhang, X. Liu, X.Q. Chen, M.Q. Xu, L. He, S. Li, and N. Guo, *Differential behavioral responses of zebrafish larvae to yohimbine treatment.* Psychopharmacology (Berl), 2015. **232**(1): p. 197-208.

135. Zhao, Z., G. Li, Q. Xiao, H.-R. Jiang, G.M. Tchivelekete, X. Shu, and H. Liu, *Quantification of the influence of drugs on zebrafish larvae swimming kinematics and energetics.* PeerJ, 2020. **8**: p. e8374.

136. Nordgreen, J., F.M. Tahamtani, A.M. Janczak, and T.E. Horsberg, *Behavioural effects of the commonly used fish anaesthetic tricaine methanesulfonate (MS-222) on zebrafish (Danio rerio) and its relevance for the acetic acid pain test.* PLoS One, 2014. **9**(3): p. e92116.

137. Ekeberg, O. and A. Lansne, *The Neural Control of Fish Swimming Studied Through Numerical Simulatio.* Adaptive behavior, 1995. **3**.

138. Zhao, W., A. Ming, and M. Shimojo, *Development of High-Performance Soft Robotic Fish by Numerical Coupling Analysis.* Appl Bionics Biomech, 2018. **2018**: p. 5697408.

139. Keeble, J.E., J.V. Bodkin, L. Liang, R. Wodarski, M. Davies, E.S. Fernandes, C.d.F. Coelho, F. Russell, R. Graepel, M.N. Muscara, M. Malcangio, and S.D. Brain, *Hydrogen peroxide is a novel mediator of inflammatory hyperalgesia, acting via transient receptor potential vanilloid 1-dependent and independent mechanisms.* PAIN®, 2009. **141**(1): p. 135-142.

140. Valério, D.A., S.R. Georgetti, D.A. Magro, R. Casagrande, T.M. Cunha, F.T.M.C. Vicentini, S.M. Vieira, M.J.V. Fonseca, S.H. Ferreira, F.Q. Cunha, and W.A. Verri, *Quercetin Reduces Inflammatory Pain: Inhibition of Oxidative Stress and Cytokine Production.* Journal of Natural Products, 2009. **72**(11): p. 1975-1979.

141. Kiasalari, Z., T. Rahmani, N. Mahmoudi, T. Baluchnejadmojarad, and M. Roghani, *Diosgenin ameliorates development of neuropathic pain in diabetic*

rats: Involvement of oxidative stress and inflammation. (1950-6007 (Electronic)).

142. Ribeiro, R.A., S.M. Vale Ml Fau - Thomazzi, A.B. Thomazzi Sm Fau - Paschoalato, S. Paschoalato Ab Fau - Poole, S.H. Poole S Fau - Ferreira, F.Q. Ferreira Sh Fau - Cunha, and F.Q. Cunha, *Involvement of resident macrophages and mast cells in the writhing nociceptive response induced by zymosan and acetic acid in mice.* 2000(0014-2999 (Print)).
143. Maximino, C., *Modulation fo nociceptive-like behavior in zebrafihs (Danio rerio) by environmental stressors* Psychology Neuroscience 2011. **4**: p. 7.
144. Schroeder, P.G. and L.U. Sneddon, *Exploring the efficacy of immersion analgesics in zebrafish using an integrative approach.* Applied Animal Behaviour Science, 2017. **187**: p. 93-102.
145. McHenry, M.J. and S.M. van Netten, *The flexural stiffness of superficial neuromasts in the zebrafish (Danio rerio) lateral line.* J Exp Biol, 2007. **210**(Pt 23): p. 4244-53.
146. Tytell, E.D., M.C. Leftwich, C.-Y. Hsu, B.E. Griffith, A.H. Cohen, A.J. Smits, C. Hamlet, and L.J. Fauci, *Role of body stiffness in undulatory swimming: Insights from robotic and computational models.* Physical Review Fluids, 2016. **1**(7).
147. Lin, Y.Y., *Muscle diseases in the zebrafish.* Neuromuscul Disord, 2012. **22**(8): p. 673-84.

8 List of Figures and Tables

9 Abbreviations

HTS	High Throughput Screening
Dpf	Days Post-fertilization
BMP	Bone Morphogenetic Protein
AD	Alzheimer's disease
FAD	Familial Alzheimer's disease
CFD	Computational Fluid Dynamics
CNS	Central Nervous System
MSS	Morphine Sulfate Solution
NSAIDs	Nonsteroidal Anti-Inflammatory Drugs
PIV	Particle Image Velocimetry
RPE	Retinal Pigment Epithelium
DPH	Diphenylhydantoin
LED	Light Emitting Diode
Hpf	Hours Post-fertilization
SIMPLE	Semi-Implicit Method for Pressure-Linked Equations
PISO	Pressure Implicit with Splitting of Operator
cDNA	Complementary Deoxyribonucleic Acid
FSI	Fluid-structure Interaction
DAE	Differential-Algebraic Equation
EMG	Electromyography
GSH	Glutathione

10 Nomenclature

Δt	Physical time step
$\overline{H}$	Mean height of the bell
D_{max}	Maximum diameter of the bell
υ	Kinematic viscosity
k_i	Hinge stiffness
Y_C	Centroid displacement in y direction
V_C	Centroid velocity in y direction
W_h	Power required to activate hinges
A_i	Area of body i
J_i	Body moment of inertia i
$\dot{E}_b$	Power of the body system
P_{com}	Centre of mass of fish body
m_{body}	Total mass of fish body
l_{body}	Length of fish body
f	Tail beat frequency
J_{body}	Fish body moment of inertia
ω_{body}	Fish body angular velocity
M_i	Torque of body i
ω_i	Angular velocity of body i
M_j	Torque generated at the joint j
F_j	Force generated at joint j
P_m	Power per unit mass
$W_{external}$	Work done to the fish by the surrounding fluid
$W_{internal}$	Work done by fish muscle
T	Motion period
P	Flow pressure

$P_{external}$	Hydrodynamic power
$P_{internal}$	Mechanical power from fish muscle
ρ	Fluid density